Bergslagen, etapp 2

Geochemical and geophysical assessment of c. 1.8 Ga granites associated with W-F ± Mo mineralisation, western Bergslagen

Edward Lynch, Robert Berggren & Stefan Bergman

september 2023

SGU-rapport 2023:13

SGU Sveriges geologiska undersökning

Cover photos: GP-suite granitic dyke crosscutting metavolcanic rock, Bångbro area (western Malingsbo granite). Hammer is 80 cm long. Photographer: Edward Lynch

Authors: Edward Lynch, Robert Berggren & Stefan Bergman
Reviewed by: Magnus Ripa & Lena Persson
Head of unit: Ildikó Antal Lundin

Editor: Lina Rönnåsen

Geological Survey of Sweden
Box 670, 751 28 Uppsala, Sweden
phone: 018-17 90 00
e-mail: sgu@sgu.se

www.sgu.se

TABLE OF CONTENTS

SAMMANFATTNING

Denna rapport presenterar resultaten av en petrologisk, geokemisk och geofysisk undersökning av cirka 1,8 miljarder år gamla granitintrusioner som tillhör den regionala granit-pegmatitsviten (GP-sviten) i Bergslagen. I västra Bergslagen är graniter i GP-sviten associerade med W-F ± Mo ± Cu- och intragranitisk Mo ± F-mineralisering i skarn, medan det i hela distriktet finns en genetisk koppling med pegmatiter som innehåller en del ovanliga metaller. Flera av dessa grundämnen (t.ex. W, F, Ta, Li) anses vara ”kritiska” eller ”strategiska” råvaror av Europeiska unionen.

Intrusioner i GP-sviten sydost om västra Bergslagens gränszon (WBBZ), en sammansatt deformationszon i regional skala, omfattar huvudsakligen odeformerad, jämnkornig till megakristförande biotit- ± muskovit- ± hornbländeförande syenogranit till alkalifältspatgranit som saknar mineralisering. Nordväst om WBBZ förekommer också liknande odeformerade, jämnkorniga till megakristförande biotitgraniter som lokalt innehåller sidobergsxenoliter eller mafiska mikrogranulära enklaver (t.ex. Malingsbo- och Enkullengraniter). I närheten av kända skarn-W-mineraliseringar förekommer rödrosa, massiv, jämnkornig alkalifältspatgranit associerad med aplit-pegmatitsegregationer och gångar. I sådana områden uppvisar graniterna texturella egenskaper som tyder på höga grader av fraktionering, inklusive aplit-pegmatitvarianter utan mafiska mineral, kvartsrika segregationer, och alkalimetasomatos.

Geokemiskt är graniterna kisel- och alkalirika (K + Na), peraluminösa och ferroiska intrusioner med höga halter av U, Th, Ta och Y, och låga halter av Ca, Mg, Ti, Nb, Zr och REE. Det finns en tydlig regional geokemisk trend som visar ökande fraktionering från ofyndiga graniter i sydost till skarnproximala ofyndiga och mineraliserade graniter i nordväst, vilket innebär att fraktionerad kristallisation har en nyckelroll för grundämnesanrikning i differentierade magmor associerade med W ± Mo ± F-mineralisering. Variationer i petrofysiska egenskaper (densitet, magnetisk susceptibilitet) för granit överensstämmer med de observerade regionala geokemiska och mineralogiska trenderna.

U-Pb-zirkon- och Re-Os-molybdenglansdatering av granit- och skarnprover avgränsar tidsperioden för granitintrusion och Mo- (± W-) mineralisering till ca 1,81–1,77 miljarder år, och identifierar alltså en relativt kortlivad, senorogen magmatisk-metallogen epok. Huvud- och spårelement-geokemi och Sm-Nd-isotopdata indikerar att graniterna huvudsakligen har överlappande fraktionerad I- och A2-typsaffinitet och bildades genom uppsmältning av cirka 1,9 miljarder år gamla metamagmatiska ± suprakrustala källbergarter som påverkats av tidigare subduktions-, metamorfos- och vittringshändelser. En kombination av dekompressionssmältning (vid netto-extension av jordskorpan) och värmeadvektion från likåldrig öbågerelaterad magmatism kan ha initierat uppsmältning av undre till mellersta jordskorpan och migrering av felsiska smältor vilket ledde till bildning av granit i mellersta till övre jordskorpan.

Förutom ursprungsmagmans sammansättning, som huvudsakligen återspeglar källbergartens egenskaper, var lokala företeelser vid enskilda mineraliseringar som t.ex. förekomsten av värd-bergarter som marmorhorisonter, förekomsten av äldre strukturer i sidoberget och differentiella höjnings- och erosionseffekter viktiga förutsättningar för bildning och bevarande av W-skarn-mineraliseringar i västra Bergslagen.

ABSTRACT

This report presents the results of a petrological, geochemical, and geophysical investigation of c. 1.8 Ga granitic intrusions in Bergslagen assigned to the regional Granite-Pegmatite (GP) igneous suite. In western Bergslagen, GP-suite granites are associated with skarn-hosted W-F ± Mo ± Cu and intragranitic Mo ± F mineralisation, while across the district, a genetic link with some rare metal-bearing pegmatites is also envisaged. Several of these associated commodities (e.g., W, F, Ta, Li) are considered "critical" or "strategic" raw materials by the European Union.

GP-suite intrusions southeast of the western Bergslagen boundary zone (WBBZ), a regional-scale composite deformation zone, comprise mainly undeformed, equigranular to megacrystic biotite ± muscovite ± hornblende-bearing syenogranite to alkali feldspar granite that lack mineralisation (e.g., Fellingsbro granite). Northwest of the WBBZ, similar undeformed equigranular to megacrystic biotite granites also occur that locally contain country rock xenoliths and/or mafic microgranular enclaves (e.g., Malingsbo and Enkullen granites). Closer to known skarn W prospects, reddish pink, massive, equigranular alkali feldspar granites associated with aplite-pegmatite segregations and dykes occur. In these areas, the granites show textural features consistent with high degrees of fractionation including aplite-pegmatite variants lacking mafic minerals, quartz-rich segregations, and alkali metasomatism.

Geochemically, the granites are high-silica, peraluminous and ferroan intrusions enriched in SiO_2, total alkalis (K + Na), U, Th, Ta and Y, and depleted in Ca, Mg, Ti, Nb, Zr and total REEs. A regional geochemical trend of increasing bulk fractionation from barren granites in the SE to skarn-proximal barren and mineralised granites in the NW is evident, suggesting fractional crystallization represents a key control on element enrichment in late-stage differentiated magmas associated with W ± Mo ± F mineralisation. Variations in granite petrophysical properties (density, magnetic susceptibility) are consistent with the observed regional geochemical and mineralogical trends.

Zircon U-Pb and molybdenite Re-Os dating of granite and skarn samples constrains the timing of granite emplacement and Mo (± W) mineralisation from c. 1.81–1.77 Ga, and thus identifies a relatively short-lived, late-orogenic magmatic-metallogenic epoch. Major and trace element geochemistry, and Sm-Nd isotopic data indicate the granites have mainly overlapping fractionated I- and A2-type affinities and formed via infracrustal anatexis of Svecofennian (c. 1.9 Ga) metaigneous ± supracrustal source rocks affected by earlier subduction, metamorphic and weathering events. A combination of decompression melting (via net crustal extension), mafic magma underplating and/or heat advection from coeval arc-related magmatism at c. 1.8 Ga may have initiated lower to mid-crustal anatexis and melt migration leading to granite formation in the mid- to upper crust.

Aside from parental magma compositions that mainly reflect granite source rock characteristics, local deposit-scale features including the availability of target/host marble horizons, the prevalence of preexisting structural fabrics in country rocks, and differential uplift/erosion effects were important controls on skarn W mineralisation development and preservation in western Bergslagen.

INTRODUCTION

The late Svecokarelian (c. 1.8 Ga) granite-pegmatite suite in Bergslagen (Stephens et al. 2009), in this report called the GP-suite, is associated with three main types of mineralisation:

1. Pegmatite-hosted niobium-yttrium-fluorine and/or lithium-cesium-tantalum ± tin ± beryllium mineralisation.
2. Granite-hosted molybdenum mineralisation.
3. Skarn-hosted tungsten-fluorine-molybdenum ± copper mineralisation.

Of these commodities, Be, F, Li, Nb, Ta, W and Y are designated "critical raw materials" by the EU based on economic and supply risk considerations, with W having the highest designation in terms of economic importance (e.g., Blengini et al. 2020). Since January 2021, the importation and use of Sn, Ta and W (along with Au) are also governed by an EU "Conflict Minerals" regulation, meaning the sourcing of these metals from politically unstable regions should be avoided by EU-based industries (e.g., Partzsch 2018). Although not deemed a critical material at present, Mo is one of several strategic metals considered important for the European defense industry (e.g., Pavel et al. 2020).

In the Bergslagen ore district, the "Western Bergslagen W-Mo" metallogenic area includes more than 100 known W ± Mo ± F ± Cu deposits or occurrences (Bergman 2012). Of these, numerous skarn-hosted W prospects occur that show a spatial and/or genetic association with GP-suite granitic intrusions. The southeastern boundary of the W-Mo metallogenic area coincides in general with the "Western Bergslagen Boundary Zone" (WBBZ, Beunk & Kuipers 2012), a composite regional-scale structure comprising discontinuous northwest-southeast shear zones between Garpenberg and Älvlången (Fig. 1). Thus, the WBBZ acts as a major structural-deformational boundary separating mineralisation-related GP-suite intrusions to the NW from equivalent, generally barren granites in the SE.

The aim of this project is to assess factors controlling the enrichment of W, Mo, F and Cu in western Bergslagen, with a particular focus on mineralisation types 2 and 3 mentioned above. Geological field mapping, petrography, lithogeochemistry, geochronology (U-Pb, Re-Os) and tracer isotope analysis (Sm-Nd) have been combined with geophysical investigations (e.g., petrophysics, ground surveys, inversion modelling) to assess the character and mineralisation potential of c. 1.8 Ga granitic intrusions to the SE and NW of the WBBZ. The project was active during the period 2019-2021, and results from the first field season are presented in Bergman et al. (2020). Coordinates for sample locations and outcrops are given in the SWEREF99 TM grid system.

REGIONAL SETTING

The Bergslagen W-Mo metallogenic area is located in the western part of the Bergslagen lithotectonic unit of the Paleoproterozoic Svecokarelian orogen (Fig. 1). To the immediate west, mafic to felsic plutonic rocks of the Transscandinavian Igenous Belt (TIB) and the eastern limit of the Sveconorwegian orogen occur. A more detailed account of these units is given by Stephens et al. (2009), Stephens & Jansson (2020), Wahlgren & Stephens (2020), and references therein.

The oldest lithological unit in Bergslagen is a c. 1.9 Ga Svecofennian supracrustal sequence mainly comprising intermediate to felsic metavolcanic rocks with lesser interbedded marble and skarn layers. The supracrustal rocks host numerous metallic mineral deposits, with the most economically important types being iron oxide and base metal sulfide deposits. The metavolcanic rocks are both underlain and overlain by clastic metasedimentary units.

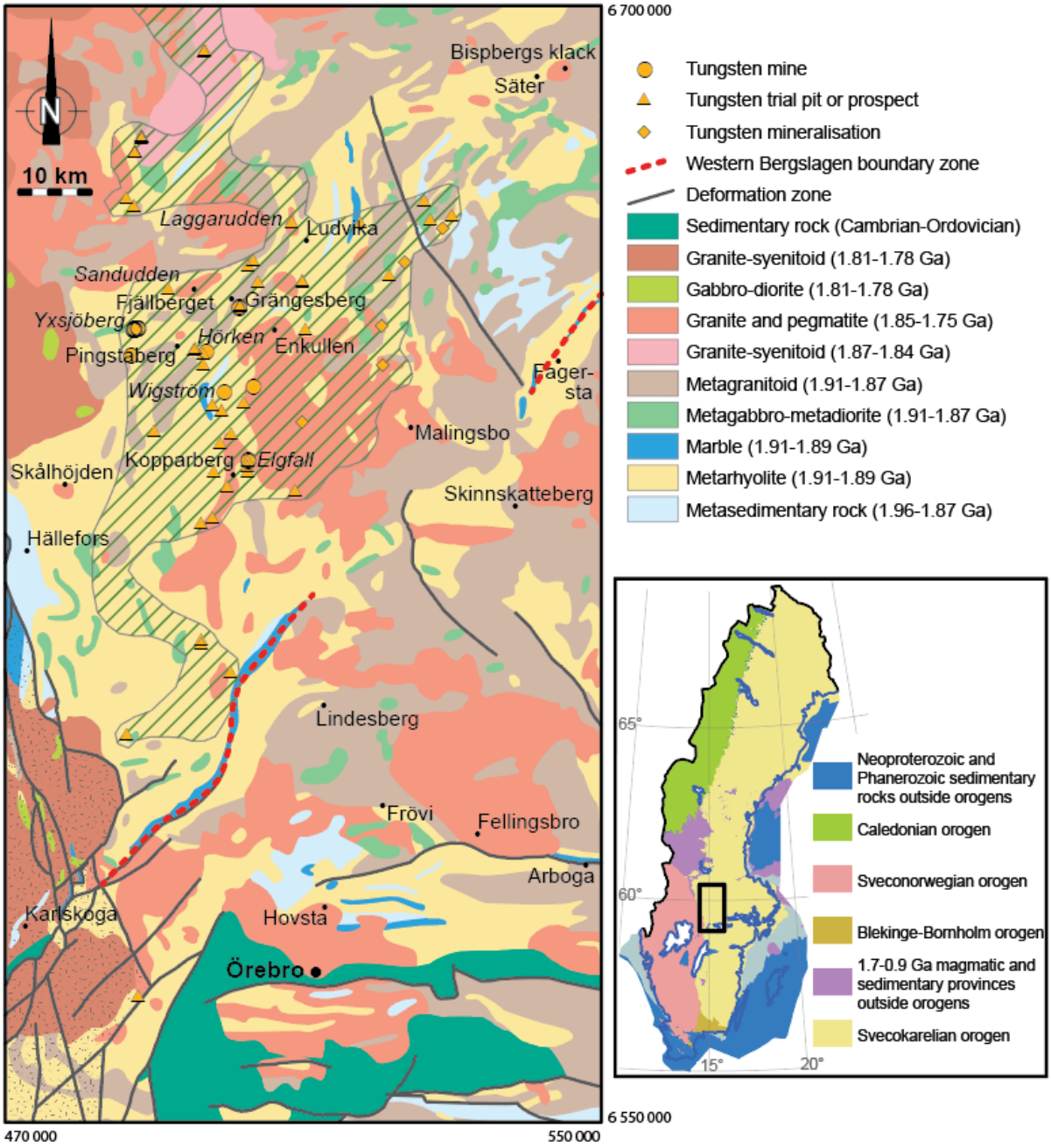

Figure 1. Bedrock map of parts of western Bergslagen, modified from Bergman et al. (2012). The area with speckled pattern in the southwestern part was affected by ductile deformation during the Sveconorwegian orogeny. The hatched area is the metallogenic area "Western Bergslagen W-Mo" (Bergman 2012). The location in Sweden is shown in the small map with the main lithotectonic units.

Based on the scheme devised by Stephens et al. (2009), supracrustal rocks in Bergslagen are intruded by six plutonic rock suites. These are (from oldest to youngest):

1. Abundant c. 1.91–1.88 Ga granitoid-dioritoid-gabbroid intrusions (older GDG suite).
2. Subordinate c. 1.87–1.85 Ga granitoid-dioritoid-gabbroid intrusions in SW Bergslagen (younger GDG suite).
3. C. 1.87–1.84 Ga granite-syenitoid-dioritoid-gabbroid ± monzonitoid intrusions in northern and southern Bergslagen (older GSDG suite)
4. Minor c. 1.85–1.83 Ga granite-pegmatite intrusions in NE and central Bergslagen (older GP suite).
5. A zone of c. 1.81–1.78 Ga granite-syenitoid-dioritoid-gabbroid ± monzonitoid intrusions in western Bergslagen that form part of the TIB (younger GSDG suite).
6. Abundant c. 1.81–1.75 Ga granite-pegmatite intrusions (younger GP suite).

The younger GP suite intrusions are associated with the granite- and skarn-hosted W-Mo-F-Cu mineralisation in western Bergslagen and are the focus of this report.

Two main episodes of regional deformation and metamorphism affected Bergslagen supracrustal and plutonic rocks at c. 1.87–1.86 Ga and c. 1.84–1.81 Ga (M1/D1 and M2/D2 event, respectively) and separate the emplacement of the older and younger GSDG and GP intrusive suites. A more localized deformation-metamorphic event also occurred at around 1.82–1.80 Ga (D3), although its timing and significance remains uncertain (cf. Stephens & Jansson 2020). Svecokarelian-related regional deformation-metamorphism (M1 and M2, above) is characterized by repeated ductile deformational episodes that formed structural fabrics, folding, and shearing in pre- to syn-orogenic lithologies at variable temperatures and low to medium pressures. Sveconorwegian-cycle orogenesis to the west of Bergslagen was active at c. 1.1–0.9 Ga. Remnants of a Cambrian–Ordovician sedimentary cover partly bounded by faults is preserved near Örebro in central Bergslagen.

PREVIOUS WORK

Two generations of GP-suite intrusions with crystallization ages of c. 1.85–1.83 Ga and 1.82–1.75 Ga have been recognized in Bergslagen (e.g., Stephens & Jansson 2020, and references therein). In southern Finland, comparable late Svecofennian leucogranites were simultaneously emplaced between c. 1.85 Ga and c. 1.79 Ga (Kurhila et al. 2011). Plan (2020) presented a zircon U-Pb LA-ICP-MS age of c. 1.79 Ga for the Högberget granite (Bergman et al. 1995) adjacent to the Wigström skarn W deposit. This date is considered more accurate than a multigrain U-Pb zircon TIMS age of c. 1.75 Ga previously acquired by Bergman et al. (1995). Overlapping c. 1.8 Ga ages for both magmatic and hydrothermal zircons from the Wigström-Högberget system suggests coeval granite emplacement and skarn W-F-Mo mineralisation (Plan 2020). A Re-Os molybdenite age of c. 1.8 Ga for the Wigström deposit was presented without details in a conference abstract by Stein et al. (1996). The Högberget granite adjacent to the Wigström W-F skarn deposit is a high-silica, peraluminous intrusion and a fractionated character is indicated by its high Th and Rb/Sr contents, and by flat REE patterns that show increases in light REEs and negative Eu anomalies (Bergman et al. 1995).

The Mo-mineralised Pingstaberg granite (Billström et al. 1988) has a preliminary igneous age of c. 1805 Ma (Lynch et al. 2019). The Fjällberget granite (Åberg & Bjurstedt 1988) has a LA-ICP-MS U-Pb zircon age of c. 1.79 Ga and zircon $\varepsilon_{Hf(T=1.79\ Ga)}$ values of +1.1 to +3.7 (Andersen et al. 2009). Patchett et al. (1987) presented Sm-Nd isotopic data for the Malingsbo and Fellingsbro granites (the latter with a TIMS U-Pb zircon age of 1.78 Ga), giving $\varepsilon_{Nd(T=1.79\ Ga)}$ values of +1.5 and +1.7, and -0.1, respectively. Valbracht et al. (1994) reported a wider range of initial ε_{Nd} values

between -0.3 and +7.7 for granites in the "Fellingsbro-Malingsbo suite". In the Yxsjöberg-Pingstaberg area, the Mo-mineralised Pingstaberg granite is more fractionated than comparable barren GP-suite intrusions (Ripa & Antal Lundin 2020). During magma fractionation, both Y and Yb behaved incompatibly, whereas Zr and Ba contents in parental magmas decreased.

Skarn and granite-related W and Mo mineralisation in western Bergslagen were considered by most early researchers (Magnusson 1940, Hübner 1971, Ohlsson 1979) to be related to a younger generation of granitic intrusions (variously referred to as "late Svecofennian", "serorogenic", or "GP-suite" in the literature). Although this view was challenged by Hellingwerf & Baker (1985) who suggested the mineralisation was genetically related to older c. 1.9 Ga intrusive rocks ("urgranit", "primorogenic", or "GDG-suite"), subsequent work (e.g., Sundblad et al. 1993, Romer & Öhlander 1994, Bergman et al. 1995, Lynch et al. 2019, Plan 2020, Ripa & Antal Lundin 2020) has strengthened the original interpretation.

Tungsten occurrences in Bergslagen were described and interpreted regarding their mode of formation by Ohlsson (1979). The W-mineralised skarn bodies at Elgfall and Laggarudden are spatially related to granite or granitic pegmatite, and the mineralisation was interpreted to be of contact metasomatic origin with some influence of thermal metamorphism (Ohlsson 1979). Similarly, hydrothermal solutions exsolved from evolved felsic magma were suggested to have formed the stratabound Yxsjöberg W-Cu-F skarn deposit. Romer & Öhlander (1994) obtained a U-Pb titanite age of c. 1790 Ma from the Yxsjöberg deposit and concluded that post-kinematic granites were the source of heat, metals and probably fluids responsible for the formation of the skarn deposit. Sulfur isotopic data for molybdenite from the Pingstaberg, Hörken and Wigström deposits show $\delta^{34}S$ values within the narrow range +1.8 ‰ to +3.1 ‰, which is compatible with a single igneous (granitic) source (Hellingwerf et al. 1987).

Geophysical modelling suggests that the contacts of the Pingstaberg and Yxsjöberg granites are moderately outwards dipping (Ripa & Antal Lundin 2020). The Fellingsbro granite (Holmquist 1906) is shown by geophysical modelling to have a stock-shaped southern part reaching a depth of 15–20 km, and considerably thinner, laccolithic central and northern parts (Zuber 1985).

Airborne geophysical data, including magnetic, electromagnetic, and radiometric measurements that cover the project area have been made by SGU during several campaigns, with flight directions from east-west or northwest-southeast (cf. Stephens et al. 2009). During the most recent work (2007–2020), "Very low frequency" (VLF) electromagnetic data was acquired using two radio transmitters, which allows calculation of the apparent resistivity of the bedrock.

SGU performs gravity measurements on the ground with a point separation of about 1 km on an on-going basis. Geophysical ground surveys of selected exploration targets have been performed by LKAB and SGAB using magnetometry and slingram methods in the study area. The surveyed prospects include Finnstängselmossen near Pingstaberg (analogue slingram data by LKAB, year unknown), Hörken (analogue magnetic data by LKAB, 1977), and Ställdalen near Wigströms-gruvan (analogue and digital data by LKAB and SGAB, 1985–1986). Krigstjärn, Kumlan, Lortbromossen and Rundberget are other exploration areas near Wigström that were surveyed during the years 1981–1988.

Petrophysical data acquired by SGU are available from Hörken (13 samples up to 1991), the Pingstaberg area (21 samples from 1990–1992 and 2017) and the Wigström-Högberget area (10 samples up to 1990).

METHODS

Field work and sampling

After initial assessment of available geological and geophysical data, three field areas were selected to compare GP-suite granites in different settings. These were:

1. The Lindesberg–Örebro area SE of the WBBZ and distal to the known skarn W mineralisation.
2. The Malingsbo–Kloten area NW of the WBBZ also distal to known skarn W prospects to the west.
3. The Kopparberg–Ställdalen area NW of the WBBZ where known skarn W mineralisation including the Yxsjöberg, Sandudden, Hörken, Wigström-Högberget and Elgfall prospects occur, and the Mo-mineralised Pingstaberg granite (cf. Fig. 1).

For comparative purposes, the Mo-mineralised Bispbergs klack granite near Säter about 55 km to the northeast was also included as part of area 3 (Fig. 1). An overview map of areas 2 and 3 showing magnetic and gravity field strengths can be seen in Figure 2.

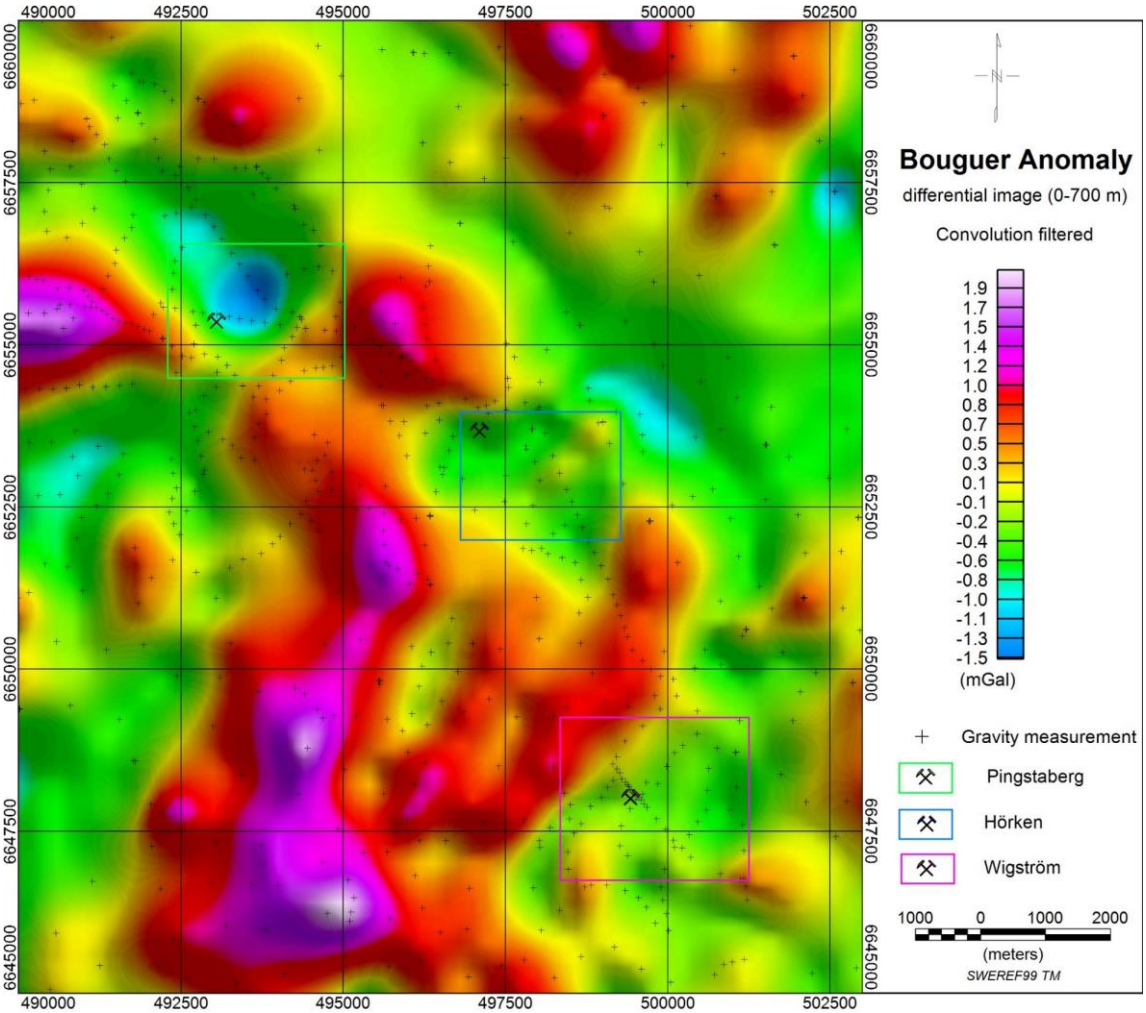

Figure 2A. An overview of the study area showing the gravity field. The rectangles called Hörken and Pingstaberg represent areas studied in more detail. Bouguer Gravity Anomaly with black dots showing locations for survey. The gravity image has been modified, and filtered, to enhance the surficial part of the bedrock.

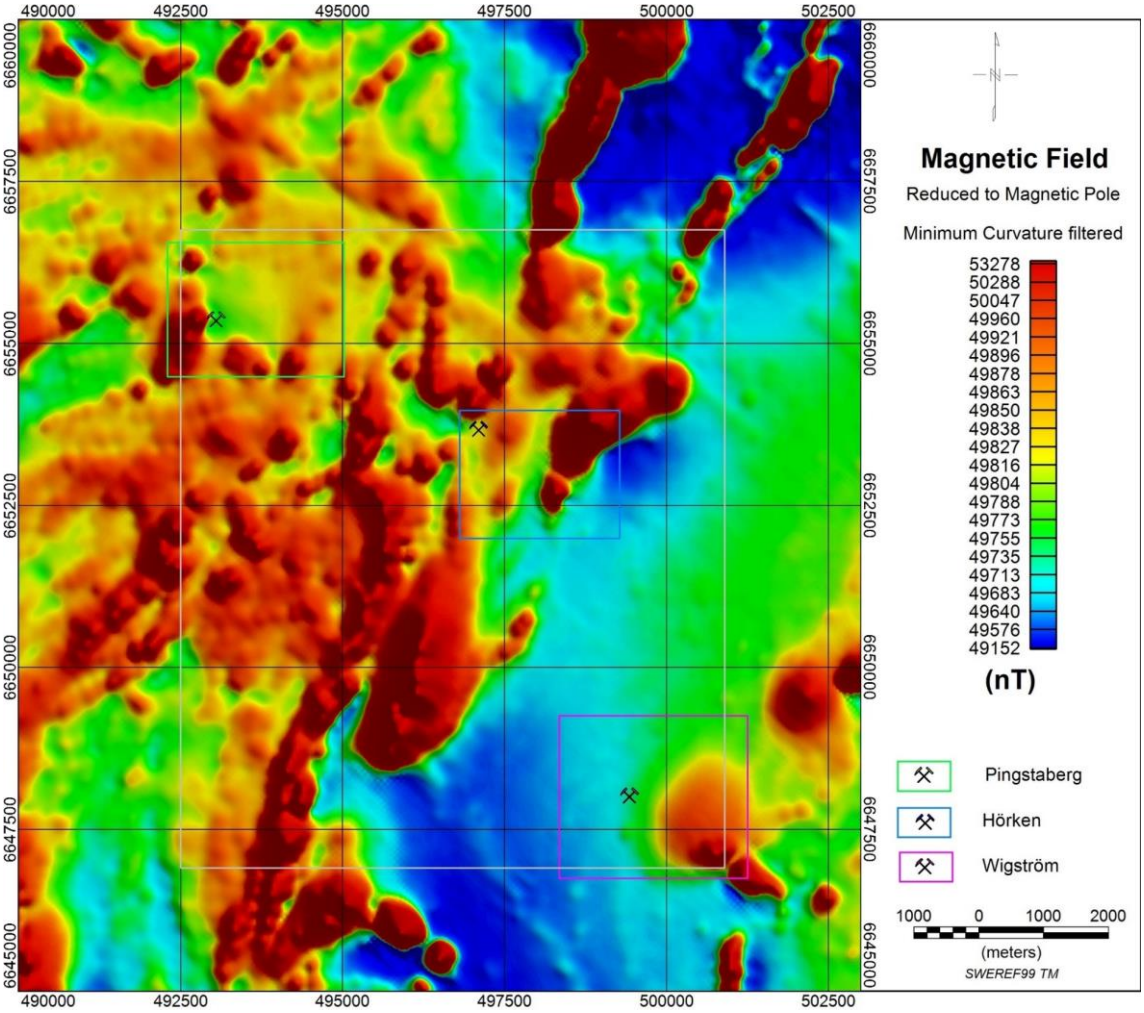

Figure 2B. An overview of the study area showing the magnetic field. The rectangles called Hörken and Pingstaberg represent areas studied in more detail. Airborne survey of the magnetic field where reduction to the magnetic pole (RTP) has been applied, as well as filtering to suppress minor features. The grey box relates to the overview inversion of magnetic susceptibility (Fig. 9).

Field work was performed during the summer in 2019 and 2020. Outcrops were visited where rock type, structural orientations and field relations were documented. Fresh and altered rock samples of texturally and mineralogically variable granitic rocks (e.g., equigranular, megacrystic, biotite, biotite + muscovite) were hammered from outcrops for lithogeochemical, petrophysical, and geochronology analysis. Representative samples of meta-igneous and metasedimentary country rocks were also sampled for further analysis. In addition, the assessment and sampling of historical drill core from several Bergslagen W and Mo prospects were undertaken during September 2020 at the Swedish National Drill Core Archive in Malå, Västerbotten County.

Ground geophysical measurements

Across the study area, magnetic susceptibility measurements of the main lithologies were made using hand-held susceptibility meters (SM20, GF Instruments). Additionally, K, U, and Th contents were estimated for some exposed rock surfaces using a Radiation solutions 230 spectrometer. Detailed ground geophysical profiles over the Hörken, Högberget and Pingstaberg granites were surveyed using a combined magnetometer and Very Low Frequency (VLF) electromagnetic instrument (GSMV-19). Electromagnetic VLF measurements were made using three different frequencies (signals from three different radio transmitters). The 16.4 kHz signal from Novika, Norway, was selected as the most favourable direction for the calculation of bedrock apparent resistivities. Gravity field profiles were also surveyed in the Hörken, Pingstaberg, and Wigström–Högberget areas using a Scintrex CG-5 autograv instrument with a point separation of 10–100 m.

Petrophysical analysis

In total, 32 rock samples were analyzed for density, magnetic susceptibility, and natural remanent magnetisation at the petrophysical laboratory at SGU, Uppsala. During sampling and if conditions allowed, petrophysical samples were oriented relative to time and sun angle. The orientation and strength of the remanent magnetisation was measured for oriented samples, but analysis of the direction of remanent magnetisation was not possible because of the small number of samples.

Processing and 3D-modelling of geophysical data

Geophysical modelling was made using both inversion and forward modelling. The software Oasis Montaj, VOXI was used for inversion of the magnetic and gravity data. The results are 3D models of the variation of density and magnetic susceptibility, respectively, corresponding to the measured field strengths.

The apparent resistivity was calculated along the measured VLF-profiles using the 2D-code Rebocc implemented in the Oasis Montaj software. The 2D apparent resistivity sections have been used together with the 3D models from inversion of gravity and magnetic data to support the forward modelling of the bedrock units in the area.

The forward modelling was done using the software Model Vision. The model building started by using relatively big and simple rock-bodies, with petrophysical properties observed in the field, to suit the main features of the geophysical response. The workflow was repeated successively to arrive at more detailed models that fit the observed geophysical data.

Whole-rock geochemical and Sm-Nd isotopic analysis

Thin sections were examined with a petrographic microscope at SGU, Uppsala. In total, 48 representative rock samples were sent to ALS in Öjebyn, Sweden, for crushing, milling and lithogeochemical analysis. Rock powders were analyzed for major, minor and trace elements by ALS in Galway, Ireland, using LECO, ICP-MS and ICP-AES. In addition, whole-rock Sm-Nd isotopic analysis of a subset of 24 granitoid and metamorphic samples was undertaken by ALS in Luleå, Sweden, using MC-ICP-MS. Geochemical data analysis and plotting was performed using ioGAS-64 and GCDkit 6.0 software.

Zircon U-Pb dating

Zircons were obtained from density separates of crushed rock samples using a Wilfley water table at SGU. Magnetic minerals were removed using a hand magnet. Handpicked zircons were mounted in transparent epoxy resin together with grains of the reference zircon 91500. The zircon mounts were polished, gold coated and examined by backscattered electron imaging at the Department of Earth Sciences, Uppsala University, Sweden. Secondary ion mass spectrometer (SIMS) analysis was carried out using the Cameca IMS 1280 ion microprobe instrument at the NORDSIM laboratory, Swedish Museum of Natural History, Stockholm. Detailed descriptions of the analytical procedures are given in Whitehouse et al. (1999) and Whitehouse & Kamber (2005). A c. 6 nA O^{2-} primary ion beam was used during analysis, yielding spot sizes of c. 15 µm. U/Pb isotopic ratios, U, Th and Pb concentrations, and Th/U ratios were calibrated relative to the zircon 91500 standard which has an age of c. 1065 Ma (e.g., Wiedenbeck et al. 2004). Common Pb-corrected isotope values were calculated using modern common Pb composition (Stacey & Kramers 1975) and measured ^{204}Pb, in cases where the ^{204}Pb count rate was above the detection limit. U-Pb decay constants follow the recommendations of Steiger & Jäger (1977). Isochron diagrams and age calculations of U-Pb isotopic data were made using Isoplot 4.15 (Ludwig 2012). All age uncertainties are presented at the 2σ or 95% confidence level.

Molybdenite Re-Os dating

Sample preparation for molybdenite Re-Os dating was undertaken at SGU in Uppsala and the Department of Earth Sciences, Uppsala University, while isotopic analysis was conducted at the Department of Earth Sciences, Durham University, UK. Re-Os dating utilized the single occurrence 'whole-rock' sampling and mineral separation approach advocated by Stein (2006). Sample crushing, molybdenite separation (Frantz magnetic and LST heavy liquid methods), the isolation of pure aliquots of Re and Os, and the measurement of ^{187}Re and ^{187}Os concentrations by N-TIMS followed the analytical procedure outlined by Selby & Creaser (2001). Model ages were calculated using the ^{187}Re decay constant of Smoliar et al. (1996) and the results are reported at the 95% (2σ) uncertainty level.

RESULTS

Granite types and petrology

In this study, the investigated GP suite intrusions have been subdivided into four groups based on geographical location relative to the WBBZ, their petrological characteristics, and proximity to known skarn W-Mo-F mineralisation. The sub-types are summarized in Table 1 and a description of each is given in the following sections, with an emphasis on field petrology and textures.

Table 1. Classification used in this study for GP-suite granitoid rocks in western Bergslagen.

Name	Location, setting	Rock types[1]	Host rocks	Key field and petrological features	Example intrusions (this study)	Correlation with previously named massifs & plutons[2]
Southeast granitoids (SEG)	Southeast of the WBBZ,	1. Bt granite 2. Bt-ms granite 3. Granitic pegmatite	c. 1.91–1.88 Ga metagranodiorite, metagreywacke, metarhyolite, metadioritoid, metacarbonate rocks	Megacrystic; MME-bearing; massive Equigranular to megacrystic variants; massive; late aplitic-pegmatitic segregations, dykes	Fellingsbro	Fellingsbro-type Malingsbo-type Örebro-type
Skarn-distal granitoids (SGD)	Northwest of the WBBZ,	1. Bt granite 2. Granitic pegmatite	c. 1.90–1.88 Ga felsic metarhyolite, metagranodiorite	Equigranular to megacrytic variants; xenolith-bearing; MME-bearing; massive, but tectonic foliation locally occurs; late pegmatite, typically unzoned	Malingsbo Enkullen (Malingsbo north)	Malingsbo-type Enkullen-type
Skarn-proximal barren granitoids (SPB)	Northwest of the WBBZ	1. Bt granite 2. Granitic pegmatite	c. 1.90–1.88 Ga felsic metarhyolite, metagranodiorite, metacarbonate rocks	Equigranular to megacrystic variants; late aplitic-pegmatitic segregations, dykes, vein dykes (unzoned); massive	Hörken	Högberget-type Pingstaberg-type (barren facies) Stockholm-type
Skarn-proximal mineralised granitoids (SPM)	Northwest of the WBBZ	1. Bt granite 2. Bt microgranite 3. Aplite 4. Granitic pegmatite	c. 1.90–1.88 Ga felsic metarhyolite, metagranodiorite, metacarbonate rocks	Equigranular to aplitic-pegmatitic variants with systematic biotite-depletion; local IMT; disseminated fluorite, molybdenite, rare chalcopyrite; late aplitic-pegmatitic segregations, dykes, vein dykes (unzoned); massive	Pingstaberg (mineralised facies) Bispbergs klack	Pingstaberg-type (mineralised facies) Bispbergs klack-type Skålhöjden-type

Notes: [1]Listed in general decreasing abundance, [2]Based on names listed in Ahl et al. (2001) and earlier publications.
Abbreviations: Bt = biotite, ms = muscovite, IMT = interconnected miarolitic texture; MME = mafic microgranular enclave, WBBZ = western Bergslagen boundary zone

Type 1: Barren granites in the southeast sector

These granites occur southeast of the WBBZ and lack known mineralisation or an association with adjacent mineralised skarns. The largest intrusion in the southeast is the Fellingsbro granite (c. 350 km^2) which exhibits a partly rounded shape at the present erosional surface (Fig. 1). Other granites are irregularly shaped and oriented roughly east–west. North of Örebro, three irregular intrusions occur adjacent to several smaller granitic bodies and intrude older (c. 1.9 Ga) Svecofennian metavolcanic rocks.

In the Lindesberg area, greyish red, leucocratic and equigranular biotite ± muscovite granite belonging to the Fornaboda massif dominates (Fig. 3A). The rock is generally massive and only locally has an obvious tectonic lineation. A gradation from equigranular to megacrystic texture has also been noted (Lundström 1983). Dykes of aplite and muscovite pegmatite, and amphibolite xenoliths are also present. A similar grey granite occurs further south, in the Frövi–Hovsta area (Fig. 3B). Locally, this granite contains quartzofeldspathic gneiss and metagranitoid xenoliths (Fig. 3C), and biotite-rich schlieren, which marks a difference to the Lindesberg granite.

Coarse-grained granitic biotite ± muscovite pegmatite occurs in large areas west of Frövi. Xenoliths and schlieren are similar to those in the Lindesberg granite. Contacts between pegmatite and medium-grained equigranular granite are gradational or sharp, and they may be wavy (Fig. 3D) or straight. Contacts with quartzofeldspathic gneiss is also gradational or sharp (Fig. 3E). Swarms of pegmatite dykes that are discordant to gneissic foliation in the country rock are commonly observed (Fig. 3F). Pegmatite and granite grade into migmatite and gneiss with all intermediate variations. In metatexitic migmatite, aplitic to pegmatitic veins are concordant to discordant to a gneissic foliation. Early veins are isoclinally folded and may be strongly stretched and boudinaged, while later granitic veins tend to be planar and discordant (Fig. 3E & G).

A megacrystic granite in the southeast (Fellingsbro granite, Holmquist 1906) is a medium-grained biotite ± hornblende granite with c. 1–3 cm K-feldspar megacrysts and lacking muscovite. The megacrysts may be rectangular or rounded and are in places oriented to define a magmatic foliation. Gradation into equigranular types has not been encountered. Only mafic xenoliths have been observed. Common components are 5–10 cm large mafic magmatic enclaves (Fig. 3H), indicating the presence of coeval mafic and felsic magmas, and distinguishing the Fellingsbro granite from the other types described above.

► **Figure 3**. Examples of granitic rocks in the southeast sector. **A.** Biotite-muscovite granite, Fornaboda massif (dating sample locality STB191003). **B.** Biotite-muscovite granite (STB191045). **C.** Biotite leucogranite crosscutting foliated metagranodiorite (dating sample locality STB191023). Contact highlighted. **D.** Biotite pegmatite with wavy contact to medium-grained equigranular biotite granite. (STB191019). **E.** Pegmatite with diffuse contact to gneiss and a cross-cutting, straight vein (STB191017). **F.** Irregular network of pale grey, pegmatitic granite dykes crosscutting dark grey, intermediate metavolcanic rock (STB191029). **G.** Sawed sample of metatexite (U-Pb dating sample STB181050Aa and STB181050Ab). Pale red granitic leucosome occurs as stretched veins and boudins in banded grey gneiss. **H.** Biotite granite with outlined mafic enclave (dating sample locality STB191044).

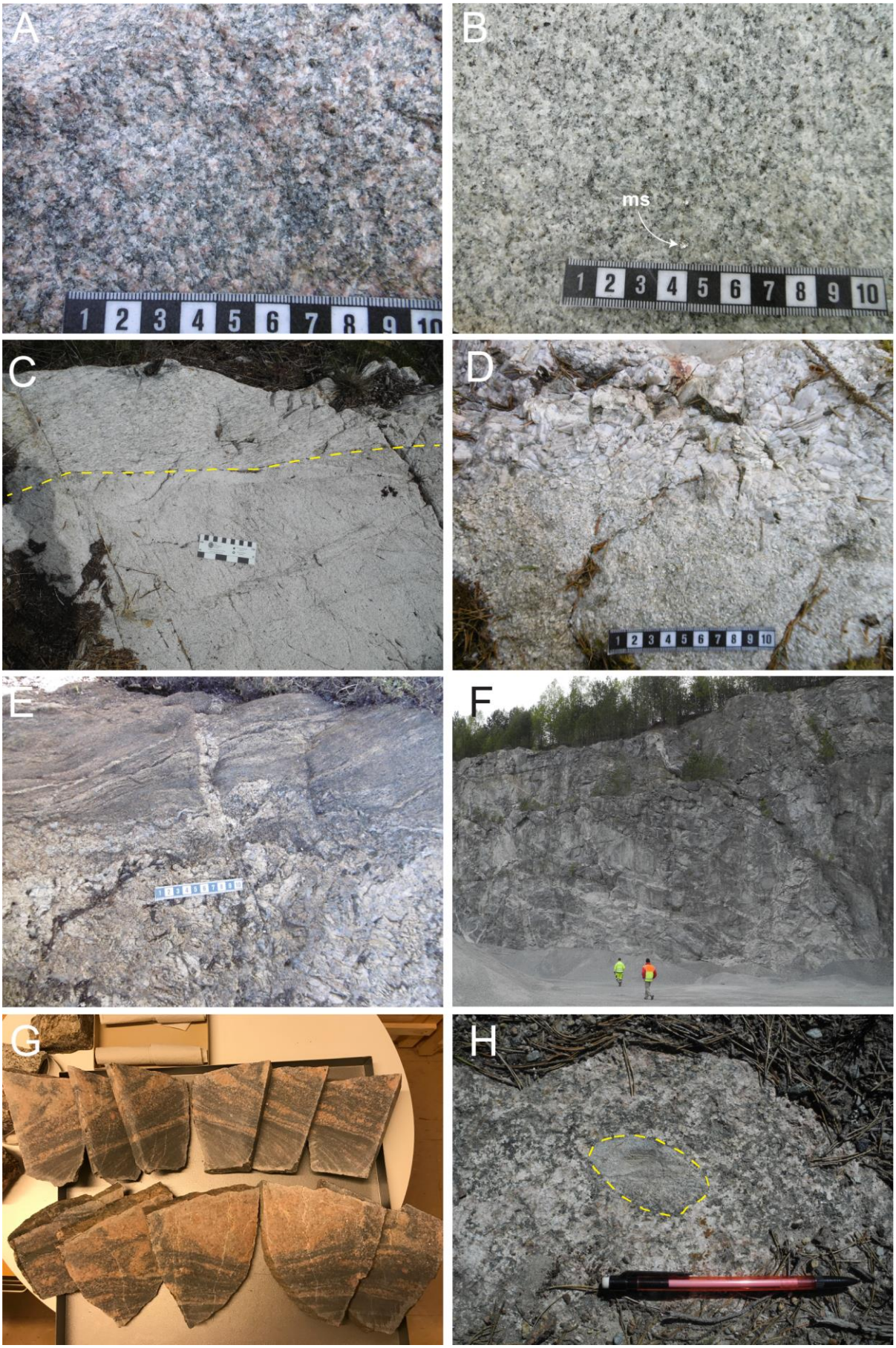
A
B
ms
C
D
E
F
G
H

Type 2: Barren, skarn-distal granites in the northwest sector

These granites occur northwest of the WBBZ, lack significant lithophile element mineralisation and are geographically distal (> 5 km) to the known skarn tungsten deposits and prospects to the west. The main example is the Malingsbo granite (Magnusson & Lundquist 1932), a relatively large granite batholith (c. 500 km^2) occurring southeast of Grängesberg and east of Kopparberg (Fig. 1). At the current erosion level, the Malingsbo granite has an irregular oblate shape and intrudes c. 1.89 Ga intermediate to felsic metavolcanic rocks in the north, south and west, and c. 1.89–1.88 Ga metagranitoids in the southeast and east. Along its margin in the NE and SW, the granite extends laterally and is discordant to ductile structures and lithological contacts in host rocks (Fig. 1). On the periphery of the intrusion, numerous smaller (c. 0.5–10 km^2), irregular to subrounded granite plutons and stocks also occur (Fig. 1).

The Malingsbo granite is a texturally composite batholith comprising grey to red, medium- to coarse-grained (c. 3–10 mm), equigranular to seriate biotite granite and subordinate K-feldspar megacrystic biotite granite. Contacts between these internal units are mainly gradational/transitional where encountered. At the type locality near Malingsbo village (Fig. 1), the main rock type is a pale- to reddish-pink, massive, medium- to coarse-grained (c. 1–7 mm) equigranular biotite granite (Fig. 4A–B). Here, the granite contains coarse (c. 5–15 mm) muscovite pegmatite occurring as irregular, cm- to m-sized segregations, zones, dykes, and veins (e.g., Fig. 4A). Granite-pegmatite contacts are narrow gradational or sharp/igneous (e.g., dykes and vein dykes), while the pegmatite is typically unzoned and internally massive.

Locally, the Malingsbo granite contains xenoliths comprising irregular to oblate, melanocratic to mesocratic, fine-grained (< 1 mm) biotite- or amphibole-rich rocks with internal tectonic foliations (Fig. 4C–D). Xenolith contacts are generally sharp to narrow diffuse, with the latter style suggesting a degree of resorption or assimilation (Fig. 4D). Overall, the xenolith petrology suggests they represent fragments of Svecofennian rocks assimilated during magma ascent and emplacement. On a larger scale, numerous country rock inlier domains or blocks of varying sizes are included by the Malingsbo granite, particularly in the east. Structurally, the Malingsbo granite is undeformed or may show a weakly developed alignment of biotite crystals that may represent a syn-emplacement fabric. Along its SE margin, however, it contains an augen fabric defined by preferentially aligned and partly lenticular feldspar phenocrysts, mantled by a fine-grained and foliated biotite-rich matrix (Fig. 4E). This structural characteristic suggests late ductile deformation affected the batholith locally.

▶ **Figure 4.** Examples of skarn-distal granitic rocks in the northwest sector. **A.** Equigranular biotite granite with pegmatitic parts (U-Pb dating sample locality ELH190002). **B.** Detail of equigranular biotite granite shown in A (ELH190002). **C.** Irregular xenolith (arrow) in biotite granite (ELH190001). **D.** Oblate xenolith (outlined) in biotite granite (ELH190016). **E.** Foliated biotite granite with augen texture (dating sample locality ELH190029). **F.** Biotite granite with feldspar megacrysts, Enkullen area (ELH190050). **G.** Mafic enclave in feldspar-phyric biotite granite, Enkullen area (ELH190050). **H.** Mafic enclave or xenolith with internal felsic banding in biotite granite, Enkullen area (ELH200004).

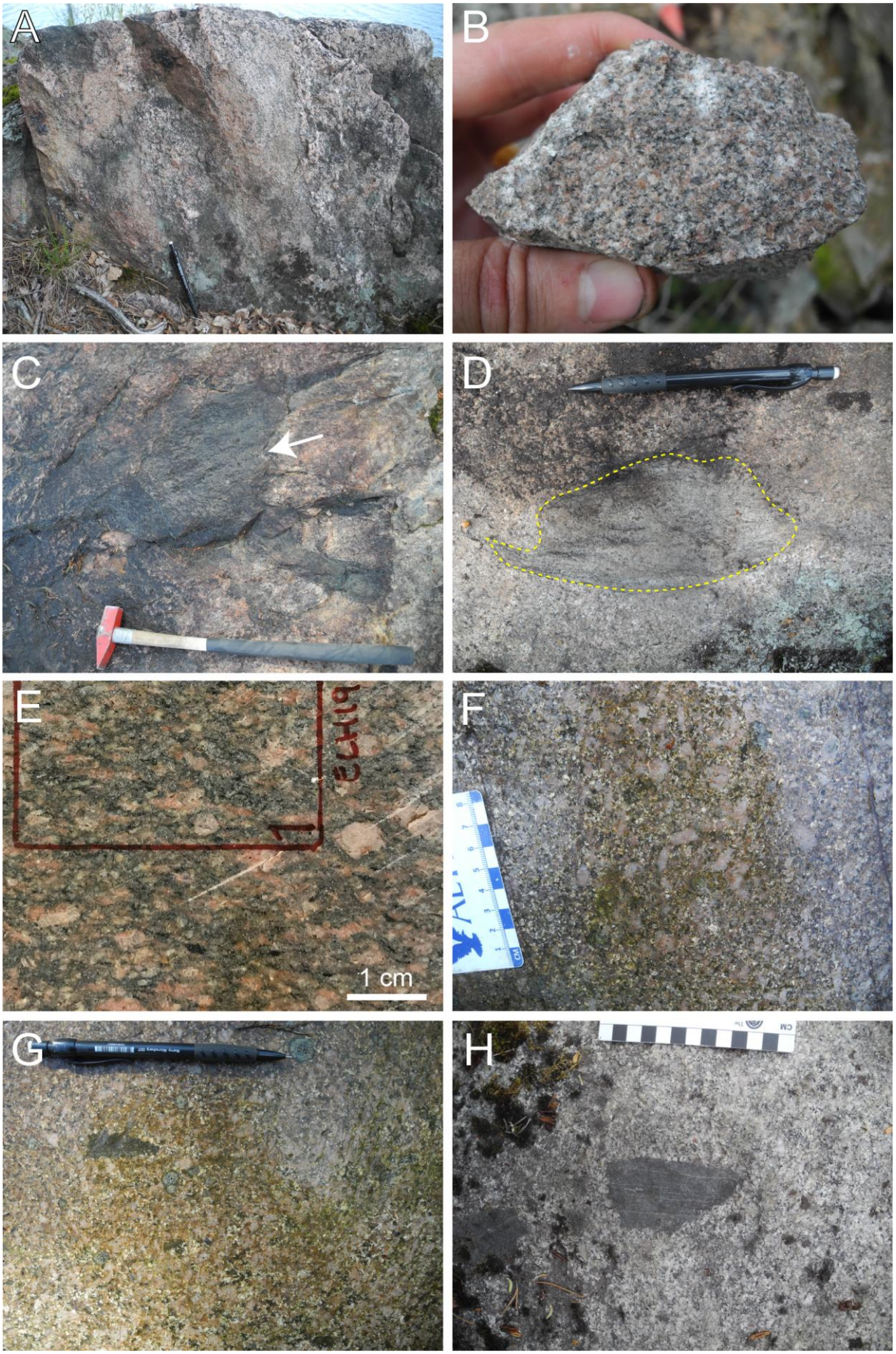
A
B
C
D
E
1 cm
F
G
H

In the northern part of the Malingsbo batholith (Enkullen, Fig. 1), a grey to pale pink, massive, medium- to coarse-grained (c. 3–15 mm) K-feldspar megacrystic biotite granite occurs (Fig. 4F), the Enkullen granite (Magnusson & Lundquist 1932). Feldspar phenocrysts tend to be randomly oriented and, locally, the rock is crosscut by narrow aplite-pegmatite vein dykes. Characteristically, the granite contains oblate to lenticular, biotite-rich mafic microgranular enclaves (MMEs) or clots ranging from c. 2–8 cm in length (Fig. 4G). Near Enkullberget, flattened enclaves have a preferred ENE–WSW alignment on horizontal outcrop surfaces which parallels the trend of the country rock contact to the north. Whether this structural relationship exists along other parts of the intrusion contact is not known, however. Less flattened, polygonal xenoliths also occur in the Enkullen granite and display an internal planar fabric (Fig. 4H). Overall, the petrology of the Enkullen granite is similar to the megacrystic parts of the Malingsbo granite occurring to the south and SE, although the latter granite type tends to lack MMEs.

Type 3: Skarn-proximal granites in the northwest sector

These granites occur northwest of the WBBZ and are closer (< 5 km) to known skarn tungsten and intragranitic Mo mineralisation (Fig. 1). For this sub-type, the studied granites are either non-mineralised individual intrusions (e.g., Hörken granite) or the barren parts of an intrusion that elsewhere contains localised lithophile element mineralisation and related hydrothermal alteration (e.g., eastern part of the Pingstaberg granite).

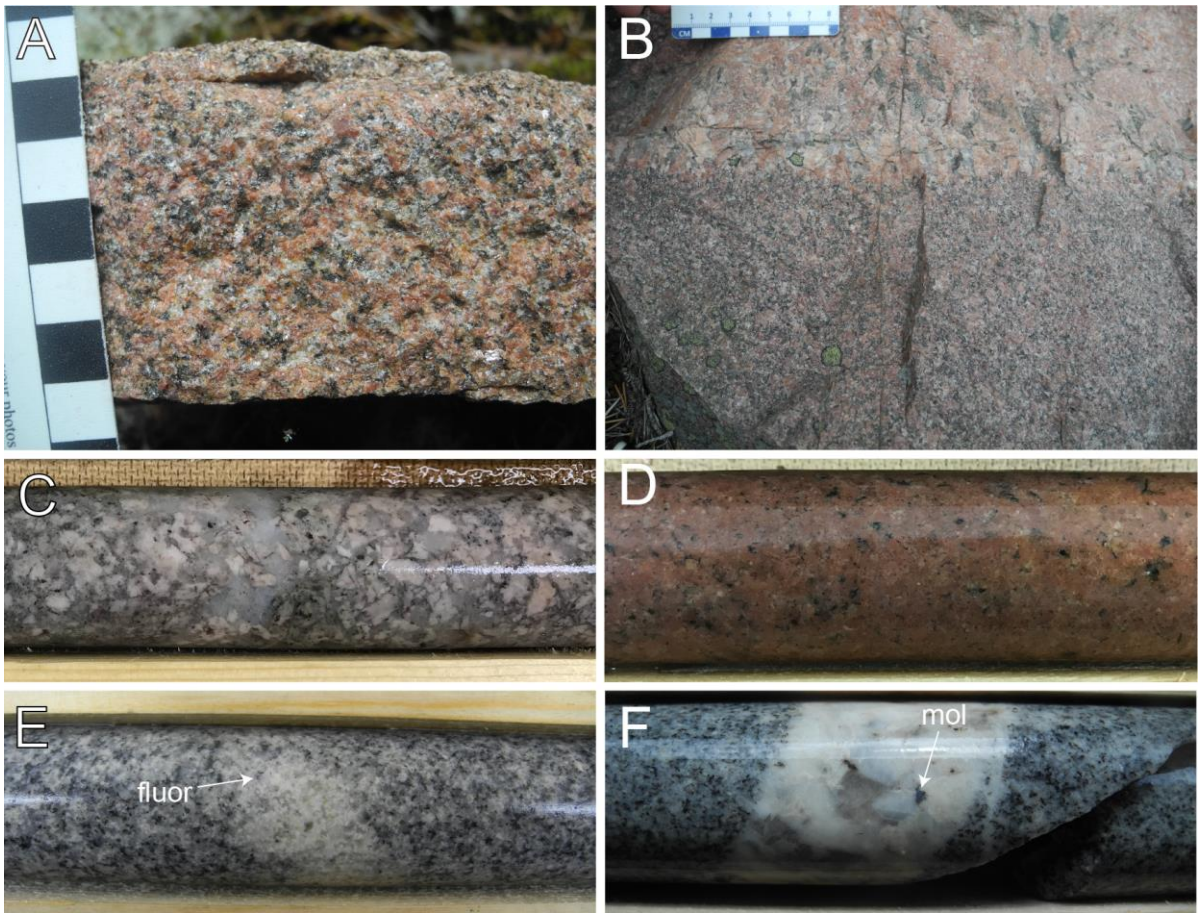

Figure 5. Examples of skarn-proximal granitic rocks in the northwest sector. **A.** Equigranular biotite granite (ELH200020). **B.** Narrow, gradational contact between biotite granite and pegmatite (ELH190039). **C.** Megacrystic biotite granite, Elgfall (ELH200108). Drill core is 4 cm in diameter. **D.** Biotite granite, Grantorpsgruvan (ELH200105). **E.** Equigranular biotite granite with pale biotite-depleted zone containing fluorite (fluor), Wigström–Högberget (ELH180050). **D.** Pegmatite dyke with molybdenite (mol) crosscutting equigranular biotite granite, Wigström–Högberget (ELH180051).

In general, the skarn-proximal intrusions comprise grey to red, medium- to coarse-grained (c. 1–10 mm), equigranular to megacrystic biotite granite (Fig. 5A–C). Examples include the Hörken granite adjacent to the several Mo ± W prospects, and the SW margin of the Malingsbo granite close to the Kolheden and Elgfall skarn W prospects (Fig. 1). Although the granites are undeformed/massive, several show a preferential alignment of biotite crystals that is typically steeply dipping (c. 80–90°) on vertical outcrop surfaces. Mineralogically, the granites are dominated by intergranular quartz and alkali feldspar (e.g., orthoclase), minor plagioclase feldspar, and biotite. Accessory zircon, magnetite and rare fluorite also occurs. Biotite modal abundances typically range from c. 5–15 vol. % (Fig. 5A–D). Late-stage pegmatite veins, dykes and leucocratic segregations with lesser biotite occur in the granites and show narrow gradational contacts (e.g., Fig. 5B & E). The pegmatites are internally homogenous, unzoned and massive, but may show a preferred crystal growth direction near their margins (Fig. 5B). Locally, these late-stage features may contain rare, disseminated fluorite and molybdenite (Fig. 5E–F).

Type 4: Mineralised and/or altered skarn-proximal granites in the northwest

These granites also occur northwest of the WBBZ and represent volumetrically minor intrusions or parts of intrusions associated with variable granite-hosted Mo and/or adjacent skarn-hosted W ± Mo ± F mineralisation and related hydrothermal alteration. Examples include the Bispbergs klack granite near Säter and minor granitic intrusions in the Wigström and Yxsjöby areas (Fig. 1). The latter example is located c. 1.5 km north of the Yxsjöberg W-Cu-F deposit and presently represents the closest known granite to the Yxsjöberg mineral system.

Overall, mineralised skarn-proximal granites comprise a range of texturally diverse granitic rocks that includes medium- to coarse-grained (c. 2–8 mm) equigranular biotite granite, coarser (> 10 mm) pegmatitic biotite granite, leucocratic 'saccharoidal' microgranite, and biotite-poor aplite and pegmatite (Fig. 6). At Bispbergs klack (Fig. 1), a c. 2 × 3 km, NE-aligned biotite granite intrudes c. 1.9 Ga meta-igneous rocks and locally contains intragranitic-style Mo ± F mineralisation. The area is historically significant, being the discovery location for tungsten (W) and molybdenum (Mo) and their respective ore minerals scheelite and molybdenite (e.g., Lassner & Schubert 2005). In the eastern part of the intrusion, medium-grained, feldspar-phyric biotite granite and coarser pegmatitic segregations contain disseminated, medium- to coarse-grained (c. 3–10 mm) molybdenite that is locally associated with chalcopyrite, pyrite and fluorite (Fig. 6A). Scheelite, bismuthinite, bornite and galena have also been reported from this area (Sundblad & Bergman 1997).

In the SW part of the Pingstaberg granite (Fig. 1), disseminated molybdenite and minor fluorite occur within a medium- to coarse-grained (c. 2–8 mm), grey to reddish pink, massive, equigranular biotite granite and in aplite-pegmatite (Fig. 6B; cf. Billström et al. 1988). Comparable biotite granite and microgranite with accessory molybdenite occur at Yxsjöbyn and at the Wigström tungsten deposit (Fig. 6C–D). Granitic dykes at Wigström are inferred to represent apophyses of the adjacent c. 1.79 Ga Högberget granite to the east (cf. Plan 2020). Additionally, at Wigström, an irregular greenish-grey, feldspar-rich rock containing disseminated molybdenite and lacking mafic minerals crosscuts hanging wall metavolcanic rocks close to the mineralised skarn zone (Fig. 6E). This rock is similar to pegmatitic vein dykes crosscutting pyroxene skarn at the Yxsjöberg deposit c. 12 km to the NW (Fig. 6F). The occurrence of disseminated scheelite in the Yxsjöberg vein dykes (Fig. 6F), molybdenite and fluorite in nearby comparable granitic rocks (e.g., Yxsjöbyn, Wigström), and scheelite, molybdenite and fluorite in calc-silicate skarn zones close to the granites provides evidence for a magmatic-hydrothermal origin for the skarn W-F-Mo systems.

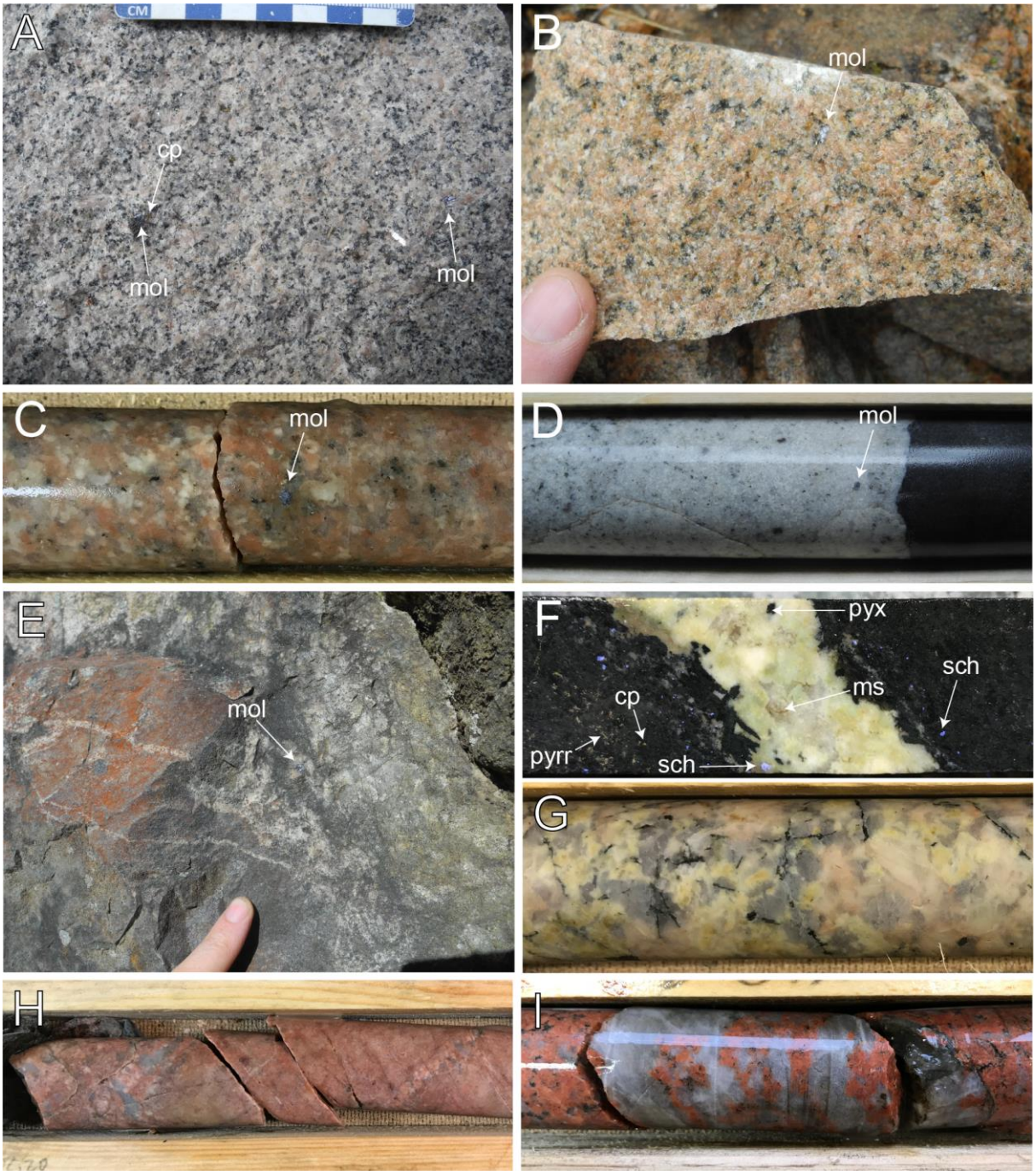

Figure 6. Examples of mineralised and altered skarn-proximal granitic rocks in the northwest sector. Where shown, drill core diameter is c. 4 cm. **A.** Biotite granite with disseminated molybdenite (mol) and chalcopyrite (cp), Bispbergs klack (ELH190052). **B.** Biotite granite with disseminated molybdenite (mol), SW Pingstaberg granite (ELH190073). **C.** Biotite granite with disseminated molybdenite (mol), Yxsjöby (dating sample locality ELH200106). **D.** Aplite dyke with molybdenite (mol) crosscutting intermediate metavolcanic rock, Wigström (ELH180054). **E.** Pale greenish-grey and irregular feldspar-quartz zone and veins with molybdenite cross-cutting medium grey metavolcanic rock, Wigström (ELH180015). **F.** Sericite-altered quartz-feldspar vein dyke crosscutting pyroxene-rich skarn rock associated with scheelite (sch), chalcopyrite (cp), muscovite (ms) and pyroxene (pyx), Yxsjöberg (ELH200097). Note scheelite crystal in the pegmatite vein dyke. The photo was taken under partial illumination with short-wavelength UV light. **G.** Coarse (pegmatitic) biotite granite showing moderate sericite alteration of feldspar, Sandudden (ELH200109). **H.** Biotite-depleted aplite dyke, Pingstaberg, with interconnected miarolitic texture and moderate potassic alteration (ELH200103). **I.** Quartz-rich pegmatitic segregation or vein in potassic-altered biotite granite, SW Pingstaberg granite (ELH200104).

Hydrothermal alteration associated with the skarn-proximal and mineralised granites in the NW mainly comprises moderate to intense sericite and K-feldspar ± hematite alteration overprinting feldspar, and chlorite replacing primary biotite (e.g., Fig. 6G–I). A relatively consistent depletion in biotite abundances when comparing granite with late-stage residual phases (aplite, pegmatite) affected by hydrothermal alteration is also evident.

Older (c. 1.9 Ga) Svecofennian rocks

Several Svecofennian (c. 1.9 Ga) country rock samples have been included in this study for the purpose of acquiring comparative geochemical, U-Pb dating and Sm-Nd isotopic results (see sections "Geochemical characteristics", "Zircon U-Pb Geochronology" and "Molybdenite Re-Os Geochronology", respectively). These include metagabbro, metavolcanic, migmatitic gneiss and metagranitoid samples from the SE sector, and samples of metavolcanic rock and amphibolite hosted by the Malingsbo granite in the NW sector (Appendix Table A1).

Geophysical results

Petrophysics

The petrophysical data used in this study, as presented below, are samples taken during this project combined with samples from earlier work (SGU petrophysical database). Figure 7 shows the distribution of density and magnetic susceptibility for various rock types from the mineralisation-proximal areas of Hörken, Pingstaberg and Wigström, as well as for the larger granite intrusive bodies Malingsbo, and in the Lindesberg–Frövi area.

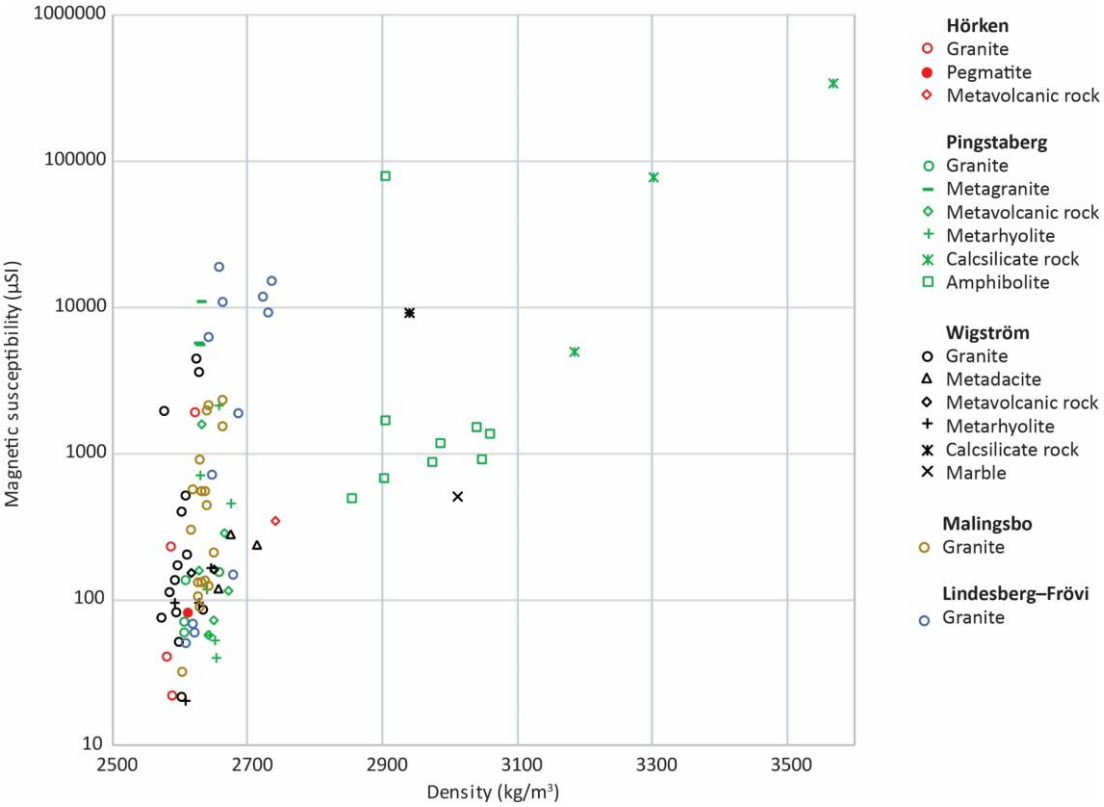

Figure 7. Distribution of density and magnetic susceptibility in various rock samples from the Hörken, Pingstaberg and Wigström areas located NW of the WBBZ. Five samples fall out of the range of visibility in this diagram because of having either density above 3600 kg/m³ or magnetic susceptibility above 1. Diagram ranges have been selected to prioritize visibility of the sample population. Data from the Malingsbo granite and for granitic intrusions in the Lindesberg–Frövi area to the south-east are also included.

The average petrophysical properties of granitic rock samples (Table 2) from the mineralisation proximal Hörken, Pingstaberg and Högberget granites and the larger Malingsbo granite intrusion can be seen in Table 2.

Figure 8 shows a plot of the density and magnetic susceptibility of individual granite samples.

The Högberget granite has slightly lower density (mean value 2601 kg/m^3) compared to the Malingsbo granite (mean value 2634 kg/m^3). A statistical comparison (T-test using 95% level of confidence) between the Högberget and Malingsbo granite also indicate that their average densities differ significantly. The Hörken and Pingstaberg granite also show low densities (mean value 2606 and 2619 kg/m^3, respectively) but the samples are too few to make any statistical analysis.

The magnetic susceptibility for all sampled granites is generally low but show large variations (Table 2, Figure 8). A comparison of the magnetic susceptibility of the Malingsbo granite to the three smaller, occurrence related, granites shows that the mean values of magnetic susceptibility does not differ significantly in the granites.

Natural Remanent Magnetisation (NRM) has been measured in the petrophysics laboratory for all the collected rock samples. The NRM has been used to compare the granites from the three mineralised areas, and the Malingsbo granite. Based on the NRM of samples of the three mineralisation-proximal granites they cannot be said to differ significantly from each other. However, the mean of NRM in samples collected from the Malingsbo granite differ at a 95 % confidence level from the NRM means of samples from the mineralisation-proximal granites. The statistical result for this significant difference is based on 51 measured samples (Table 3). As seen in Table 3, the sample variance of the three mineralisation-proximal granites differs, and the statistical calculation has been done assuming unequal variance. Regardless, the results show NRM to differ between the two groups of samples and the result likely reflects petrographic and compositional variations between the Malingsbo granite, and the three mineralisation-proximal granites.

Table 2. Statistical values for the Hörken, Pingstaberg and Högberget granites, and for comparison also from the Malingsbo intrusion. One of the 5 samples measured from Hörken has negative magnetic susceptibility and thus it cannot be plotted on the logarithmic scale of Figure 8.

Granite	Number of samples	Mean of magnetic susceptibility (SI)	Mean of density (kg/m3)	Mean of natural remanent magnetisation (mA/m)
Hörken	5	0.00014 ± 0.00073	2606 ± 29	16.03 ± 21.2
Pingstaberg	4	0.000098 ± 0.00004	2619 ± 22	9.76 ± 3.9
Högberget	15	0.00023 ± 0.00136	2601 ± 17	24.06 ± 53.4
Malingsbo	18	0.00035 ± 0.00076	2634 ± 14	5.22 ± 8.9

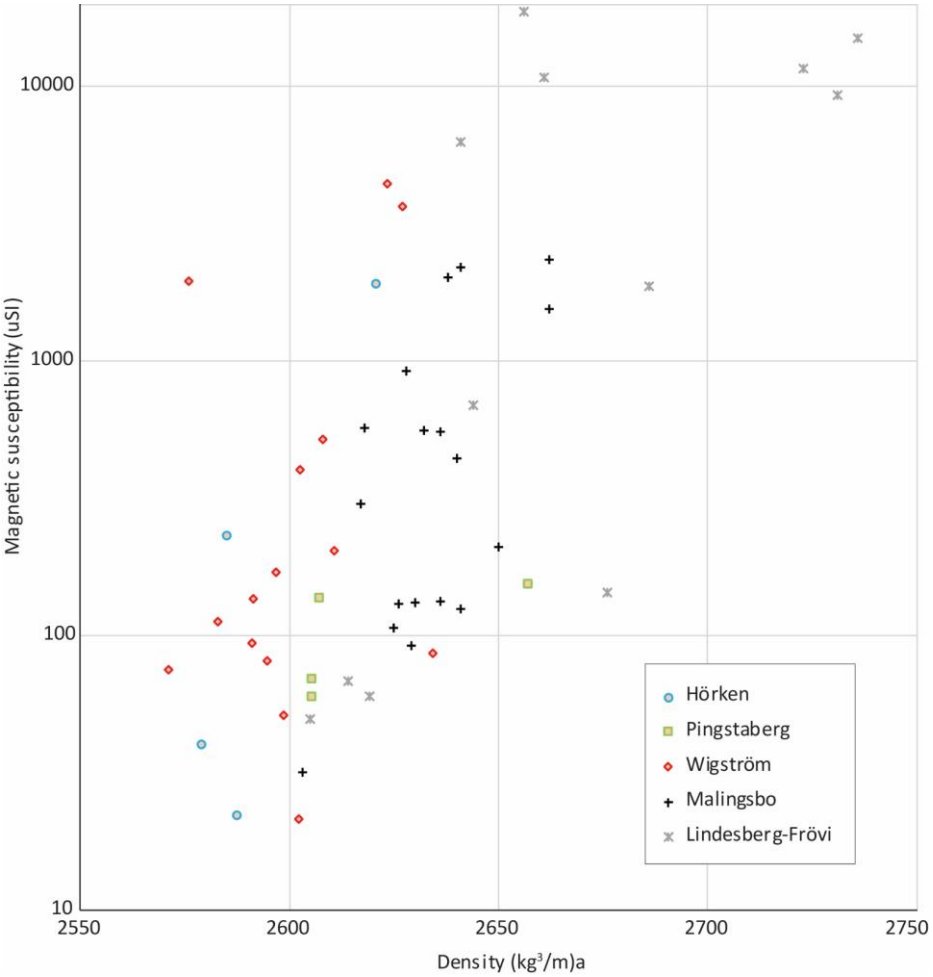

Figure 8. Magnetic susceptibility and density data for the skarn-proximal Hörken, Pingstaberg and Högberget granites, the skarn-distal and barren Malingsbo granite in the NW sector, and for barren granitic intrusions in the Lindesberg-Frövi area in the SE. One sample from the Hörken granite showed diamagnetic properties and negative magnetic susceptibility and could not be added due to the logarithmic scale.

Table 3. Statistical properties of the NRM (mA/m) measurements on samples collected from the Malingsbo, and the Hörken, Pingstaberg, and Högberget granites.

	Malingsbo granite	**Hörken, Pingstaberg, Högberget granites**
Mean (mA/m)	7.52	29.21
Standard Error (mA/m)	2.17	9.43
Median (mA/m)	4.53	17.37
Mode (mA/m)	#N/A	5.18
Standard Deviation (mA/m)	9.20	45.23
Sample Variance (mA/m)	84.70	2045.45
Kurtosis	9.83	18.09
Skewness	3.04	4.09
Range	38.37	221.49
Minimum (mA/m)	1.64	4.70
Maximum (mA/m)	40.01	226.19
Sum	135.38	671.93
Count	18	23
Confidence level (95%)	4.58	19.56

Overview inversion model

An overview model of magnetic susceptibility of an area including the Hörken, Pingstaberg and Högberget granites was determined using 3D inversion of airborne magnetic field data (Fig. 2B). The model (Fig. 9) shows a northeast to north-northeast trend for the rocks with higher magnetic susceptibility than 0.002 SI. The petrophysical overview (Fig. 7) shows that granite rock generally has lower magnetic susceptibility than that which means that the magnetic structural trend of Figure 9 can be expected to come from amphibolite and calcsilicate rocks. Granite situated close to the deposits Pingstaberg, and Wigström does not seem to be a part of the strongly magnetic trend, and instead occur related to low magnetic field strength.

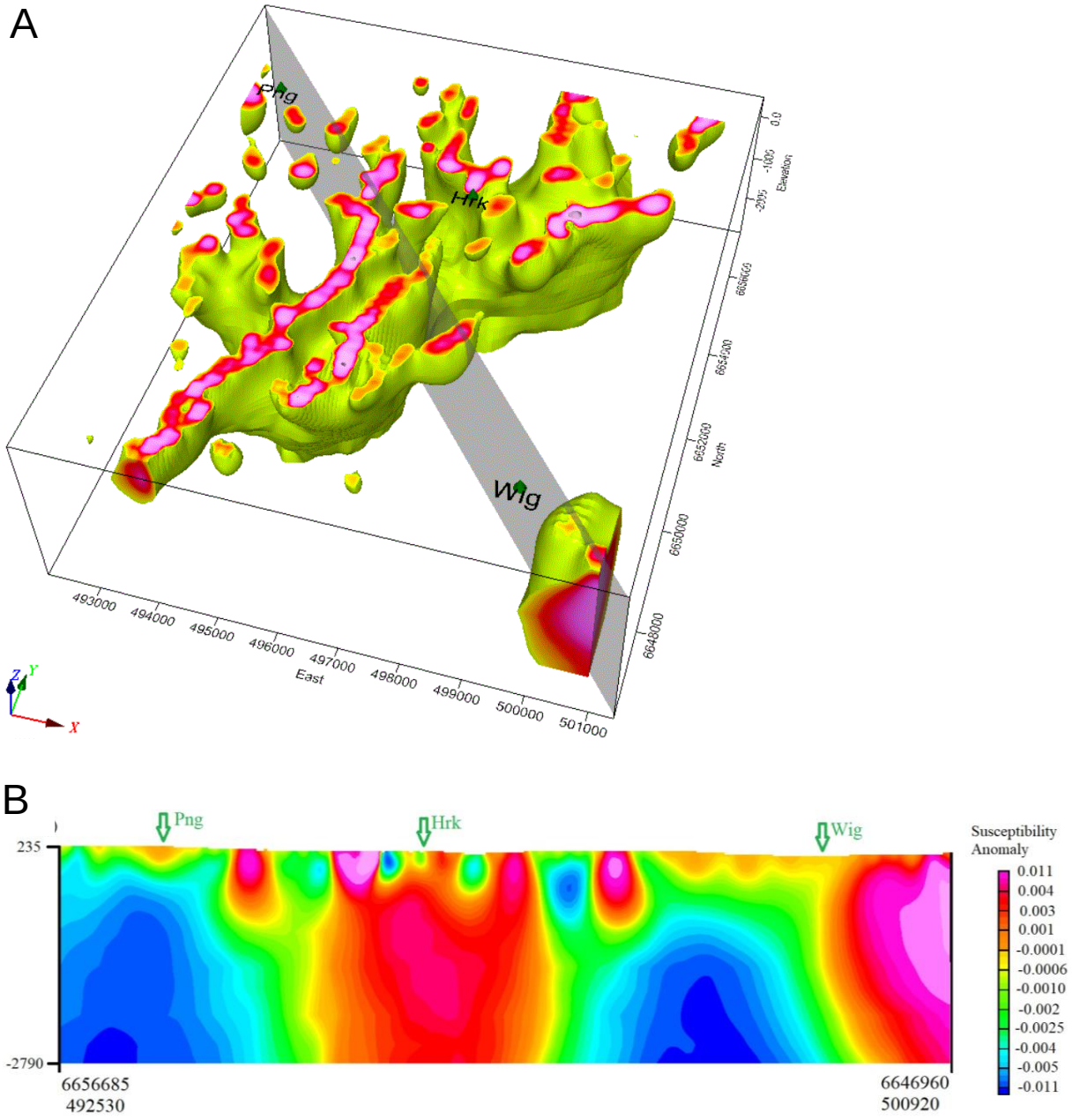

Figure 9. A. Inversion model (voxel size 10m) showing the highest magnetic susceptibilities of the surrounding area to the three mineralisation-proximal granites. The location of the mineral deposits Hörken (Hrk), Pingstaberg (Png), and Wigström (Wig), are displayed as green cones. The colour scale (yellow to pink) relates to magnetic susceptibilities from 2000 to 450000 (µSI). The grey envelope is the section of B. **B.** Apparent susceptibility section cut from the inversion model in A. The green arrows show the projection of each occurrence on this profile.

Geophysical modelling of the Hörken area

The area of the Hörken deposit (Fig. 10) has been investigated with geophysical survey of the magnetic field and gravity field. The bedrock map (from the SGU map database Bedrock 1:50 000–1:250 000) shows an elongate granite body with a north-northeast strike, and the Hörken deposit is situated at its western flank.

A magnetic susceptibility inversion model was calculated from airborne magnetic field data. However, the model does not provide any significant information and is not shown here. Likewise, the result of a Very low Frequency (VLF) electromagnetic survey is not shown since it does not seem to hold information helpful to decide the geometry of the granite body.

A forward model (Fig. 11) along the line shown in Figure 10 was made using magnetic and gravity data. The susceptibility means can clearly differ between the rock types, but large variance of magnetic susceptibility have been observed within each group. Hence, the gravity data was supporting the interpretation of rock type and geometry.

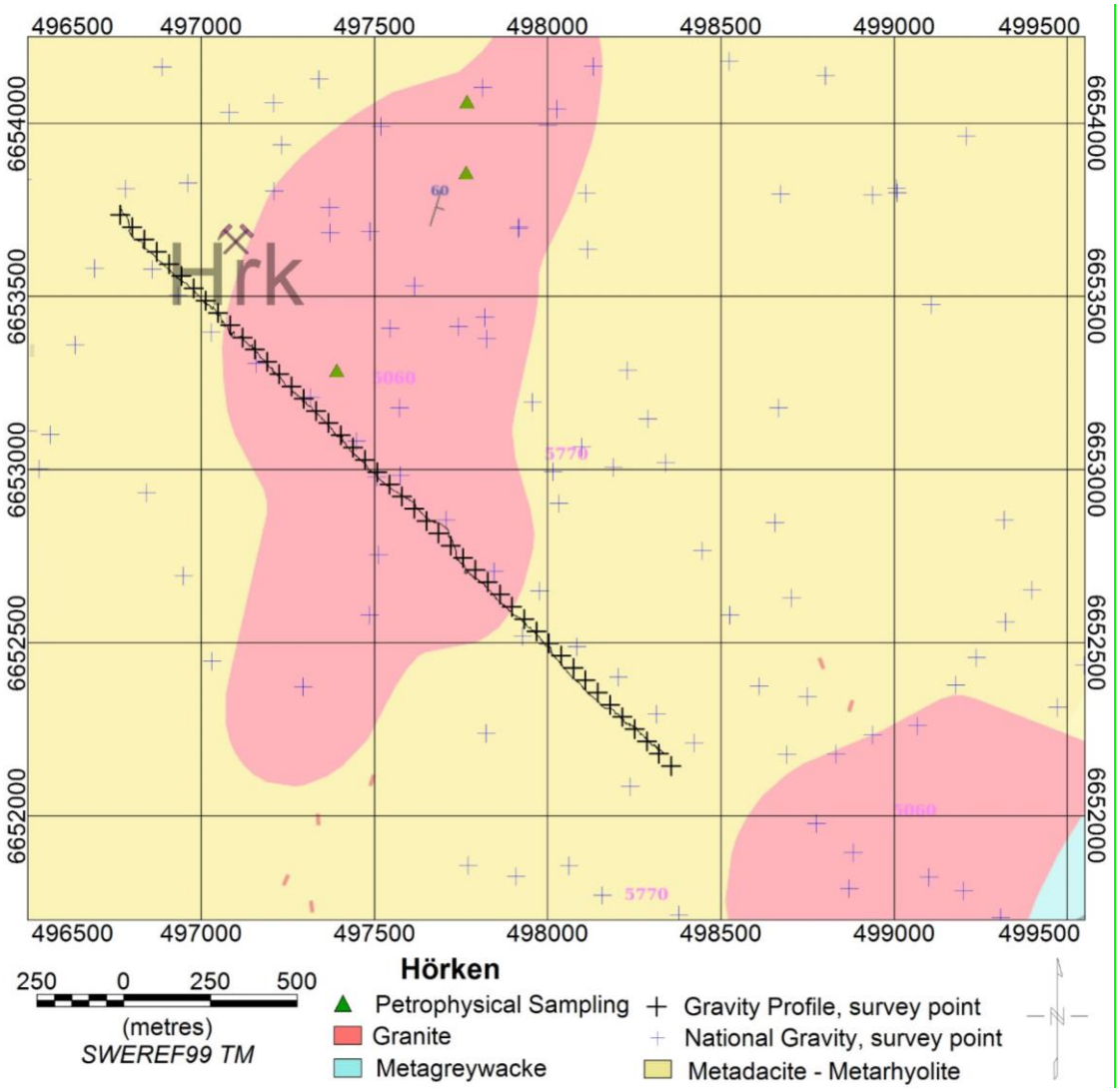

Figure 10. Bedrock map (from the SGU map database Bedrock 1:50 000–1:250 000) of the Hörken area. The black line shows the geophysical ground survey of the gravity-, and magnetic field as well as a survey of electromagnetic response, using VLF-sensor. Outcrop of the granite have been sampled and the results act as a base for the forward model (Fig. 11).

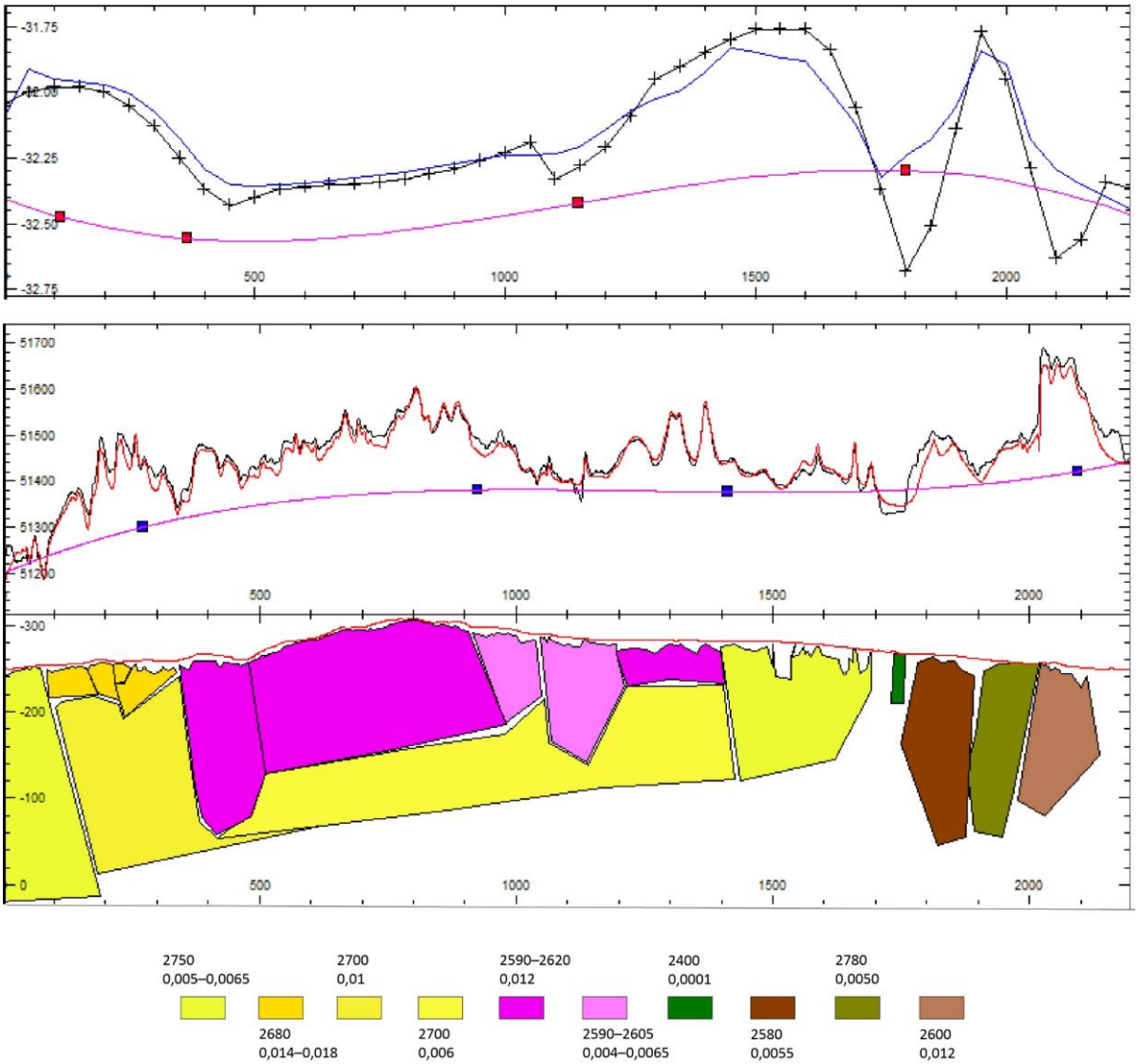

Figure 11. Forward model of the magnetic- and gravity profile of the Hörken deposit area. The modelling and interpretation of geologic bodies is based on gravity and magnetic data. The areas not coloured are represented by density 2600 kg/m^3 and magnetic susceptibility of 200 µSI.

The forward model (Fig. 11) suggests granite (pink) to be placed on top of a rock with higher density (yellow), c. 2700 kg/m^3, and a magnetic susceptibility of 6000 µSI inferred to be a volcanic rock, which complements some field observation. Furthermore, the gravity survey suggests greater masses to be present toward the west, which in the forward model has been satisfied by adding greater depth to the volcanic rock.

The northwestern contact of the granite is interpreted to have a steep, but southeastwardly dip (c. 80–85 degrees, which is an apparent dip considering the direction of the modelled profile). Such a dip has been concluded for the granite body's contacts with surrounding rocks, as well as for the internal changes that give contrast in density and magnetism.

The forward model suggests the granite to be about 1000 m wide along the section, having a depth of 250 m thinning towards the east, and having internal magnetic contrasts with steep dips towards east-southeast. The geophysical results do not suggest the granite to continue quite as far eastward as shown on the geological map (Strömberg 1983).

Geophysical modelling of the Pingstaberg area

The area chosen for examination during this investigation is located within the area from which geophysical results and models were presented by Ripa & Antal Lundin (2020). Figure 12 shows the surrounding area to the Pingstaberg deposit where the deposit is located on the western flank of an east-northeast elongated granite body.

A magnetic susceptibility inversion model was calculated from airborne magnetic field data. The inversion model was analysed by using iso-surfaces (Fig. 13) designed to match the magnetisation of sampled rock types. A north-northeast band of high magnetisation can be seen on the western side of a body of low magnetisation, corresponding to the Kalkåsen skarn iron body. The inversion model shows a body of low magnetisation and westerly dip that underlies what Figure 12 presents as a granite. Four samples of the granite show homogenous, low magnetic susceptibility.

The granite body is suggested to have an eastward dip of approximately 45 degrees. It seems present down to about 1000 m from the surface level. Likewise, the gravity data has been used to calculate a 3D inversion model (Fig. 14) and a prominent feature is a low-density volume in the center, which is interpreted to be a granite body. It has inward-dipping contacts and appears to have the shape of a bowl. The body is about 1000 m wide and seems present down to a depth of 800 m.

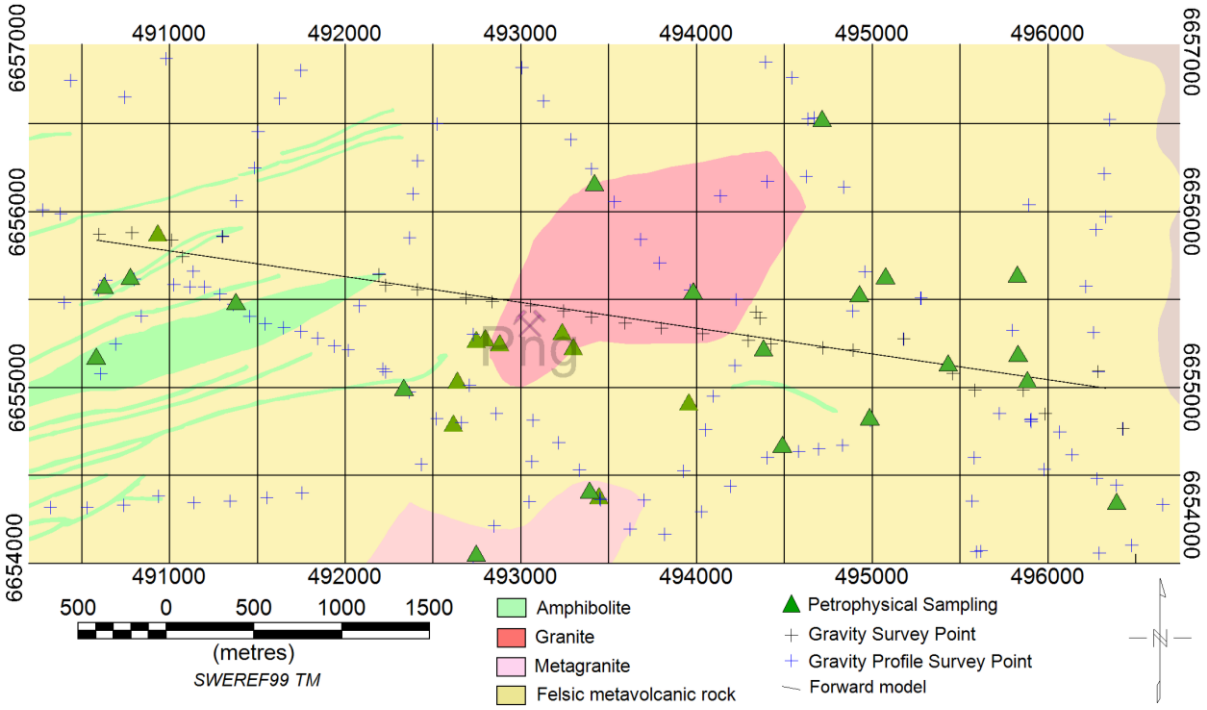

Figure 12. Bedrock map of the Pingstaberg area (from the SGU map database Bedrock 1:50 000–1:250 000). Symbols show petrophysical samples as well as gravity survey stations. The black line shows the WNW-ESE direction of the forward model (presented in Figure 15).

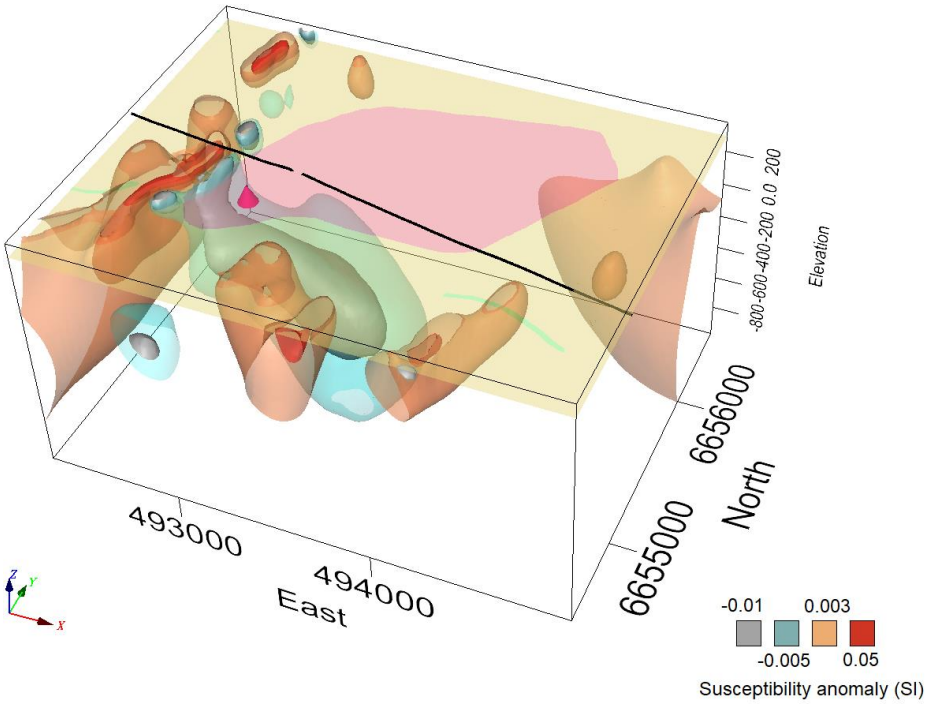

Figure 13. Iso-surfaces from inversion (voxel size 25 m) of magnetic susceptibility based on airborne magnetic field data from the surrounding area to the Pingstaberg deposit. The extent of the inversion can be seen in Figure 2B and the bedrock map from Figure 12 is shown as a semi-transparent surface at 290 m level. The models grey, and light blue surfaces represent the lowest-, and the low anomaly of magnetic susceptibilities, respectively, while the orange, and red surfaces represent the high and the highest anomaly of magnetic susceptibilities, respectively. The deposit is marked with a magenta cone and the black line shows a part of the path of the geophysical forward model (Fig. 15).

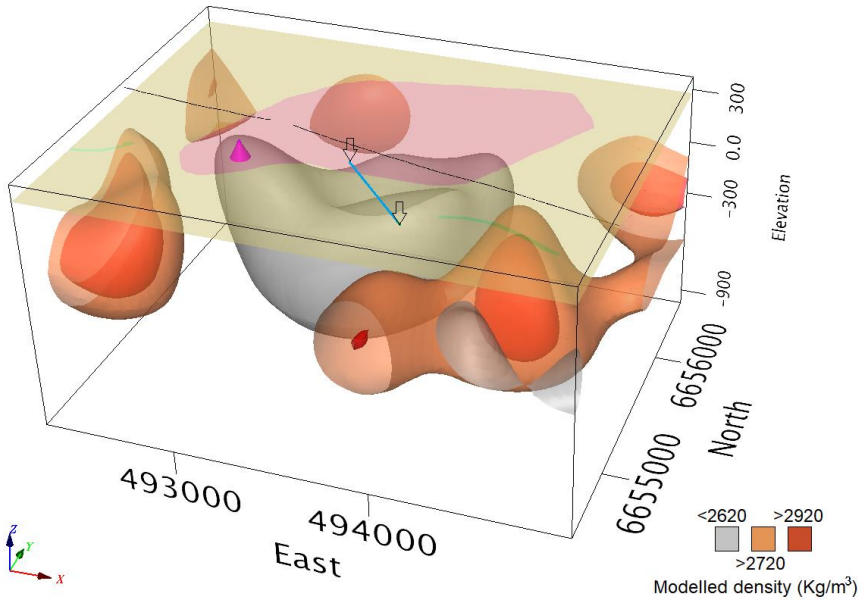

Figure 14. Iso-surfaces from inversion (voxel size 25 m) of bouguer anomaly based on the gravity field surveyed in the surroundings of the Pingstaberg deposit, see Figure 2. The inversion model shows a body of low mass (<2620 kg/m^3) in the central part. The orange surfaces are modelled as rock volume of densities of at least 2720 kg/m^3, and the red surface shows rock volumes of more than 2920 kg/m^3 which is commonly seen in amphibolite and skarn. The deposit is marked with a magenta cone and the black line shows the geophysical ground gravity survey. The arrows and the blue line show the interpretation of width of the body interpreted to be granite. The bedrock map from Figure 12 is shown as a semi-transparent surface at 280 m of elevation.

The gravity data from ground survey has been used, along with magnetic field data from the airborne survey, to create a forward model (Fig. 15). The ground gravity survey is presented as a black line in the inversion figures and in the overview (Fig. 12). The magnetic data was the year 2016 airborne survey with identification 'FECA' that used flight direction 130 degrees, elevation 60 m, and line separation 200 m.

In the eastern part (east dipping bodies) there is a unit with high density and high magnetic susceptibility that has been interpreted by Ripa & Antal Lundin (2020) as a metamorphosed mafic rock located at a shallow depth.

The forward model has not been completely perpendicular to the strike, hence naturally giving a longer measure for the granite width (1300 m). The model proposes the depth of the granite body to be more than 400 m, and with a westerly dip along the profile direction.

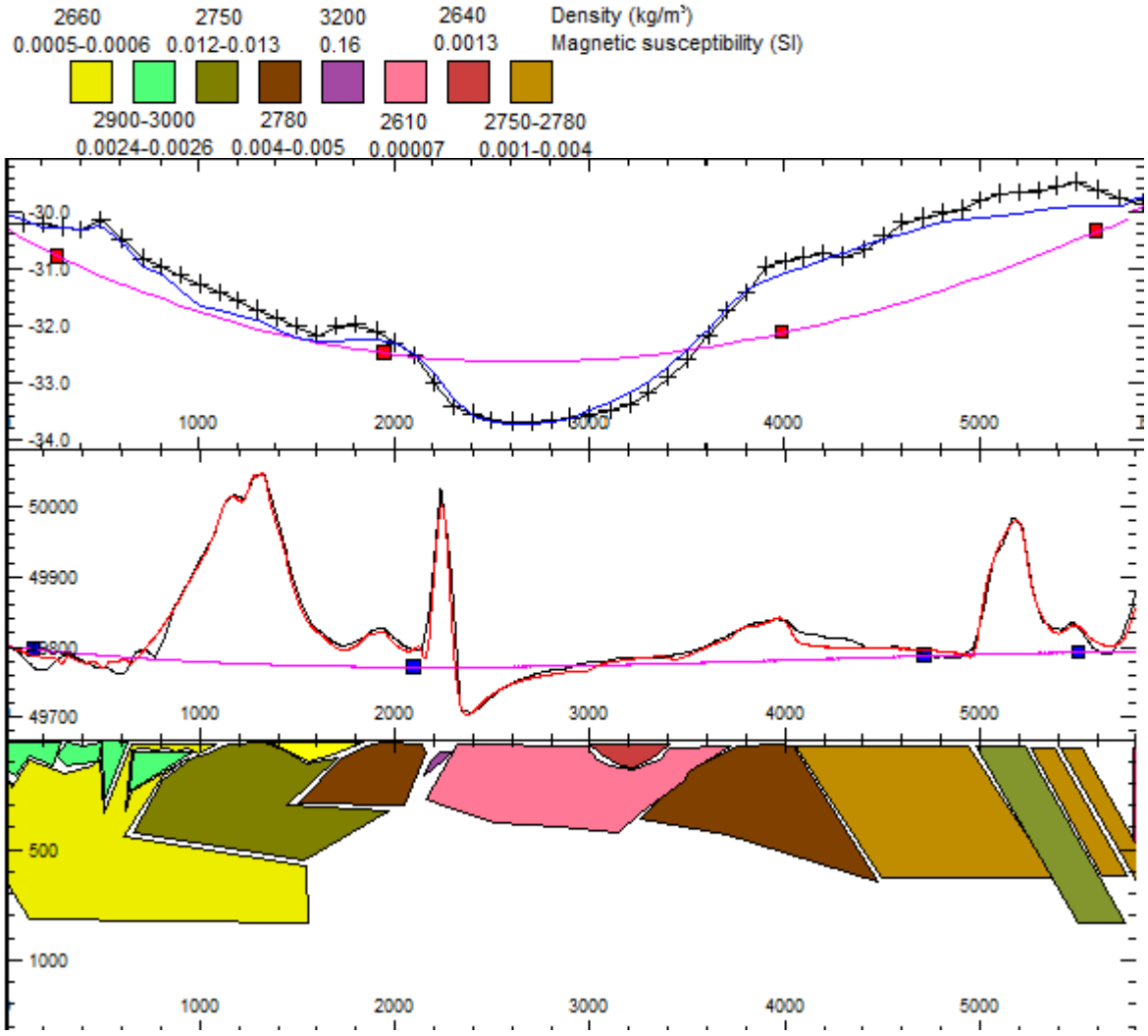

Figure 15. Forward model of geophysical data in the Pingstaberg deposit area. Focus of the profile was to investigate the mapped granite body which is represented as a pink body. The location of this section can be seen as a black line in the overview map (Fig. 12). The profile is also visible in the inversion figures (Fig. 13 & 14). The areas not coloured are of density 2600 kg/m^3 and magnetic susceptibility of 1000 µSI. The pink lines in the 'field strength' windows of the model act as subtracted reference fields, that is used to account for regional variation.

A summary of the analysis and modelling is that the Pingstaberg granite seem to be nearly 1000 m wide, and over 800 m deep. The dips of the granite contacts could not be established but in the forward model a westerly dip has been chosen since it matches the interpretation of the skarn iron body (at c. 2300 m), of great influence on the magnetic field.

Geophysical modelling of the Wigström-Högberget area

The geological map of the Wigström deposit area (Fig. 16) shows the position of the Wigström deposit, surrounded by volcanic rock, and with a granite rock on its eastern side. A geophysical survey was planned to cross the granite body, the mineralisation, and the volcanic rock, ending in the sedimentary rock. However, the wetland condition of the area restricted the survey in both the western and eastern parts. The results of the magnetic field ground survey showed contrasts in magnetisation of about 100 nT in the western part, while the magnetisation in the granite and metavolcanic rock in the east is less than 50 nT. The weak contrasts in magnetisation made modelling of the data insignificant.

The result of the electromagnetic Very Low Frequency (VLF) ground survey has been used to calculate an inversion model of resistivity (Fig. 17), which shows a resistivity contrast and a significant conductive zone around the Wigström deposit. The resistive body between 750 and 1100 m represents the Högberget granite. The rock type in the eastern part of the model (1100–1500 m) is interpreted to be a volcanic rock, which is principally in accord with the geological map (Fig. 16) even though the position of the contact differs somewhat. A significantly more conductive unit is found between 0 and about 300 m in Figure 17. It is interpreted to represent a lithological change within the metavolcanic unit. Steep linear features of increased resistivity at c. 900 and 1200 m may be due to thinner intrusive bodies.

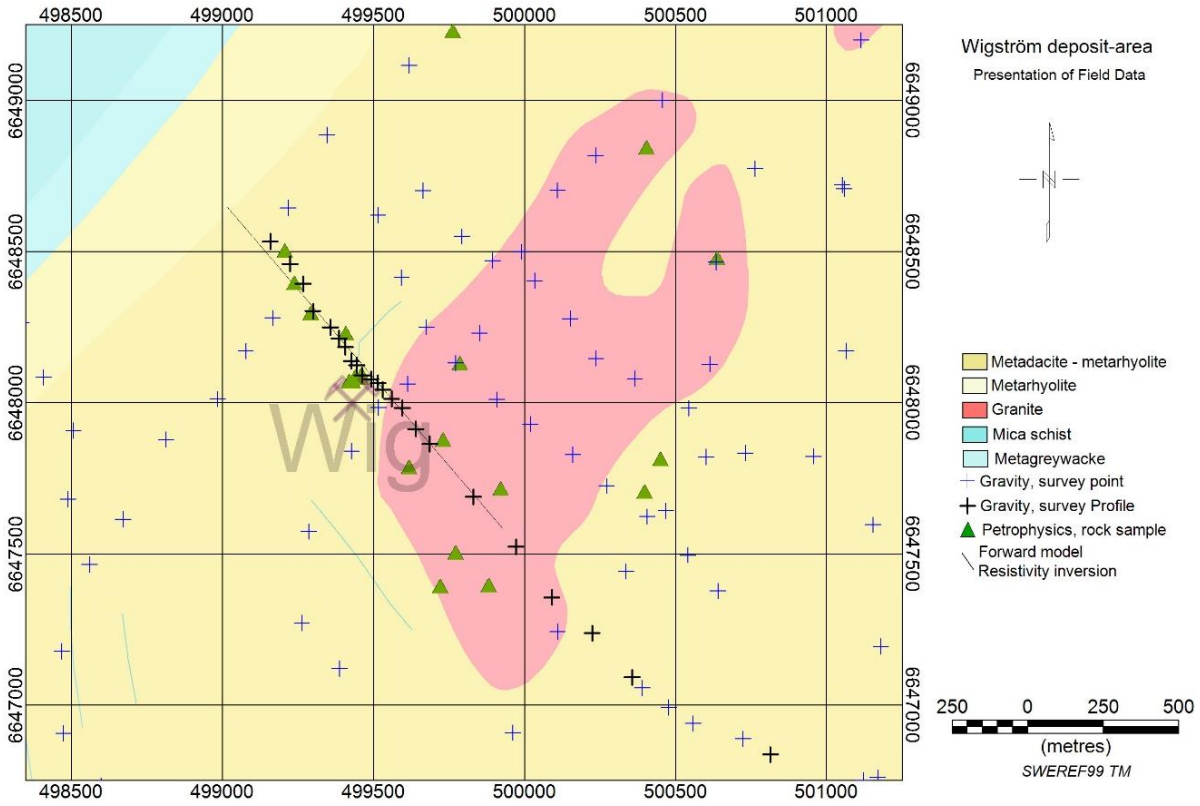

Figure 16. Bedrock map (from the SGU map database Bedrock 1:50 000–1:250 000) of the Wigström–Högberget area. The gravity measurements, the petrophysical samples, as well as the location of the resistivity inversion (Fig.17) is shown in the map.

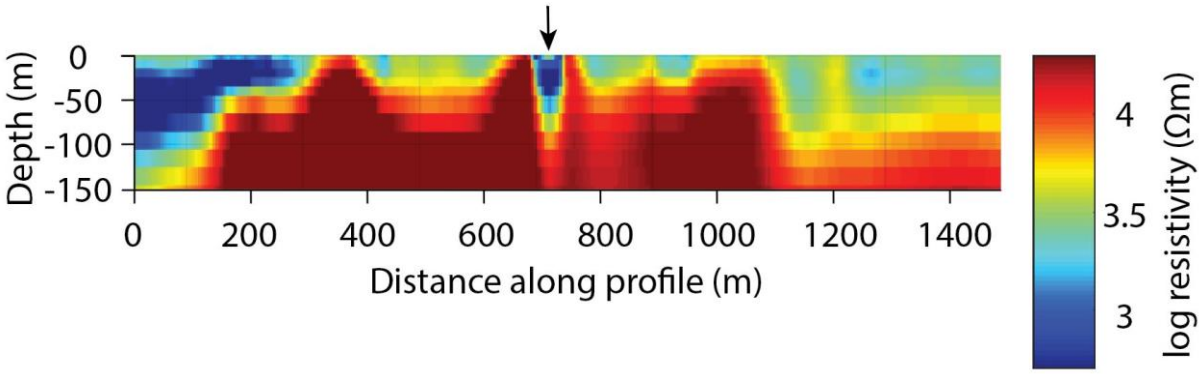

Figure 17. 2D inversion model of the apparent resistivity along a section across the Wigström deposit and its surroundings. The profile is displayed from northwest (0 m) toward southeast (1500 m). The Wigström deposit (arrow) is clearly marked as an anomaly of low resistivity.

Geochemical characteristics

Major and trace elements

The results of whole-rock geochemical analysis are summarized in Figures 18 to 22. In terms of major element oxides, the analysed samples have high silica (SiO_2 = 64.0–77.6 wt. %), high total alkali ($Na_2O + K_2O$ = 6.00–14.46 wt. %) and low CaO (0.29–4.44 wt.%), MgO (0.02–1.69 wt. %), Fe_2O_3T (0.34–7.16 wt. %) and TiO_2 (0.01–0.99 wt.%) contents. In general, GP suite granitic samples are more geochemically evolved compared to the older (c. 1.9 Ga) metagranitoid samples. Several skarn-proximal and mineralised aplite-microgranite samples of the former group, however, have relatively low SiO_2 (c. 65–68 wt. %) and elevated total alkali contents (c. 11.8–14.5 wt. %), reflecting lower modal abundances of quartz and higher alkali feldspar, respectively. In part, the petrological and geochemical character of some of these late-stage, alkali feldspar-rich bodies (e.g., SW Pingstaberg granite; Fig. 6H) are reminiscent of quartz-depleted episyenite (microclinite) rocks locally associated with late- to post-orogenic granitoids (e.g., Suikkanen & Rämö 2019).

On a total alkali-silica plot, the analysed samples mostly fall within the 'granite' field and have mainly subalkaline affinities (Fig. 18A). On a QAP plot, they classify as 'syenogranite' to 'alkali feldspar granite' *sensu stricto* based on calculated normative mineralogy values (Fig. 18B). The latter 'alkali feldspar granite' classification is consistent with relatively high modal abundances of K-feldspar and albite (c. 45–70 vol. % combined), particularly for granitic rocks in the NW sector which generally contain low modal abundances of plagioclase (c. 1–5 vol. %). On a modified Shand plot (Fig. 18C; Frost et al. 2001), the granitoids are mainly peraluminous and show a diagonal compositional trend consistent with feldspar and/or mica fractionation (cf. Abdel-Rahman 2001), and fertile granites associated with LCT pegmatites (cf. Černý 1991). On the ferroan-magnesian classification plot of Frost et al. (2001), the granitoids have mainly ferroan compositions indicative of granitoids formed in anorogenic, infracrustal settings (Fig. 18D), and have mainly calc-alkalic to alkali-calcic series affinities.

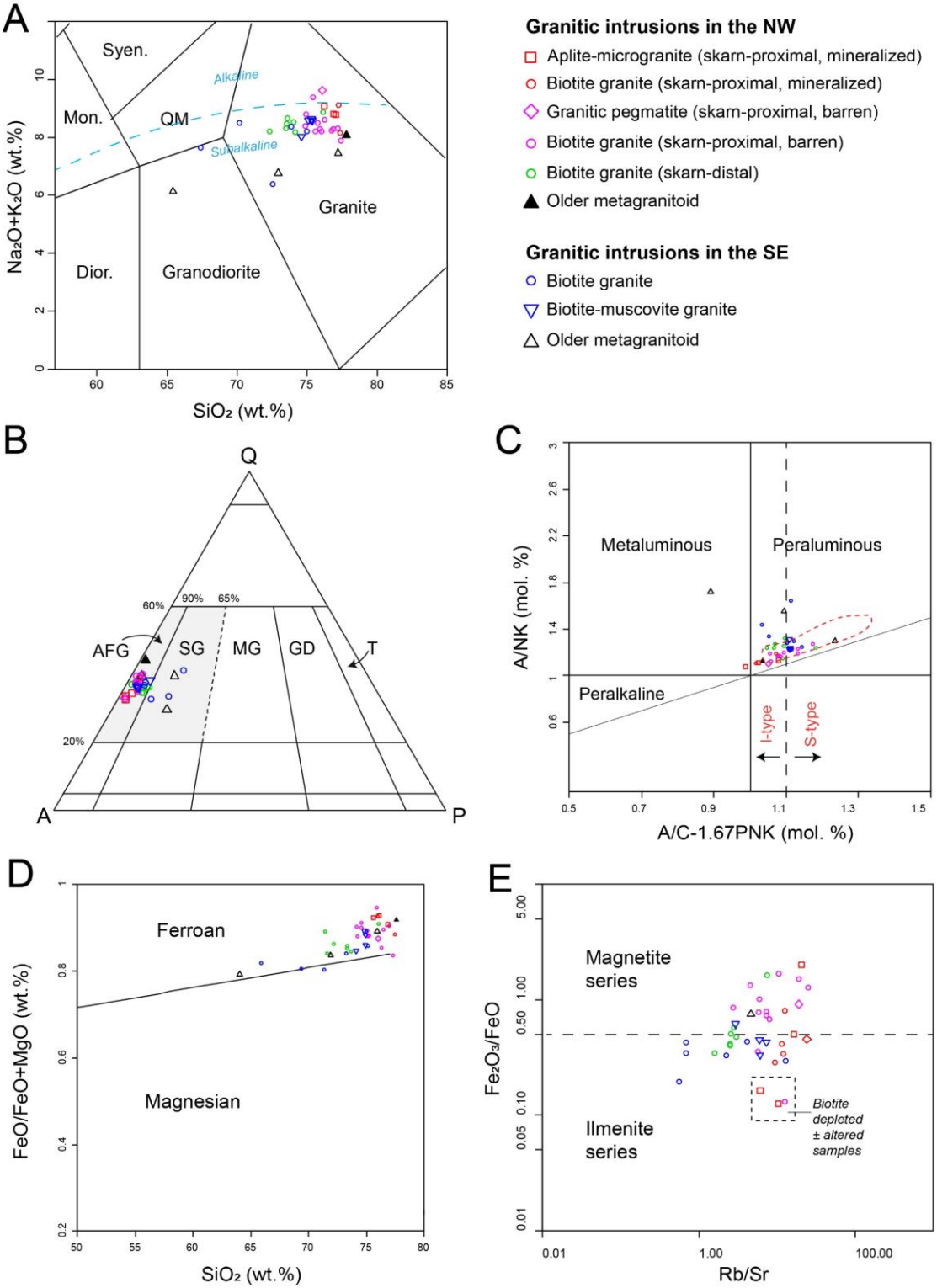

Figure 18. Classification of GP suite and older granitic intrusions. **A.** Total alkali vs silica plot of Middlemost (1994). Dashed line denoting alkaline/subalkaline series is from Wilson (1989). QM = quartz monzonite. **B.** QAP (quartz-alkali feldspar-plagioclase) ternary plot for granitoid classification (after Le Bas & Streckeisen 1991). Data points based on calculated granite mesonorm values (Mielke & Winkler 1979). Abbreviations: AFG = Alkali feldspar granite, SG = syenogranite, MG = monzogranite, GD = granodiorite, T = tonalite. **C.** Modified Shand plot for relative aluminium saturation (Frost et al. 2001). The vertical dashed line at ASI = 1.1 and dividing I-type and S-type granites is from Chappell & White (2001). Dashed red line corresponds to fertile granite/LCT pegmatite field from Černý (1991). **D.** Ferroan-magnesian classification plot of Frost et al. (2001). **E.** Relative oxidation (Fe_2O_3/FeO) versus fractionation (Rb/Sr) plot of Blevin and Chappell (1995). Horizontal dashed line dividing magnetite-ilmenite series granitoids is from Baker et al. (2005). Skarn-proximal granitic samples depleted in biotite and other mafic minerals are highlighted.

On a relative oxidation versus fractionation plot (Fig. 18E), the analysed samples straddle the ilmenite-magnetite series boundary ($Fe_2O_3/FeO \approx 0.5$; cf. Baker et al. 2005) and show a weak covariation trend controlled by relative fractionation, with the more evolved skarn-proximal intrusions in the NW (Rb/Sr ≈ 5–24) mainly falling in the magnetite series field. A wide scatter of Fe_2O_3/FeO values for the skarn-proximal and mineralised rocks likely reflects variable biotite and/or sericite abundances, and the effects of 'red rock'-style hematite exsolution/oxidation associated with K-feldspar metasomatism (e.g., Pirajno 2013, p. 211). For the GP-related samples in general, the redox signatures reflect the predominance of magnetite as the main accessory Fe-Ti oxide mineral and are consistent with parental magmas derived from mixed igneous and sedimentary source rocks (cf. Sato 2012; see Discussion). Their main compositional traits are also consistent with their main petrological characteristics and the evolved and generally restricted geochemistry of other GP-suite granitic intrusions in Bergslagen (e.g., Stephens et al. 2009).

Bivariate plots for several element pairs further highlight comparative compositional variations and trends for the different granites (Fig. 19). For example, decreasing TiO_2 values are linearly correlative with decreasing FeOt and MgO concentrations ($R^2 = 0.90$ and 0.92, respectively), and highlight decreasing compositional trends from barren skarn-distal granites in the SE and NW to skarn-proximal barren and mineralised granitic rocks in the NW (Fig. 19A–B). These trends generally reflect variations in mafic minerals abundances (e.g., biotite) for the different granite subgroups, with skarn-proximal mineralised granitic rocks in the NW (e.g., leucocratic aplite, pegmatite variants) generally having lower amounts of mafic minerals. This compositional variation is also evident on a Ta/Nb vs Ti plot which shows increasing Ta/Nb ratios relative to decreasing Ti contents (Fig. 19C) — a trend consistent with biotite fractionation (e.g., Halley 2020).

Compositional variations partly controlled by mafic mineral fractionation is further illustrated on a V/Sc vs Sc plot, with the analysed samples clustering within a compositional range expected for low Fe-, V- and Sc-bearing rocks lacking normative amphibole, pyroxene and/or ilmenite and associated with magnetite fractionation (Fig. 19D). Although an overall positive linear correlation is evident on a Hf vs Zr plot (Fig. 19E), skarn-proximal granitic rocks in the NW delineate a steeper Hf/Zr trend compared to skarn-distal granites in the NW and SE, reflecting an increased degree of zircon fractionation (cf. Halley 2020). On a P_2O_5 vs Rb/Sr plot (Fig. 19F), skarn-proximal barren and mineralised granitic rocks in the NW mainly have lower P_2O_5 contents compared to less fractionated (Rb/Sr ≈ 0.5–7) skarn-distal granites in the SE and NW. These characteristics suggest compositional variations controlled by the fractionation of apatite and other P-bearing accessory minerals (e.g., xenotime). They also suggest a general petrogenetic affinity between the GP suite granitic intrusions and highly fractionated 'peraluminous low phosphorous granites' associated with Nb-Ta-Sn mineralisation (cf. Černý et al. 2005).

On a spider plot comprising lithophile and high field strength trace elements, normalized to an average upper continental crust (UCC) composition, the analysed samples show variable relative enrichment/depletion patterns that reflect varying degrees of fractionation and/or the effects of deuteric alteration (Fig. 20). Older metagranitoid samples from the NW and SE show relatively weak enrichments in U, La, Nd, Y, Tm and Yb, and weak to moderate depletions in Nb, Sr, P, Zr and Ti (Fig. 20A). GP-related biotite granites in the SE have similar patterns, while two-mica granites in the SE show more pronounced enrichments in Rb, Th and U, and larger depletions in most other elements compared to the SE biotite granites (Fig. 20B). Skarn-proximal barren and mineralised granitic rocks in the NW show the largest enrichments and depletions, with the latter intrusions having moderate to strong enrichments in Rb, Th, U, Y, Tm and Yb (median range of c. 2.5–7 > UCC = 1), and relatively large depletions in Ba, La, Ce, Sr, P and Ti (median range of c. 0.03–0.6 < UCC = 1; Fig. 20C). In general, skarn-distal barren granitic rocks in the NW (e.g., Malingsbo granite) have less pronounced element enrichments and depletions compared to those for the skarn-proximal barren and mineralised intrusions, and have broadly comparable patterns to the skarn-distal granites in the SE (Fig. 20B–C).

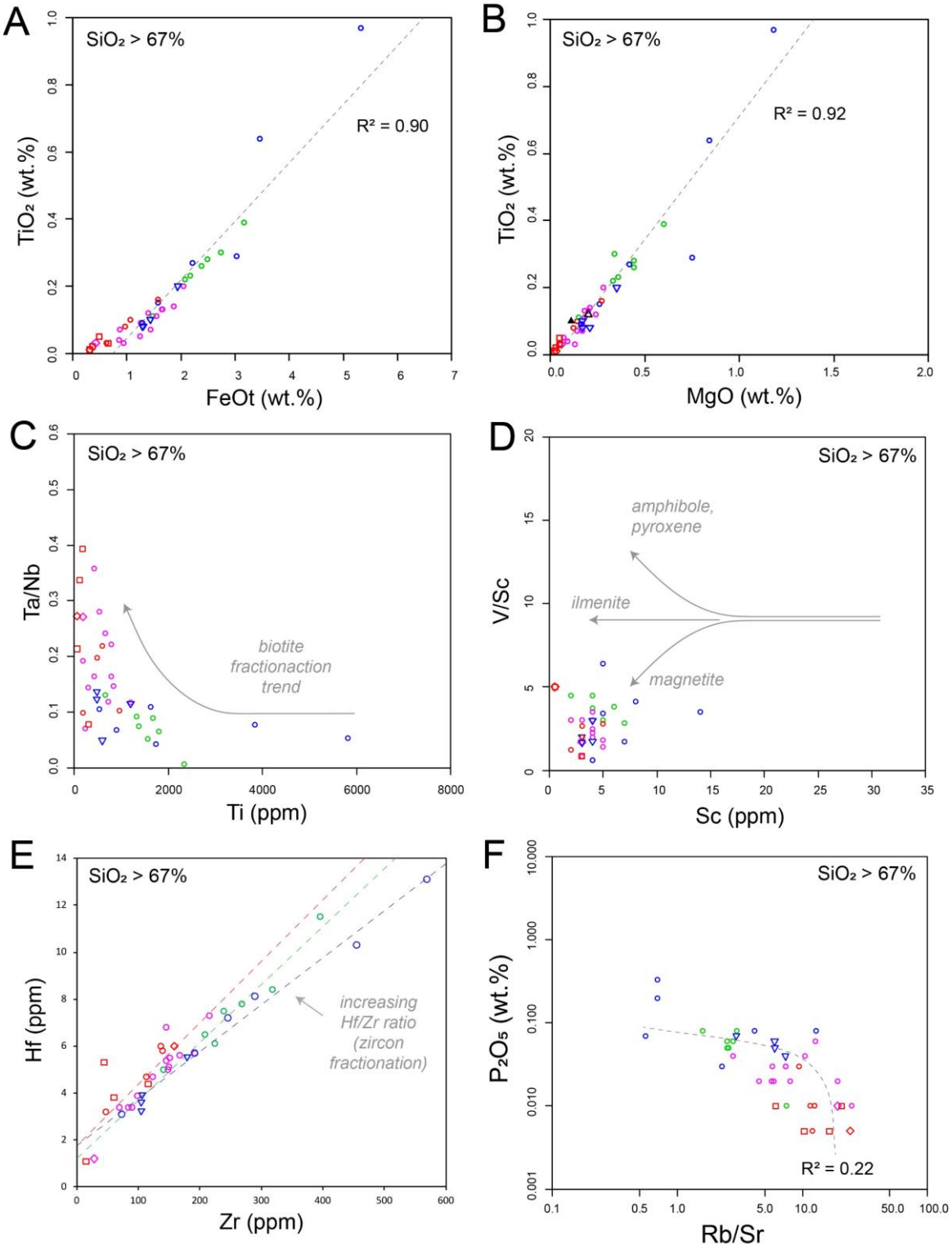

Figure 19. Geochemical compositional trends for the c. 1.81–1.78 Ga granitic intrusions (excludes older country rocks). Symbols are the same as those shown in Fig. 18. **A.** TiO_2 vs FeOt. **B.** TiO_2 vs MgO. **C.** Ta/Nb vs Ti. Arrow indicates biotite fractionation trend from an andesitic precursor magma (after Halley 2020). **D.** V/Sc vs Sc. Arrows indicate named mineral fraction trends from a basaltic-andesitic precursor magma (after Halley 2020). **E.** Hf vs Zr, with dashed ratio lines for granitic intrusions in the SE (blue), skarn-distal granitic intrusions in the NW (green), and skarn-proximal granitic intrusions in the NW (red). **F.** P_2O_5 vs Rb/Sr. Dashed line and R^2 value is derived from a linear regression.

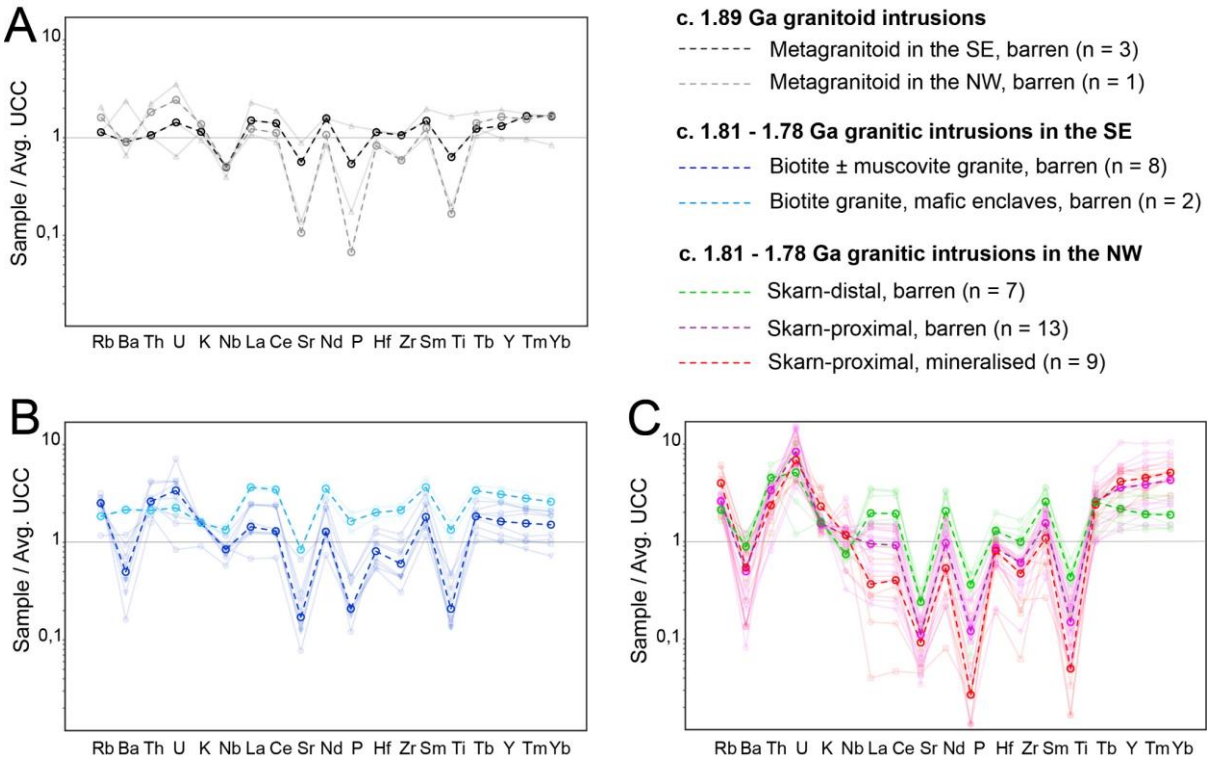

Figure 20. Spidergrams showing granitoid lithophile element compositional patterns normalized to an average upper continental crust (UCC) reference composition from Taylor & McLennan (1981). Dashed lines show median values for granitoid samples broadly classified by geographical location, proximity to skarn mineralisation and age (see Table 1). Background symbols for rock types (faded) are the same as those shown in Fig. 18. **A.** Older (c. 1.89 Ga) metagranitoid intrusions in the NW and SE. **B.** Younger (c. 1.81–1.78 Ga) granitic intrusions in the SE. **C.** Younger (c. 1.81–1.78 Ga) granitic intrusions in the NW.

Rare earth elements

Figure 21 shows chondrite-normalized rare earth element (REE) plots for the grouped granitic rock, with dashed lines representing median patterns. Older (c. 1.89 Ga) metagranitoid rocks in the NW and SE sectors have similarly fractionated, light (L)REE-enriched, negatively sloping patterns ($(La/Yb)_N$ = 5.84–25.00) with variable weak to moderate negative Eu anomalies (Eu/Eu* = 0.24–0.68; Fig. 21A). Barren c. 1.80 Ga granites in the SE sector have fractionated, LREE-enriched, negatively sloping patterns ($(La/Yb)_N$ = 5.62–18.73) with weak to moderate negative Eu anomalies (Eu/Eu* = 0.16–0.55; Fig. 21B). Skarn-distal barren granites in the NW also have LREE-enriched patterns ($(La/Yb)_N$ = 5.91–18.01) with weak to moderate negative Eu anomalies (Eu/Eu* = 0.19–0.29; Fig. 21C). In contrast, skarn-proximal barren and mineralised granitic rocks in the NW have more horizontal (i.e., less fractionated) LREE-depleted patterns ($(La/Yb)_N$ = 0.08–4.50) and more pronounced negative Eu anomalies (Eu/Eu* = 0.04–0.56; Fig. 21C). A systematic steepening or enrichment of heavy (H)REEs (Gd–Lu) relative to LREEs (La–Sm) is also evident for the skarn-distal to -proximal barren and skarn-proximal mineralised granitic rocks in the NW sector (Fig. 21C). The latter group also shows a weakly developed REE 'tetrad effect', especially for the Gd–Ho (tetrad 3) and Er–Lu (tetrad 4) pattern segments (e.g., Irber 1999).

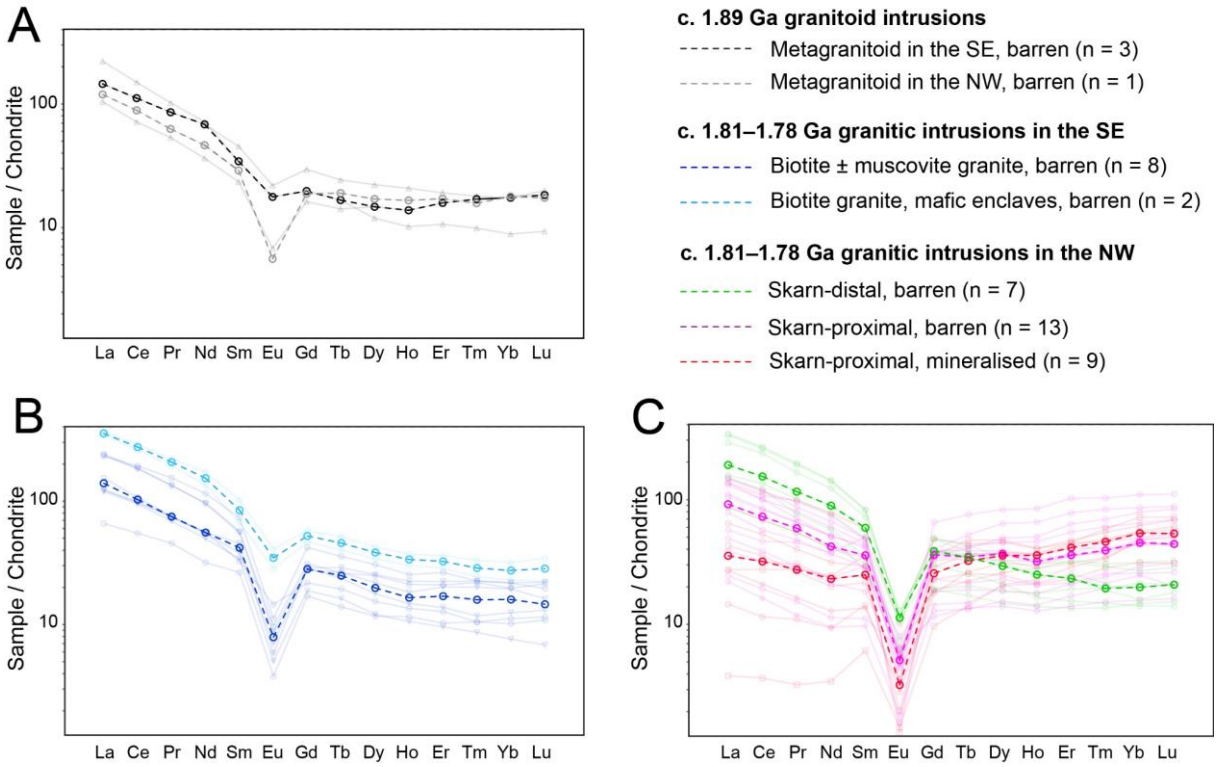

Figure 21. Spidergrams showing granitoid rare earth element (REE) compositional patterns normalized to the average chondrite composition of Boynton (1984). Dashed lines show median values for granitoid samples broadly classified by geographical location, proximity to skarn mineralisation, and age (see Table 1). Background symbols for rock types (faded colours and symbols) are same as those shown in Fig. 18. (A) Older (c. 1.89 Ga) metagranitoid intrusions in the NW and SE. (B) Younger (c. 1.81–1.78 Ga) granitic intrusions in the SE. (C) Younger (c. 1.81–1.78 Ga) granitic intrusions in the NW.

Bivariate plots for several REE parameters further highlight variations in the REE systematics of the c. 1.80 Ga granitic rocks (Fig. 22). Overall, total REE contents range from 38–550 ppm, with skarn-proximal barren and mineralised granites in the NW having lower total REE abundances compared to skarn-distal barren granites in both the NW and SE (combined means of 147 and 307 ppm, respectively; Fig. 22A–B). Total REE contents also show moderate, negative linear correlations with Zr/Hf and FeO (R^2 = 0.60 and 0.66, respectively), reflecting overall compositional variations controlled by increasing feldspar fractionation and decreasing mafic and accessory mineral abundances (e.g., biotite; Fig. 22A–B). Values for the La_N/Yb_N parameter that reflects light (L-) vs heavy (H)REE fractionation range from 0.08–18.7, with skarn-proximal barren and mineralised granitic rocks in the NW having lower values compared to the skarn-distal barren granites in both the NW and SE (combined mean La_N/Yb_N values of 1.63 and 11.36, respectively). La_N/Yb_N values also show a relatively strong, negative linear correlation with Gd_N/Yb_N ratios (HREE fractionation; R^2 = 0.93) reflecting an increase in HREE abundances relative to LREEs when going from the skarn-distal to skarn-proximal samples (Fig. 22C). Finally, all of the granitic rocks show moderate to strong negative Eu anomalies (Eu/Eu* = 0.04–0.68; cf. Fig. 21), with skarn-proximal granites in the NW having the most negative Eu/Eu* values reflecting an overall trend of increasing plagioclase fractionation (Fig. 22D).

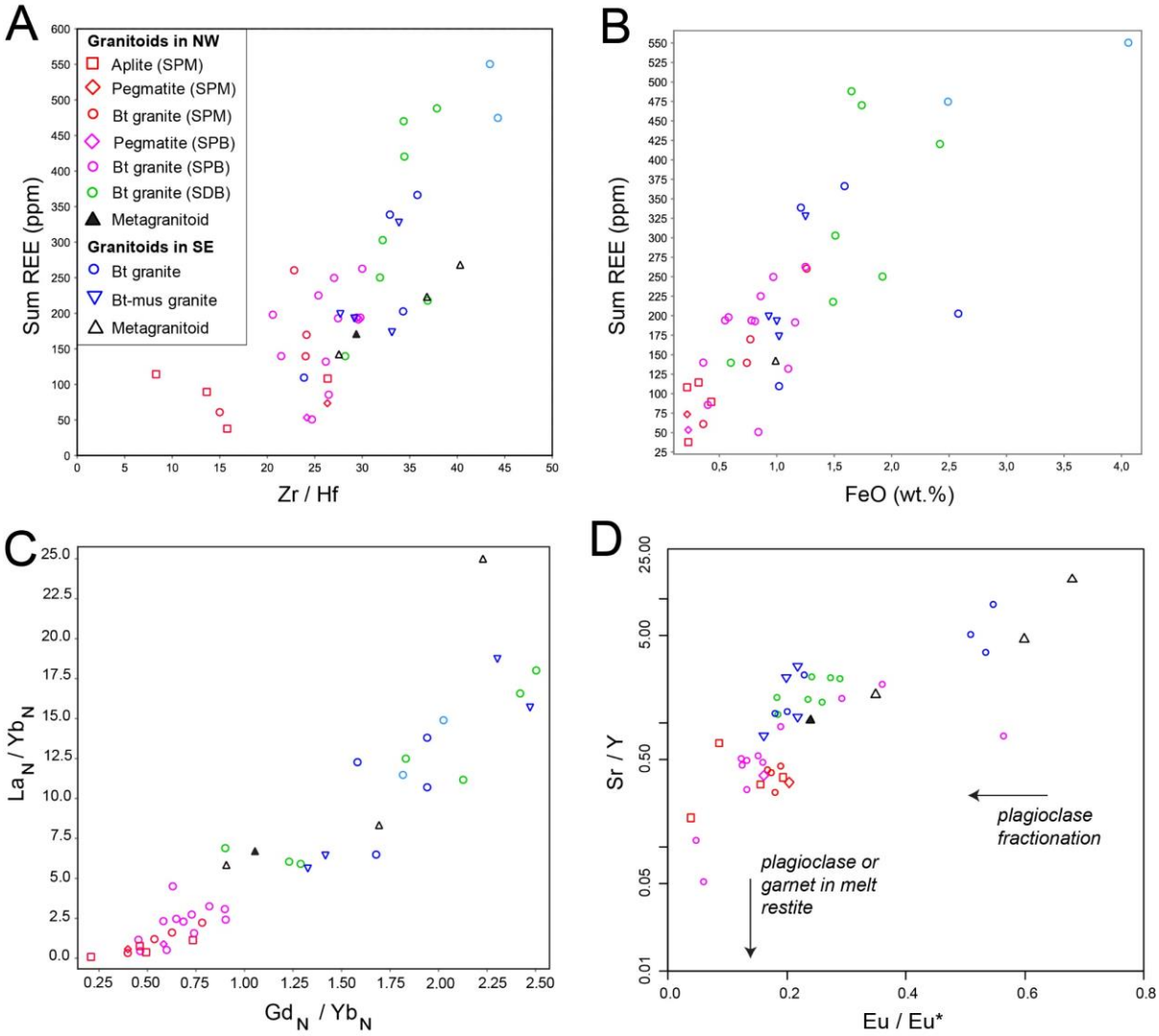

Figure 22. Rare earth and trace element bivariate plots for c. 1.9 Ga and 1.8 Ga granitic intrusion. Abbreviations shown in plot A legend: MG = microgranite, SPM = skarn-proximal mineralised, SPB = skarn-proximal barren, SDB = skarn-distal barren. Underscore 'N' denotes normalised value using the data from Boynton (1984). **A.** Sum of REEs vs Zr/Hf. **B.** Sum of REEs vs FeO. **C.** La_N/Yb_N vs Gd_N/Yb_N. **D.** Sr/Y vs Eu/Eu*.

Ore element associations and metallogeny

Geochemical compositional features that constrain magma redox state, degree of fractionation, and/or mineralisation-related element associations provide insights into the broader metallogenic potential of the analysed granitic rocks (Fig. 23). On the $Fe_2O_3/(Fe_2O_3+FeO)$ versus SiO_2 plot of Meinert (1995), barren granites in the SE and NW sectors show a general trend towards more oxidized and fractionated compositions (Fig. 23A), with skarn-proximal barren granites in the NW (e.g., Hörken granite) having redox-fractionation characteristics consistent with an average value for productive granites linked to skarn Mo mineralisation (Fig. 23A). In contrast, skarn-distal and barren granites in the NW and SE sectors, while comparatively evolved ($SiO_2 \approx 71$–75 wt. %), have a relatively reduced signature ($Fe_2O_3/(Fe_2O_3+FeO) < 0.4$) more consistent with granites associated with skarn W and Sn mineralisation (Fig. 23A).

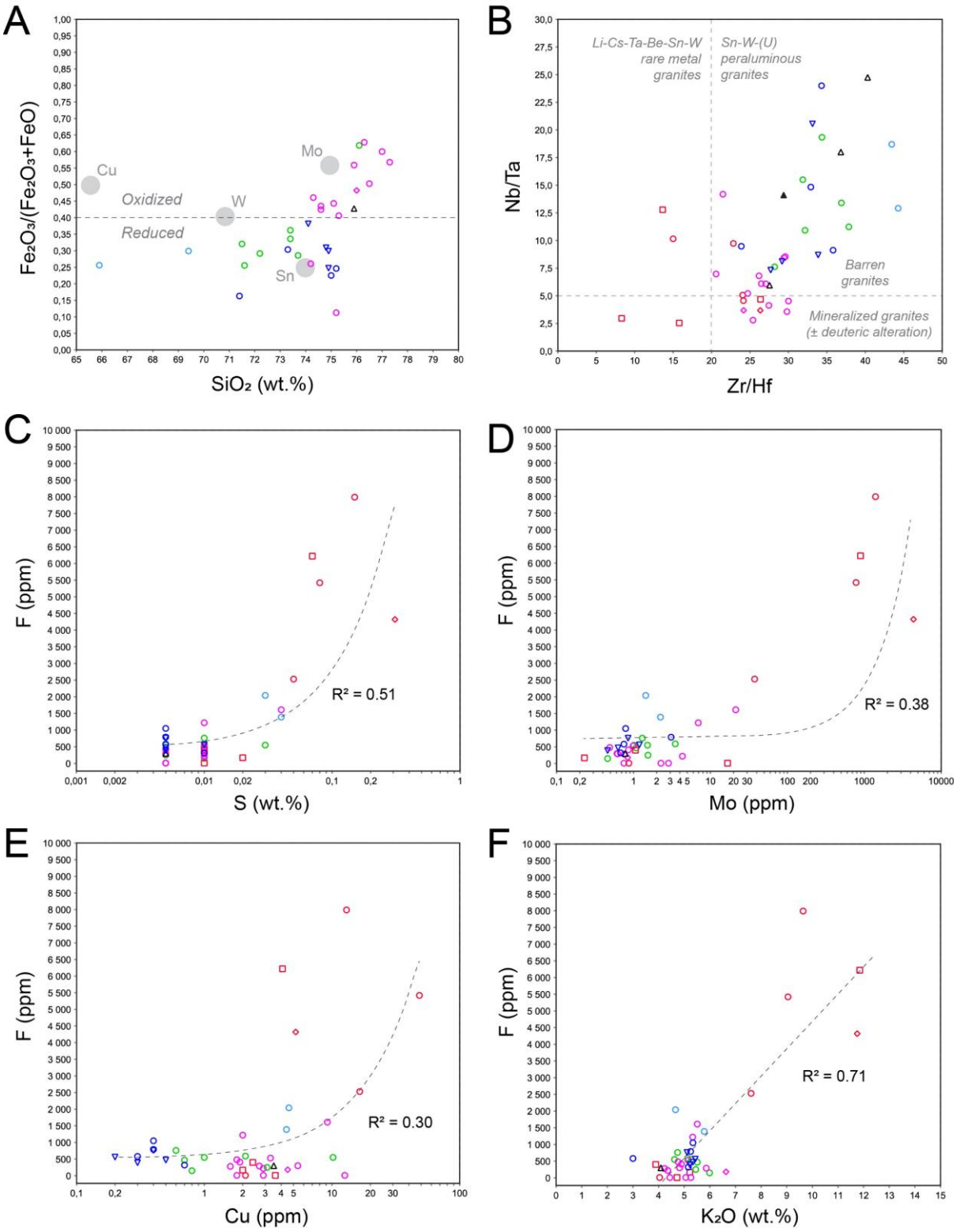

Figure 23. Metallogenic and element association plots for c. 1.8 Ga granitic intrusions in western Bergslagen. Symbols and colour scheme are same as those shown in Figs. 18 and 22. **A.** $Fe_2O_3/(Fe_2O_3+FeO)$ vs SiO_2 (after Meinert 1995). Grey circles indicate average composition of granitic rocks associated with skarn Cu, Sn, W and Mo mineralisation. **B.** Nb/Ta vs Zr/Hf plot (after Ballouard et al. 2016). **C.** F vs S. **D.** F vs Mo. **E.** F vs Cu. **F.** F vs K_2O.

On the Nb/Ta versus Zr/Hf plot of Ballouard et al. (2016), the samples define a general decreasing compositional trend from the barren to mineralised granite fields (Nb/Ta < 5; Fig. 23B). This pattern reflects increasing degrees of fractionation, concomitant with preferential Nb and Zr depletions (cf. Fig. 19C & E). In general, the skarn-proximal barren and mineralised granitic rocks in the NW have lower Nb/Ta and Zr/Hf ratios that overlap with those expected for peraluminous granites associated with rare metal and lithophile element mineralisation (cf. Ballouard et al. 2016). In contrast, skarn-distal granites in the NW (e.g., Malingsbo granite) and barren granites in the SE sector have elevated Nb/Ta and Zr/Hf signatures that reflect their less evolved petrographic and geochemical characteristics (Fig. 23B).

In western Bergslagen, skarn W ± Mo mineralisation is typically associated with increased fluorite and F abundances (e.g., Ohlsson 1979). Likewise, c. 1.8 Ga granites proximal to Bergslagen skarn W ± Mo deposits typically have F contents > 1000 ppm (e.g., Sundblad et al. 1993, Bergman et al. 1995). Moreover, F is considered an important volatile element and complexing ligand (along with Cl, B, CO_2, and S) in residual magmas and hydrothermal fluids associated with granite-related lithophile element mineralisation (e.g., Webster et al. 1997, Černý et al. 2005, Kesler 2005, Wang et al. 2021).

Taken together, the analysed samples show moderate positive linear correlations between F and the skarn-related elements S, Mo and Cu (R^2 = 0.51, 0.38 and 0.30, respectively), with skarn-proximal mineralised samples having the highest F contents (mean = 1882 ppm, n = 17; Fig. 23C–E). A comparable correlation for F and W is less evident (R^2 = 0.23; not shown in Fig. 23), although four skarn-proximal and mineralised granitic samples with elevated F contents (c. 4300 to 8000 ppm) also have relatively high W values (c. 34 to 39 ppm). In general, barren granites in the NW have low to moderate F contents (mean = 443 ppm; n = 20), and variable S, Mo and Cu concentrations that partly overlap with the mineralised granitic samples (Fig. 23C–E). Barren granites from the SE sector have comparable F contents (mean = 835 ppm; n = 10) consistent with average values for granitic rocks and the upper continental crust (c. 810 and 570 ppm, respectively; Rudnick & Gao 2014, Hayes et al. 2017). They also exhibit lower S, Mo and Cu contents compared to the granitic rocks in the NW (Fig. 23C–E).

A positive linear correlation between F and K_2O (R^2 = 0.71) is also evident from the analysed samples (Fig. 23F), although this trend is strongly influenced by skarn-proximal mineralised granites in the NW which are enriched in both F and K_2O (Fig. 23F). The K_2O compositions of five of these samples (7.61–11.85 wt. % K_2O) are greater than average K_2O values typical for orogenic granites (c. 3.0–4.5 wt. %; Artemieva et al. 2017) and reflect rock modal compositions dominated by primary K-feldspar ± biotite, and/or the effects of overprinting sericite ± K-feldspar alteration. Overall, the barren granites in the NW and SE sectors have K_2O contents (c. 4–6 wt. %) more typical for late-orogenic and high-K shoshonitic granites (cf. Eby 1992, Chappell et al. 2012), and lack correlations with their F contents (Fig. 23F).

Although the lower oxidation state of skarn-distal granites in the SE and NW suggests a proclivity for Sn mineralisation (e.g. Figs. 18E & 23A), their relatively low Sn contents (< 5 ppm) and the lack of correlations between Sn and other ore elements for both the skarn-proximal and skarn-distal granites (not shown here) suggest Sn behaved more compatibly with increasing magma fractionation or was susceptible to redistribution by late- to post-magmatic hydrothermal fluids (e.g. Lehmann 2021). Alternatively, differential uplift and erosion effects may have affected the preservation of Sn-bearing granite apical zones or vein systems, especially for the more geochemically reduced skarn-distal intrusions in the SE sector and adjacent to the WBBZ.

Zircon U-Pb Geochronology

The results of zircon U-Pb SIMS geochronology are summarized in Figures 24 to 26 and Table 4. The following sections briefly describe the dating results for each of the analysed samples.

Barren granites and older metamorphic rocks in the SE sector

STB181050Ab – Mesosome part of gneissic metatexite

This sample represents the mesosome part of a gneissic metatexite that is characteristic of higher-grade metasupracrustal rocks hosting GP-suite granites in the SE sector (cf. Fig. 3G). Zircon crystals from this sample are c. 50–250 μm long, subhedral to euhedral, short to elongate prismatic, and are pale yellow to brown in appearance. In BSE images, they commonly show medium grey central domains and narrow dark grey margins. Of 10 analysed spots, six produced a discordant array on a U-Pb (Wetherill) plot that yields an imprecise upper intercept (UI) date of 1896 ± 42 Ma (Fig. 24A). From this array, two concordant analyses have apparent $^{207}Pb/^{206}Pb$ dates of c. 1894 and c. 1862 Ma. The c. 1896 Ma UI date is interpreted as the approximate crystallisation or depositional age of the protolith.

STB181050Aa – Leucosome part of gneissic metatexite

This sample represents the felsic, leucosome part of the gneissic metatexite described above (cf. Fig. 3G). The zircons are c. 70–250 μm long, subhedral to euhedral, short to elongate prismatic, and are pale yellow to brown with several having cloudy central domains surrounded by clearer rims. In BSE images, the zircons show medium grey central domains and narrow dark grey margins. Several crystals show internal fractures, pits and/or mineral inclusions. Of a total of eight analysed spots, six produced a discordant array that gives a relatively precise upper intercept (UI) date of 1853 ± 8 Ma (Fig. 24B). The UI date overlaps with a weighted average apparent $^{207}Pb/^{206}Pb$ date of c. 1848 Ma for two concordant analyses from the same array (inset, Fig. 24B), and the c. 1862 Ma concordant $^{207}Pb/^{206}Pb$ date obtained for the mesosome part of the sample (Fig. 24A). The c. 1853 Ma UI date is interpreted to constrain the timing of leucosome segregation and protolith migmatization.

STB191023A – Metagranodiorite in the SE sector

This sample is a foliated metagranodiorite that is crosscut and included by massive biotite leucogranite (sample STB191044A; cf. Fig. 3C). The contained zircons are c. 40–270 μm long, subhedral to euhedral, short to elongate prismatic, are cloudy brown-orange, or are relatively clear (colourless). In transmitted light, several grains contain opaque mineral inclusions. In BSE images, the zircons display alternating medium grey-dark grey patterns indicative of oscillatory zoning, or more rarely have a uniform, medium grey appearance. Of 10 analysed spots, nine produced a discordant array that gives a relatively precise upper intercept (UI) date of 1896 ± 6 Ma (Fig. 24C). This date is identical to the c. 1896 Ma date determined for the gneissic metatexite (sample STB181050Ab above) and is interpreted as the crystallisation age of the metagranodiorite protolith.

STB191045A – Biotite-muscovite granite

This sample is a massive (undeformed), equigranular biotite-muscovite granite with occasional feldspar phenocrysts that intrudes foliated metasedimentary rocks. Zircon crystals are c. 40–250 μm long, subhedral to euhedral, short to elongate prismatic, are pale brown-orange or are relatively clear (colourless). Several crystals have cloudy central domains surrounded by narrower transparent rims. In BSE images, the zircons display alternating medium grey-dark grey patterns indicative of oscillatory zoning, or have a central medium grey domain mantled by darker rims. Of 11 analysed spots, seven plot on Concordia (Tera-Wasserburg) and define three distinct age

populations with corresponding weighted average $^{207}Pb/^{206}Pb$ dates of c. 1896 ± 9 Ma, 1852 ± 7 Ma, and 1817 ± 14 Ma (Fig. 24D). We interpret the younger of the three dates (c. 1817 Ma) as the approximate crystallisation age of the granite, with the other dates representing older geological events recorded by inherited zircons. Of these, the c. 1852 Ma date is similar to the c. 1853 Ma migmatization age recorded by metatexite sample STB181050Ab (Fig. 24B), while the c. 1896 Ma date is identical to the crystallisation age of metagranodiorite sample STB191023A (Fig. 24C).

STB191044A – Biotite granite

This sample is a massive, megacrystic, MME-bearing, biotite granite representing the Fellingsbro granite that intrudes foliated metasedimentary and metaigneous rocks. Zircon crystals are c. 60–350 μm long, subhedral to euhedral, short to elongate prismatic, and are generally colourless. Under transmitted light, several grains contain opaque mineral inclusions. In BSE images, the zircons have a relatively homogenous medium grey appearance, though several show internal fractures, pits and/or inclusions. A total of 10 analysed spots yields a relatively precise Concordia date of 1796 ± 10 Ma (Fig. 24E) which is interpreted as the crystallisation age of the granite.

STB191003A – Biotite-muscovite granite

This sample is a massive, equigranular biotite-muscovite granite with pegmatitic domains that includes an amphibolitic xenolith. Zircon crystals are c. 50–300 μm long, subhedral to euhedral, short to elongate prismatic, and are colourless or pale brown-orange and cloudy. Several grains contain opaque mineral inclusions. In BSE images, the zircons show oscillatory zoning patterns and commonly contain pits or inclusions. Of 10 analysed spots, eight form a discordant array giving an imprecise upper intercept (UI) date of 1784 ± 75 Ma (Fig. 24F). A concordant analysis (spot 1) with an apparent $^{207}Pb/^{206}Pb$ date of c. 1816 Ma has a large error (± 1166 Ma; 2σ) and was not used in the UI calculation, while another (spot 8) has an apparent $^{207}Pb/^{206}Pb$ date of 1903 ± 12 Ma suggesting inheritance of older crustal material. The c. 1784 Ma UI date, although based on a poorly constrained Discordia array (Fig. 24F), is interpreted as the approximate crystallisation age of the granite.

STB181051A – Biotite-muscovite granite

This sample is a massive, equigranular biotite-muscovite granite that crosscuts and includes a foliated metagranodiorite (sample STB191023A; cf. Fig. 3C). Zircon crystals are c. 30–60 μm long, subhedral to euhedral, generally short prismatic, and colourless to pale yellow. Several crystals show oscillatory zoning patterns in reflected light images, while BSE images show medium grey central domains and darker grey rims. From 33 analysed spots, seven form a discordant array that gives an imprecise upper intercept (UI) date of 1772 ± 27 Ma (Fig. 24G). A subset population of eight concordant analyses yields a Concordia date of 1905 ± 9 Ma (inset, Fig. 24G). The c. 1772 Ma UI date is interpreted as the approximate crystallisation age of the granite, while the c. 1905 Ma date represents an older magmatic event recorded by inherited zircons. The older date also overlaps with inherited age signatures in granite samples STB191045A and STB191003A, and the protolith emplacement age for metagranodiorite sample STB191023A.

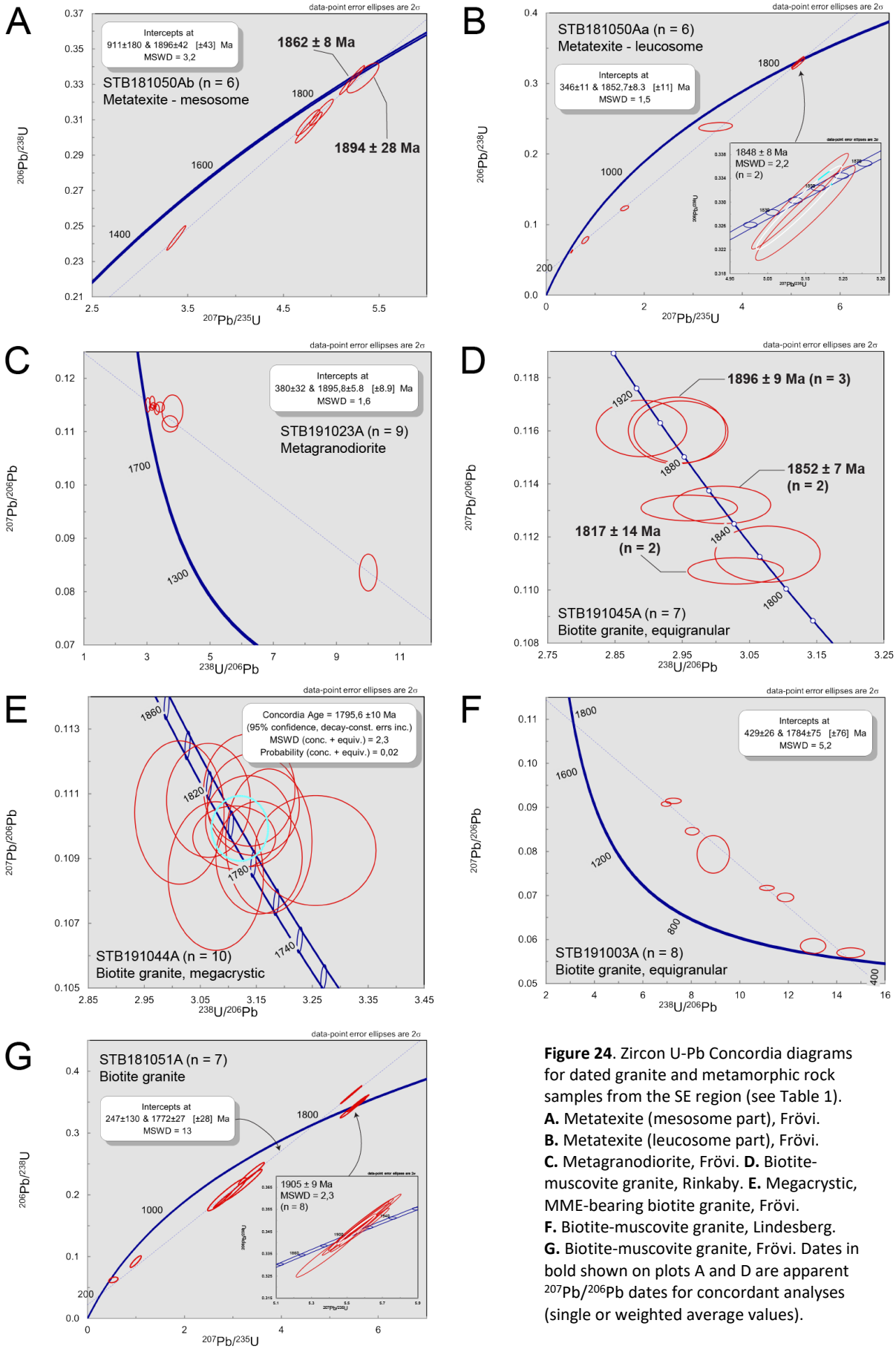

Figure 24. Zircon U-Pb Concordia diagrams for dated granite and metamorphic rock samples from the SE region (see Table 1). **A.** Metatexite (mesosome part), Frövi. **B.** Metatexite (leucosome part), Frövi. **C.** Metagranodiorite, Frövi. **D.** Biotite-muscovite granite, Rinkaby. **E.** Megacrystic, MME-bearing biotite granite, Frövi. **F.** Biotite-muscovite granite, Lindesberg. **G.** Biotite-muscovite granite, Frövi. Dates in bold shown on plots A and D are apparent $^{207}Pb/^{206}Pb$ dates for concordant analyses (single or weighted average values).

Skarn-distal barren granites in the NW sector

ELH190017A – Biotite granite (Malingsbo central)
This sample is a massive (undeformed), pale pink, seriate to megacrystic biotite granite representing the central part of the Malingsbo massif (cf. Fig. 4). Zircons from this sample are c. 40–250 μm long, subhedral to euhedral with occasional rounded edges, short to elongate prismatic, and are cloudy pale yellow to brown. In BSE and CL images, the zircons are oscillatory zoned or show medium to dark grey core domains overgrown by banded rims. Of 15 analysed spots, 13 concordant analyses yield a relatively precise Concordia date of 1860 ± 6 Ma (Fig. 25A). Based on the setting and petrological character of the granite and considering the dating results for other Malingsbo granite samples (below), the c. 1860 Ma date represents either the crystallisation age of the granite or a population of inherited zircons formed during a previous tectonothermal event (see Discussion).

ELH190051A – Biotite granite (Enkullen-Malingsbo north)
This sample is a massive, grey to pale pink, seriate to megacrystic biotite granite representing the Enkullen granite on the northwest margin of the Malingsbo massif (cf. Fig. 4). Zircons from this sample are c. 45–350 μm long, subhedral to euhedral, short to elongate prismatic, and are cloudy pale brown to orange or colourless. Of 12 analysed spots, seven concordant analyses yield a Concordia date of 1804 ± 8 Ma (Fig. 25B). This date is interpreted as the crystallisation age of the Enkullen granite.

ELH190002A – Biotite granite (Malingsbo east)
This sample is a massive, pale pink, equigranular biotite granite with late pegmatitic zones that forms part of the eastern Malingsbo massif. The zircons are c. 70–250 μm long, subhedral to euhedral, generally short prismatic, and mainly have a cloudy, pale brown to orange appearance. In BSE images, the zircons are internally fractured with pits and/or mineral inclusions and show heterogeneous medium to dark grey domains or are oscillatory zoned. Of 11 analysed spots, six plot on Concordia (Tera-Wasserburg) and define three distinct age populations with corresponding weighted average apparent $^{207}Pb/^{206}Pb$ dates of c. 1898 ± 7 Ma, 1851 ± 6 Ma, and 1804 ± 6 Ma (Fig. 25C). We interpret the younger of these dates (c. 1804 Ma) as the crystallisation age of the granite and the older dates as magmatic events recorded by inherited zircons. All three dates overlap with the c. 1817 Ma, c. 1852 Ma and c. 1896 Ma age signatures recorded in granite sample STB191045A from the SE sector (Fig. 24D).

ELH190029A – Biotite granite (Malingsbo south)
This sample is a weak to moderately foliated, reddish grey, biotite granite with augen texture and forms part of the southern Malingsbo massif (cf. Fig. 4E). The contained zircons are c. 70–350 μm long, subhedral to euhedral with occasional rounded edges, short to elongate prismatic, are commonly fractured and pitted with occasional opaque mineral inclusions and are cloudy pale brown to orange. In BSE images, the zircons show medium grey central domains and dark grey overgrowth margins or have irregular internal textures. Of 10 analysed spots, three concordant analyses yield a Concordia date of 1800 ± 14 Ma (Fig. 25D). A fourth concordant analysis (spot 10) with an apparent $^{207}Pb/^{206}Pb$ date of 1791 ± 300 Ma (2σ) was not included in the Concordia age calculation due to its large error. Despite the small number of concordant spots, we interpret the c. 1800 Ma Concordia date as the approximate crystallisation age of the granite. This date also provides a maximum (older) age limit for post-crystallisation ductile deformation in the area.

ELH190018A – Biotite granite (Malingsbo west)

This sample is a massive, pink to red, megacrystic biotite granite that forms part of the western Malingsbo massif. Zircons are c. 50–300 µm long, subhedral to euhedral, short to elongate prismatic, colourless to pale yellow/brown, and may contain opaque mineral inclusions. In BSE images, the zircons are uniform medium grey, show oscillatory zoning patterns, or have dark grey core domains surrounded by medium grey rims, or *vice versa*. Of 11 analysed spots, five concordant analyses give a Concordia date of 1795 ± 7 Ma (Fig. 25E), which is interpreted as the crystallisation age of the granite. An additional concordant analysis (spot 9) has an imprecise apparent $^{207}Pb/^{206}Pb$ date (1240 ± 236 Ma; 2σ) and was thus excluded from the age calculation.

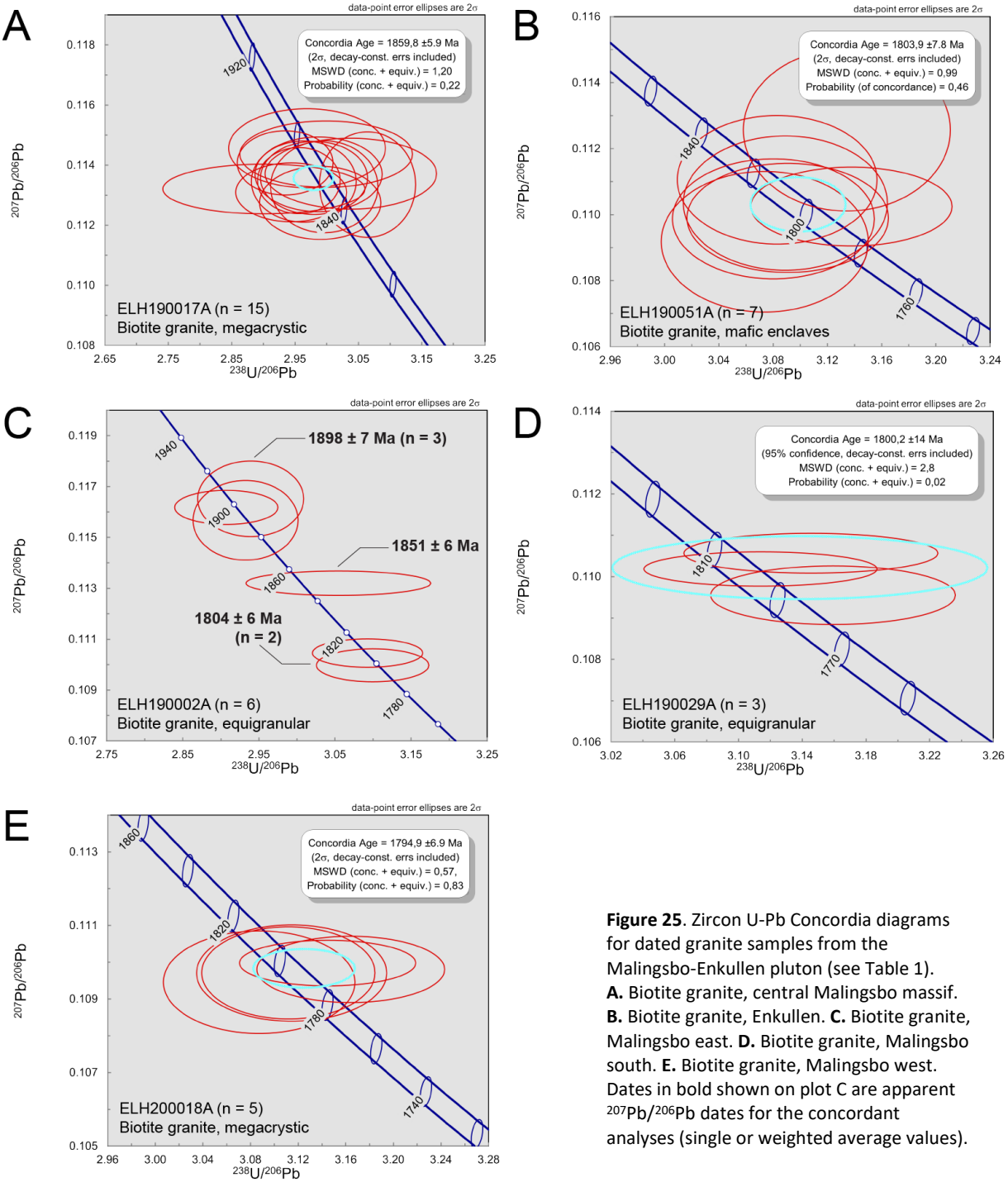

Figure 25. Zircon U-Pb Concordia diagrams for dated granite samples from the Malingsbo-Enkullen pluton (see Table 1). **A.** Biotite granite, central Malingsbo massif. **B.** Biotite granite, Enkullen. **C.** Biotite granite, Malingsbo east. **D.** Biotite granite, Malingsbo south. **E.** Biotite granite, Malingsbo west. Dates in bold shown on plot C are apparent $^{207}Pb/^{206}Pb$ dates for the concordant analyses (single or weighted average values).

Skarn-proximal granites in the NW sector

ELH200081A – Megacrystic biotite granite (Sandudden)
This sample was taken from a massive (undeformed), pale pink, seriate to megacrystic biotite granite located to the immediate west of the Sandudden skarn W ± Mo prospect (cf. Fig. 1). The contained zircons are c. 60–200 μm long, subhedral to euhedral and commonly show embayed and partly rounded edges. Zircon crystals are generally short prismatic and are cloudy pale brown to orange in appearance. In BSE images, several crystals are oscillatory zoned, while many display an internal pitted or 'spongey' texture and are fractured. Of 10 analysed spots, six produced a strongly discordant array that gives an imprecise upper intercept (UI) age of 1847 ± 39 Ma, with the least discordant analysis (spot 3) having an apparent $^{207}Pb/^{206}Pb$ date of 1820 ± 15 Ma (2σ; Fig. 26A). Based on the setting and petrological character of the granite, we interpret the single c. 1820 Ma $^{207}Pb/^{206}Pb$ date to best represent the approximate timing of granite crystallisation. We place little geological significance on the imprecise c. 1847 Ma UI date, although it overlaps with c. 1.85 Ga inherited age signatures recorded in other granite samples, and the timing of migmatization to the southeast (sample STB181050Aa). Two concordant analyses (spots 1 and 5) have apparent $^{207}Pb/^{206}Pb$ dates of c. 1897 Ma and c. 1887 Ma and likely reflect the inheritance of older crustal material.

ELH200020A – Equigranular biotite granite (Hörken)
This sample is a massive, pale pink to red, equigranular biotite granite located adjacent to several skarn W-Mo ± Cu prospects in the Hörken area (e.g., Grantorpsgruvan). The zircons are c. 50–250 μm long, subhedral to euhedral, have embayed, pitted and partly rounded edges, are short to elongate prismatic, and are colourless or cloudy pale brown to orange. In BSE images, the zircons are oscillatory zoned or show heterogeneous, medium grey central domains and dark grey rims. Mineral inclusions and/or pits are relatively common. Of 14 analysed spots, seven produced a discordant array that gives an imprecise upper intercept (UI) date of 1817 ± 23 Ma (Fig. 26B). This date is interpreted to be the approximate crystallisation age of the granite. A single concordant analysis (spot 7) has an apparent $^{207}Pb/^{206}Pb$ date of 1898 ± 11 Ma and reflects the inheritance of older crustal material.

ELH200096A – Megacrystic biotite granite (Elgfall)
This sample is a massive, pale pink to red, equigranular to pegmatitic biotite granite adjacent to the Elgfall/Älgfall skarn W prospect (cf. Fig. 1). Zircon crystals are c. 60–300 μm long, subhedral to euhedral, short to elongate prismatic, have embayed or irregular edges, and are colourless or cloudy pale brown to orange. Several crystals contain opaque mineral inclusions and are fractured. In BSE images, the zircons show medium grey central domains mantled by dark grey rims with rarer oscillatory patterns, with some examples internally heterogeneous, or showing a pitted or 'spongey' alteration texture. Of 11 analysed spots, six produced a discordant array that gives an imprecise upper intercept (UI) date of 1806 ± 46 Ma (Fig. 26C). We interpret this date as the approximate crystallisation age of the granite. Two concordant analyses (spots 10 and 11) have apparent $^{207}Pb/^{206}Pb$ dates of c. 1902 and 1894 Ma and indicate the inheritance of older crustal material.

ELH200067A – Biotite microgranite dyke (Wigström)
This sample is a massive, grey, biotite microgranite dyke that crosscuts metavolcanic rocks in the hanging wall of the Wigström skarn W-F deposit (cf. Fig. 1). Zircons from this sample are c. 40–170 μm long, subhedral to euhedral, short to elongate prismatic, and are colourless or cloudy pale yellow to brown. Several crystals contain opaque mineral inclusions. In BSE images, the zircons are oscillatory zoned with growth zones, and commonly show internal pits, inclusions, or fractures. Of 10 analysed spots, seven produced a discordant array that yields an imprecise upper

intercept (UI) date of 1798 ± 93 Ma (Fig. 26D). Of these seven, the least discordant analysis (spot 6) has an apparent $^{207}Pb/^{206}Pb$ date of 1809 ± 14 Ma (2σ). Although the dating results for this sample lack statistical robustness, the c. 1.80 Ga UI date is interpreted as the approximate emplacement age of the granite dyke. The new date is also consistent with an igneous age of c. 1778 Ma for the adjacent Högberget granite determined by zircon U-Pb LA-ICP-MS analysis (Plan 2020).

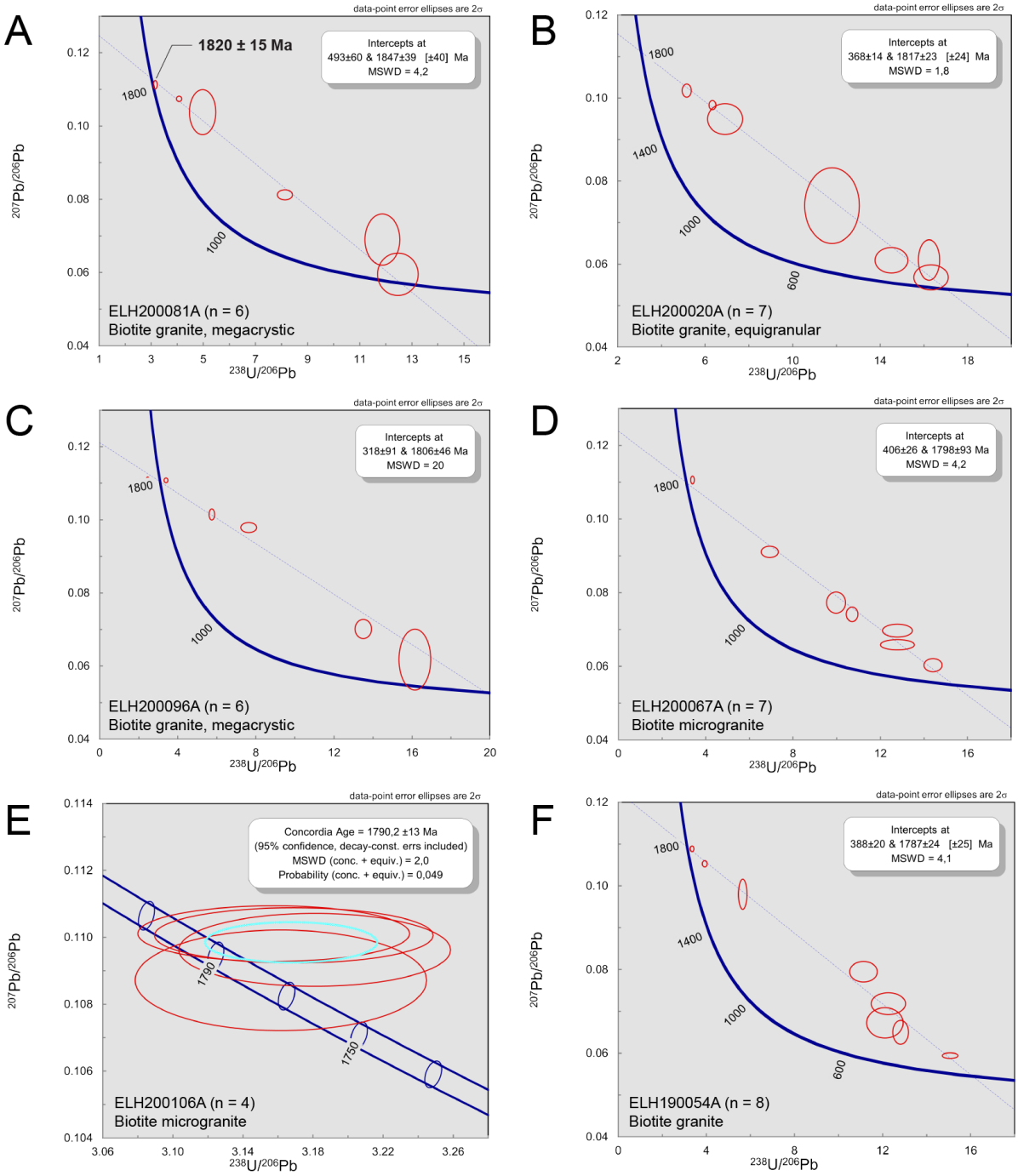

Figure 26. Zircon U-Pb Concordia diagrams for dated granites close to skarn mineralisation in western Bergslagen (see Table 1). **A.** Biotite granite, Sandudden. **B.** Biotite granite, Hörken. **C.** Biotite granite, Elgfall. **D.** Biotite microgranite, Wigström. **E.** Biotite microgranite, Yxsjöby. **F.** Biotite-molybdenite granite, Bispbergs klack. Date in bold shown on plot A is an apparent $^{207}Pb/^{206}Pb$ value.

ELH200106A – Biotite microgranite (Yxsjöby)
This sample is a massive, pale pink to red, biotite microgranite that crosscuts dacitic-rhyolitic metavolcanic rocks in the Yxsjöby area, about 1.5 km north of the Yxsjöberg skarn W-Cu-F deposit (cf. Fig. 1). The zircons are c. 50–180 μm long, subhedral to euhedral, generally short prismatic, and are cloudy yellow to brown, with several grains containing opaque mineral inclusions. In BSE images, the zircons show irregular and pitted edges and are internally heterogeneous. Of 10 analysed spots, four concordant analyses give a relatively precise Concordia date of 1790 ± 13 Ma which is interpreted as the emplacement age of the granitic dyke (Fig. 26E). The c. 1790 Ma age is similar to a titanite U-Pb date of 1789 ± 2 Ma obtained from the Yxsjöberg skarn deposit reported by Romer & Öhlander (1994).

ELH190054A – Equigranular biotite granite with molybdenite (Bispbergs klack)
This sample from Bispbergs klack is a massive, pale grey-pink to red, equigranular to seriate biotite granite containing disseminated molybdenite (cf. Fig. 6A). Zircons from this sample are c. 60–200 μm long, subhedral to euhedral, short to elongate prismatic, are colourless to cloudy pale yellow to brown, with several grains containing opaque mineral inclusions. In BSE images, the zircons are oscillatory zoned or have a more heterogeneous internal texture, and commonly contain fractures, pits and inclusions. Of 10 analysed samples, eight plot along a discordant array that gives an imprecise upper intercept (UI) date of 1787 ± 24 Ma, with the least discordant analysis (spot 9) having an apparent $^{207}Pb/^{206}Pb$ date of 1780 ± 10 Ma (2σ). Despite the U-Pb data discordance and considering a molybdenite Re-Os date of c. 1792 Ma obtained from the same sample (Table 5; see below), we interpret the c. 1787 Ma UI date to best represent the crystallisation age of the Bispbergs klack granite. The new date also overlaps with a previously determined zircon U-Pb age of 1794 ± 7 Ma for the same granite as reported by Woodward et al. (2009).

Table 4. Summary of zircon U-Pb dating results

Index[1]	Sample ID	Location	Rock type	Age ± 2σ[2]	Comment[3]
SE regional samples					
1	STB181050Ab	Frövi	Metatexite (mesosome part)	1894 ± 28 Ma	Single concordant $^{207}Pb/^{206}Pb$ date. Discordia UI date = 1896 ± 42 Ma (Fig. 24A).
2	STB181050Aa	Frövi	Metatexite (leucosome part)	1853 ± 8 Ma	Discordia UI date (Fig. 24B).
3	STB191023A	Frövi	Metagranodiorite	1896 ± 6 Ma	Discordia UI date (Fig. 24C).
4	STB191045A	Rinkaby	Biotite-muscovite granite	1817 ± 14 Ma	Wt. avg. $^{207}Pb/^{206}Pb$ date (n = 2). (Fig. 24D).
5	STB191044A	Frövi	Biotite granite	1796 ± 10 Ma	Concordia date (Fig. 24E)
6	STB191003A	Lindesberg	Biotite-muscovite granite	1784 ± 75 Ma	Discordia UI date (Fig. 24F)
7	STB181051A	Frövi	Biotite-muscovite granite	1772 ± 27 Ma	Discordia UI date (Fig. 24G).
NW skarn-distal granites					
8	ELH190017A	Malingsbo central	Biotite granite	1860 ± 6 Ma	Concordia date (Fig. 25A); Possible inherited population?
9	ELH190051A	Enkullen (Malingsbo north)	Biotite granite	1804 ± 8 Ma	Concordia date (Fig. 25B)
10	ELH190002A	Malingsbo east	Biotite granite	1804 ± 6 Ma	Wt. avg. $^{207}Pb/^{206}Pb$ date (n = 2). (Fig. 25C).
11	ELH190029A	Malingsbo south	Biotite granite	1800 ± 14 Ma	Concordia date (Fig. 25D)
12	ELH200018A	Malingsbo west	Biotite granite	1795 ± 7 Ma	Concordia date (Fig. 25E)

Index[1]	Sample ID	Location	Rock type	Age ± 2σ[2]	Comment[3]
NW skarn-proximal granites					
13	ELH200081A	Sandudden	Biotite granite	1820 ± 15 Ma	Single concordant $^{207}Pb/^{206}Pb$ date. Discordia UI date = 1847 ± 39 Ma (Fig. 26A).
14	ELH200020A	Hörken	Biotite granite	1817 ± 23 Ma	Discordia UI date (Fig. 26B).
15	ELH200096A	Elgfall	Biotite granite	1806 ± 46 Ma	Discordia UI date (Fig. 26C).
16	CMR180008A	Pingstaberg	Biotite granite	1805 ± 9 Ma	Concordia date, reported in Lynch et al. 2019
18	ELH200067A	Wigström	Biotite microgranite	1798 ± 93 Ma	Discordia UI date (Fig. 26D).
19	ELH200106A	Yxsjöby	Biotite microgranite	1790 ± 13 Ma	Concordia date (Fig. 26E)
23	ELH190054A	Bispbergs klack	Biotite granite	1787 ± 24 Ma	Discordia UI date (Fig. 26F).

Notes: [1]Index number corresponds to those shown in Fig. 27. [2]Age represents best interpreted crystallisation age. [3]Abbreviations: wt. avg. = weighted average, UI = upper intercept.

Molybdenite Re-Os Geochronology

The results of molybdenite Re-Os N-TIMS dating are summarized in Table 5 and Figure 27. The following sections provide a brief description of the dated samples and the results.

Mineralised granitoid and skarn rocks in the NE sector

ELH200033A – Pyroxene skarn with molybdenite (Hörken-Silvergruvan)
This sample is a pyroxene skarn rock with minor disseminated molybdenite, scheelite and pyrite from the Silvergruvan Mo-W prospect near Hörken (cf. Fig. 1). The skarn zone occurs within foliated, intermediate to felsic metavolcanic rocks, and is located c. 250 m from the western contact of the Hörken granite. Locally, the skarn is cut by quartz-calcite veinlets and segregations. In general, the molybdenite comprises anhedral platy to elongate prismatic or flaky crystals, is fine-grained (0.25–5 mm), has a metallic blue-grey appearance, and occurs as disseminated individual crystals, or stringer aggregates and rosettes ranging from c. 4–12 mm in size. The analysed sample gave a Re-Os model age of 1802 ± 10 Ma (2σ; Table 5 and Fig. 27) which constrains the timing of Mo-W mineralisation and associated skarn alteration at Silvergruvan. The c. 1802 Ma Re-Os age overlaps at the 2σ-level with the imprecise 1817 ± 23 Ma U-Pb age determined for the adjacent Hörken granite (Table 4 and Fig. 27), although it is older than the c. 1770 Ma Re-Os date obtained for the nearby Grantorp skarn Mo-W prospect to the east (sample ELH20002A; see below).

ELH200085A – Pyroxene-garnet-fluorite skarn with molybdenite (Wigström)
This sample is a pyroxene-garnet-fluorite skarn rock with minor disseminated molybdenite (c. 1–2 vol. %) and scheelite that is representative of high-grade skarn ore at the Wigström W-Mo deposit (cf. Fig. 1). Molybdenite is anhedral to subhedral, has a metallic blue-grey appearance, is fine-grained (c. 0.25–3 mm), and occurs as disseminated flaky and tabular crystals or aggregated clumps and rosettes associated with fluorite and minor scheelite. The analysed sample gave a Re-Os model age of 1799 ± 10 Ma (2σ; Table 5 and Fig. 27) which constrains the timing of W-Mo-F mineralisation and associated skarn alteration at Wigström. The new Re-Os age is consistent with the new c. 1798 Ma zircon U-Pb age determined for a microgranite dyke intruding the hanging wall rocks at Wigström (sample ELH200067A; Table 4), although the latter date is based on a highly discordant isochron (cf. Fig. 26D). The c. 1799 Ma Re-Os date is older than a c. 1778 ± 22 Ma zircon U-Pb age reported for the adjacent Högberget granite (Plan 2020), although both dates overlap within error.

ELH200087A – Pegmatoid dyke rock with molybdenite (Wigström)
This sample is a white to pale green feldspar-sericite-fluorite-quartz-epidote rock with minor molybdenite (c. 0.5–1 vol. %) and scheelite. Overall, the rock displays an aplitic-pegmatitic texture, is undeformed, and crosscuts hanging wall metavolcanic rocks with relatively sharp contacts adjacent to the skarn zone at the Wigström deposit (e.g., Fig. 6E). Molybdenite comprises anhedral platy to elongate prismatic or flaky crystals, is fine-grained (0.25–5 mm), has a metallic blue-grey appearance, and occurs as disseminated crystals, or clumped aggregates and rosettes ranging from c. 5–11 mm in size. The analysed sample produced a Re-Os model age of 1798 ± 10 Ma (2σ; Table 5) which is identical to the c. 1799 Ma determined for the skarn ore sample described above (ELH200085A).

ELH190054A – Biotite granite with molybdenite (Bispbergs klack)
This sample is the same reddish-pink biotite granite with molybdenite from Bispbergs klack that was used for the zircon U-Pb dating (described above). Molybdenite occurs as disseminated (c. 0.5–2 vol. %), interstitial crystals in the granite and is associated with minor fluorite and rare chalcopyrite (e.g., Fig. 6A). Molybdenite crystals range from c. 0.5–4 mm in size, are anhedral to subhedral, and occur as irregular flakes and tabular crystals, or platy aggregates typically c. 5–8 mm in size. A determined Re-Os model age for this sample is 1792 ± 10 Ma (2σ; Table 5 and Fig. 27). The new Re-Os age is marginally older than the discordant and imprecise 1787 ± 24 Ma zircon U-Pb age determined for the same sample (Table 4, Fig. 26F), although both dates overlap at the 2σ-level. The new Re-Os date, however, is identical to a c. 1794 Ma zircon U-Pb age previously reported for the Bispbergs klack granite (Woodward et al. 2009), suggesting the former date more accurately constrains the emplacement of the Bispbergs klack granite if compared to the c. 1787 Ma zircon U-Pb age determined as part of this study.

Table 5. Summary of molybdenite Re-Os dating results.

Index[1]	Sample ID	Weight (g)	Location	Description	Re (ppm)	Age ± 2σ[2]	Comment
17	ELH170002A	0.101	Pingstaberg	Intragranitic molybdenite	2.30	1801 ± 10 Ma	Reported in Lynch et al. 2019
20	ELH200033A	0.040	Silvergruvan	Skarn-hosted molybdenite	3.64	1802 ± 10 Ma	
21	ELH190085A	0.041	Wigström	Skarn-hosted molybdenite	1.45	1799 ± 10 Ma	
22	ELH190087A	0.040	Wigström	Pegmatoid-hosted molybdenite	2.24	1798 ± 10 Ma	
24	ELH190054A	0.040	Bispbergs klack	Disseminated molybdenite in granite	4.15	1792 ± 10 Ma	
25	ELH200026A	0.042	Grantorp	Skarn-hosted molybdenite	1.39	1770 ± 11 Ma	

Notes: [1]Index number corresponds to those shown in Fig. 27. [2]Re-Os model age with 2σ error that includes propagated analytical and decay constant uncertainties.

ELH200026A – Pyroxene-garnet skarn with molybdenite (Hörken-Grantorp)
This sample is a garnet-pyroxene-quartz skarn rock with rare disseminated scheelite and molybdenite (c. 0.5–1 vol. %) from the Grantorp Mo-W prospect near Hörken. In general, the molybdenite is anhedral to subhedral, has a metallic blue-grey appearance, is fine-grained (c. 0.25–3.5 mm), and occurs as disseminated, flaky prismatic and tabular crystals, or aggregated clumps and rosettes (up to c. 8 mm) that are interstitial with garnet and pyroxene. Molybdenite also occurs at the margins of quartz-garnet veinlets and quartz-rich segregations within the skarn. The analysed sample gave a Re-Os model age of 1770 ± 11 Ma (2σ; Table 5 and Fig. 27) which constrains the timing of Mo-W mineralisation and associated skarn alteration at Grantorp. The new Re-Os age at Grantorp is younger than the c. 1802 Ma molybdenite Re-Os date determined for the Silvergruvan Mo-W prospect to the west (sample ELH200033A; Table 5) and the c. 1817 Ma igneous age determined for the Hörken granite to the south (sample ELH200020A; Table 4). The dating result suggests a temporally distinct magmatic-hydrothermal event occurred in this area at c. 1770 Ma.

Notwithstanding the large analytical uncertainties associate with several of the dated zircon samples, the combined U-Pb and Re-Os geochronology results constrain four main magmatic-hydrothermal episodes at c. 1.90–1.89 Ga, c. 1.86–1.85 Ga, c. 1.81–1.79 Ga and c. 1.77 Ga (Fig. 27). A tentative fifth event at c. 1.82 Ga is also evident based on the age of the granite at Sandudden, although the overlap with the c. 1.81–1.79 Ga granite emplacement event within analytical uncertainty. Overall, the dating results reflect and granite emplacement episodes that span the c. 1.9–1.8 Ga time frame for the Svecofennian-cycle orogenesis in Bergslagen in an accretionary tectonic environment (cf. Stephens et al. 2009; see below).

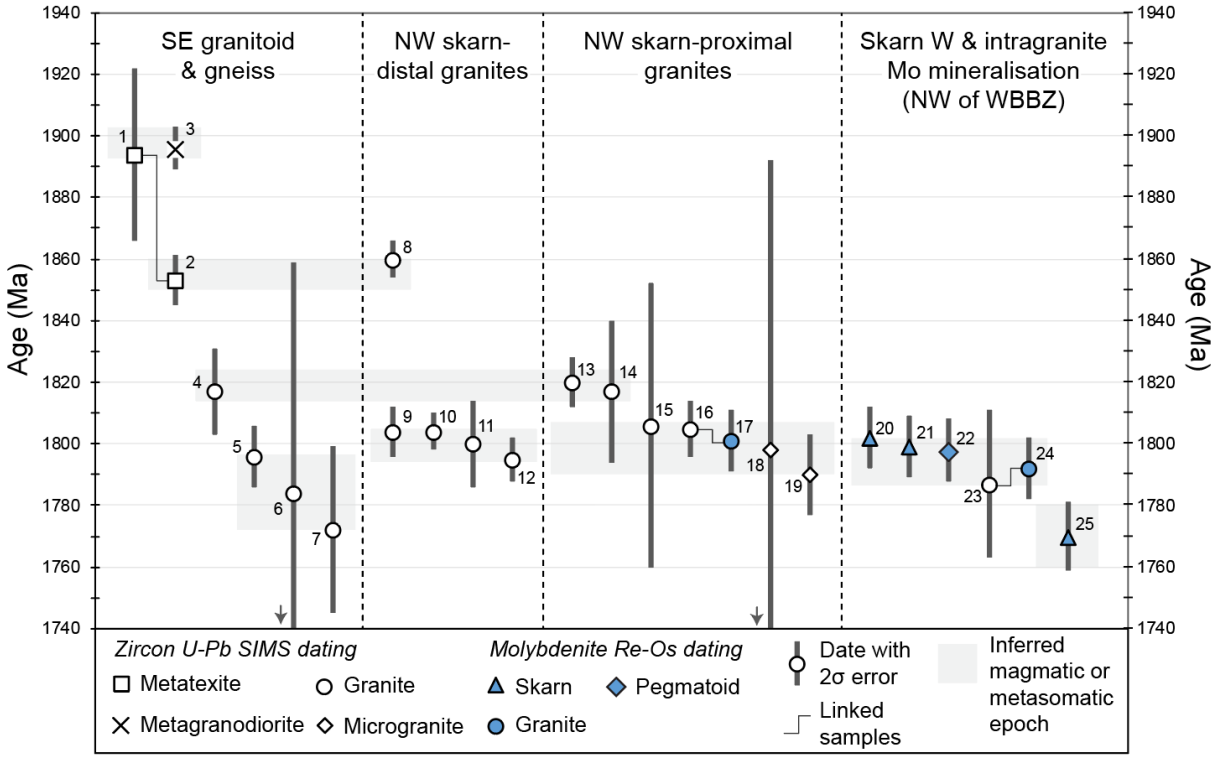

Figure 27. Summary of U-Pb and Re-Os geochronology results. Numbers beside symbols refer to the sample row numbers listed in Tables 4 and 5. Thin black lines link cogenetic or related samples.

Sm-Nd isotopic analysis

The results of whole-rock Sm-Nd isotopic analysis are listed in Table 6. Barren granites in the SE sector (e.g., Fellingsbro granite) have initial εNd values ranging from -0.2 to +4.0 (n = 4). One of these samples (STB191044A) is MME-bearing and exhibits the most isotopically juvenile signature of all the granites ($\varepsilon Nd_{1796\ Ma}$ = +4.0) which overlaps with the εNd signature of the depleted mantle at c. 1800 Ma. Older c. 1.9 Ga metagranitoid, metarhyolite and metagabbro samples in the SE have initial εNd values of +1.1, -2.0 and -0.2, respectively.

Skarn-distal barren granites in the NW (e.g., Malingsbo granite) have initial εNd values that fall within a relatively narrow range from -0.1 to +1.6 (n = 4). Skarn-proximal barren granites in the NW (e.g., Hörken) have comparable, although marginally more positive (juvenile), initial εNd values ranging from +0.5 to +3.1 (n = 6). Skarn-proximal and mineralised granitic rocks in the NW (e.g., Yxsjöby, Wigström) show the largest range of initial εNd values from -0.8 to +2.9 (n = 4) and overlap with the initial εNd signatures from the other NW granites. Finally, a metarhyolite and amphibolite sample from the NW have initial $\varepsilon Nd_{1.9\ Ga}$ values of +1.3 and +0.8, respectively.

Calculated two-stage depleted mantle model ages (T_{DM2}) for the c. 1.8 Ga granitic rocks range from 1.86 to 2.25 Ga and have a median age of 2.09 ± 0.11 Ga (±1σ; n = 18; Table 6). Older c. 1.9 Ga metamorphic rocks have T_{DM2} ages ranging from 2.08–2.41 Ga and have a slightly older median age of = 2.16 ± 0.12 Ga (n = 6). Notwithstanding certain caveats regarding the interpretation of Nd model ages (e.g., Arndt & Goldstein 1987), the T_{DM2} dates suggest GP suite granites are mainly the products of magma derived from the melting of pre-existing continental crust that, in turn, formed either directly or indirectly from mafic magmas extracted from a light REE-depleted lithospheric mantle at c. 2.0–2.3 Ga (see Discussion).

Table 6. Results of whole-rock Sm-Nd isotopic analysis (n = 24)

Sample ID	Rock type	Sm	Nd	Sm/Nd	$^{147}Sm/^{144}Nd$ [1]	$^{143}Nd/^{144}Nd$ [2]	Age (Ma)[3]	εNd(i)[4]	T_{DM2}[5] (Ga)
Barren c. 1.8 Ga granites in the SE sector									
STB191003A	Bt-ms granite	8.95	51.77	0.17	0.1040	0.511564 (14)	1784	+0.3	2.15
STB191044A	Bt granite	14.30	80.28	0.18	0.1072	0.511786 (18)	1796	+4.0	1.86
STB191045A	Bt-ms granite	5.62	27.05	0.21	0.1250	0.511757 (6)	1817	-0.5	2.23
STB181051A	Bt-ms granite	6.83	29.80	0.23	0.1380	0.511937 (16)	1772	-0.3	2.18
Older c. 1.9 Ga metamorphic rocks in the SE sector									
STB191005A	Metarhyolite	5.34	27.56	0.19	0.1167	0.511937 (18)	1900*	-2.0	2.41
STB191043A	Metagabbro	3.24	14.82	0.22	0.1316	0.511815 (22)	1900*	-0.2	2.27
STB191023A	Metagranitoid	4.21	20.94	0.20	0.1211	0.511748 (27)	1896	+1.1	2.08
STB191023A (repeat)	Metagranitoid	4.71	23.20	0.20	0.1222	0.511778 (20)	1896	+1.4	2.15
Barren, skarn-distal granites in the NW sector									
ELH190002A	Bt granite	4.77	21.48	0.22	0.1337	0.511887 (2)	1804	-0.1	2.19
ELH190017A	Bt granite	14.22	77.84	0.18	0.1100	0.511691 (4)	1800*	+1.6	2.06
ELH190051A	Bt granite	9.79	46.87	0.21	0.1258	0.511872 (16)	1804	+1.5	2.07

Sample ID	Rock type	Sm	Nd	Sm/Nd	$^{147}Sm/^{144}Nd$ [1]	$^{143}Nd/^{144}Nd$ [2]	Age (Ma)[3]	εNd(i)[4]	T_{DM2}[5] (Ga)
ELH200018A	Bt granite	7.77	38.90	0.20	0.1202	0.511784 (24)	1795	+1.0	2.10
Barren, skarn-proximal granites in the NW sector									
ELH190078A	Bt granite	8.80	37.62	0.23	0.1408	0.512000 (8)	1805	+0.5	2.14
ELH200081A	Bt granite	7.11	27.61	0.26	0.1551	0.512219 (19)	1820	+1.5	2.07
ELH200020A	Bt granite	6.75	28.64	0.24	0.1418	0.512102 (21)	1810	+2.3	2.01
ELH200105A	Bt granite	9.30	23.84	0.39	0.2350	0.513123 (18)	1810	+0.6	2.14
ELH200109A	Bt granite	2.16	6.27	0.34	0.2075	0.512804 (21)	1806	+0.7	2.13
ELH200109B	Bt granite	3.33	13.10	0.25	0.1530	0.512278 (22)	1806	+3.1	1.94
Mineralised, skarn-proximal granites in the NW sector									
ELH190073A	Bt granite	5.33	17.78	0.30	0.1804	0.512403 (12)	1805	-0.8	2.25
ELH190054A	Bt granite	11.04	45.11	0.24	0.1474	0.512202 (20)	1792	+2.9	1.95
ELH200096A	Bt granite	2.42	5.43	0.45	0.2686	0.513632 (20)	1810	+2.7	1.98
ELH200106A	Aplite-microgranite	5.13	14.15	0.36	0.2182	0.512978 (26)	1790	+1.7	2.04
Older c. 1.9 Ga metamorphic rocks in the NW sector									
ELH190026A	Metarhyolite	4.90	22.69	0.22	0.1299	0.511867 (32)	1900*	+1.3	2.16
ELH190003A	Amphibolite	3.47	15.22	0.23	0.1373	0.511938 (8)	1900*	+0.8	2.19

Notes: [1]Calculated $^{147}Sm/^{144}Nd$ value based on relative isotopic abundance method described in Faure & Mensing (2005).[2]Values in parentheses are ± 2σ error at the last one or two digit level. [3]Ages based on U-Pb dating results (Table 4) or regional geology constraints for those marked with *. [4]Initial εNd values using present-day CHUR isotopic values of $^{143}Nd/^{144}Nd$ = 0.512638 and $^{147}Sm/^{144}Nd$ = 0.1967, and ^{147}Sm decay constant $\lambda = 6.54 \times 10^{-12}$ a^{-1} (Lugmair & Marti 1978). Uncertainty associated with εNd(i) values = ± 0.4 ε-units (±2σ). [5]T_{DM2} = Calculated two-stage depleted mantle model age (after Liew & Hofmann 1988) using the following values; $^{143}Nd/^{144}Nd$ present-day depleted mantle = 0.513151, $^{147}Sm/^{144}Nd$ present-day depleted mantle = 0.219, $^{147}Sm/^{144}Nd$ present-day bulk continental crust = 0.12.

DISCUSSION

3D geometry of granite bodies

The granite bodies close to the various tungsten prospects have all been confirmed by the inversion and modelling to be oriented NNE to NE. The Hörken granite has been resolute to have a steep dip towards the ESE. Ripa & Antal Lundin (2020) present inversion modelling of gravity and magnetic data where they show the mineralisation at Pingstaberg to be dipping westward. In the forward model presented here (Fig. 15) a westward dip of the western granite contact is preferred, but the data also allow other dips.

The Hörken granite is interpreted to have a width of 1000 m and the Högberget granite to have a width of about 350 m. The granite at Hörken seems to be nearly 250 m deep. The granite close to the Pingstaberg occurrence has been more difficult to interpret but is determined to be 1000 m as well as deeper (800–1000 m).

Petrophysical properties of mineralisation proximal vs. distal granites

Mean values for density, magnetic susceptibility, and magnetic remanence for each of the investigated granites can be seen in Table 2. Rock densities for the granites associated with W-F-Mo mineralisation, combined as a group, differ significantly from that for the barren Malingsbo granite. In contrast, mean magnetic susceptibility values cannot significantly distinguish the granites from one another. This is found in harmony with the fact that the variance of magnetic susceptibility does not differ much in the granites. For the mineralisation-related granites, the Pingstaberg granite shows the biggest difference of magnetic susceptibility from the Malingsbo granite. Overall, factors such as a higher degree of fractionation and the lower abundance of mafic minerals likely influenced the lower density and magnetic susceptibility values recorded by the mineralisation-related granites in the NW. Overprinting hydrothermal alteration or retrograde weathering may also have played a role.

Timing and duration of GP suite granite emplacement in Bergslagen

The new zircon U-Pb geochronology results constrain the timing of granite emplacement in the study area from c. 1820 to 1770 Ma, with most intrusions having crystallisation ages between c. 1810 and 1780 Ma (cf. Fig. 27). Several samples, however, produced discordant U-Pb dates with relatively large errors (> ± 20 Ma) or statistically poor age solutions due to the prevalence of metamict zircons with high U, Th contents and Th/U ratios (cf. Figs. 24–26 and Table 4). Such 'disturbed', poor quality zircons tend to suffer radiogenic Pb loss and/or common Pb enrichment (e.g., Schoene 2014) and are well documented for GP-type granites and other Paleoproterozoic rock units in Bergslagen and elsewhere in Sweden (e.g., Billström et al. 1988, Högdahl et al. 2001, Woodward et al. 2009, Herrmann et al. 2021). The systematic presence of mainly U-enriched (> c. 2000 ppm) metamict zircons in Late Svecofennian granites is likely a characteristic feature of these intrusions in general and correlates with their elevated bulk U and Th contents, and anomalous U-Th-K signatures seen in airborne radiometric data (cf. Stephens et al. 2009).

While most of the dated granites yield comparable 'Late Svecofennian' crystallisation ages, the skarn-distal Malingsbo batholith produced four U-Pb dates ranging from c. 1795–1804 Ma and an older age of c. 1860 Ma (sample ELH190017A; Fig. 25, Table 4). The latter date overlaps with the 1853 ± 8 Ma crystallisation age obtained for the leucosome part of the dated metatexite in the SE sector (sample STB181050Aa; Fig. 24B) and tentatively suggests an earlier c. 1.86–1.85 Ga emplacement event for that part of the batholith, possibly associated with a phase of regional high-grade metamorphism. The c. 1.86 Ga Malingsbo sample, however, is a weakly foliated to massive, K-feldspar-phyric biotite granite that is petrologically and geochemically similar to other parts of the intrusion, and the Malingsbo-Enkullen samples dated to c. 1.80 Ga. Thus, an alternative interpretation is the older age reflects a population of inherited c. 1.86 Ga zircons incorporated during granite emplacement at c. 1.80–1.79 Ga. Assimilated country rock xenoliths occur throughout the Malingsbo batholith (cf. Fig. 4C–D & H) and highlight interactions between parental felsic magmas and Svecofennian country rocks during granite emplacement.

A younger emplacement age for the 'older' c. 1.86 Ga Malingsbo unit is indirectly supported by whole-rock Sm-Nd isotopic data also (Table 6). On a $^{143}Nd/^{144}Nd$ versus $^{147}Sm/^{144}Nd$ plot constructed for all GP-related granite samples (n = 16), the c. 1.86 Ga Malingsbo sample lies on a best-fit linear regression (isochron) with a slope equivalent to c. 1824 Ma and a $^{143}Nd/^{144}Nd$ intercept of 0.510357 (equating to $\varepsilon Nd_{(1.82\ Ga)} = +1.5$). Although the isochron has a large standard error (c. ± 0.001 or 8%) and we attach little geological meaning to the 1.82 Ga Sm-Nd 'age', the overlap between the Sm-Nd isotopic properties of the 'older' Malingsbo unit with those for the younger c. 1.81–1.78 Ga granites indicates that a c. 1.8 Ga emplacement age for the 'older' Malingsbo body may be relevant. Likewise, the initial $\varepsilon Nd_{(1.82\ Ga)}$ values of +1.8 for the Malingsbo

sample and +1.5 for the combined granites (derived from the Sm-Nd isochron) further highlights a likely GP suite petrogenetic affiliation for the 'older' Malingsbo unit.

The assimilation of Svecofennian crustal material by GP suite parental magmas is further supported by age signatures recorded by both magmatic and inherited zircons in the dated samples (Fig. 28). On a combined probability density and histogram plot showing the temporal distributions of concordant single zircon apparent $^{207}Pb/^{206}Pb$ dates, three major age peaks at c. 1.90 Ga, 1.85 Ga and 1.80 Ga are evident for all dated samples (P1–P3, respectively, on Fig. 28A). These peaks incorporate formational and inheritance ages of the dated igneous and metamorphic rocks and overlap with the timing of major crustal forming events in Bergslagen and adjacent terranes during Paleoproterozoic orogenesis (cf. Stephens & Jansson 2020). For the dated granites, apparent $^{207}Pb/^{206}Pb$ dates recorded by predominantly turbid and fractured metamict zircons produce a major inheritance peak at c. 1.90 Ga, a lesser inheritance peak at c. 1.85 Ga, and a main igneous peak at c. 1.80 Ga (P1–P3, respectively, Fig 28B). The inheritance peaks correlate with typical ages for Svecofennian meta-igneous source rocks, while the peak sizes may reflect the relative abundances of c. 1.90 and 1.85 Ga rocks in western Bergslagen and thus the availability of potential source material during anatexis. The identified age spectra also mimic age distributions for magmatism during lithospheric-scale crustal reworking and granitoid emplacement, particularly at c. 1.9 and 1.8 Ga (e.g., Condie et al. 2009).

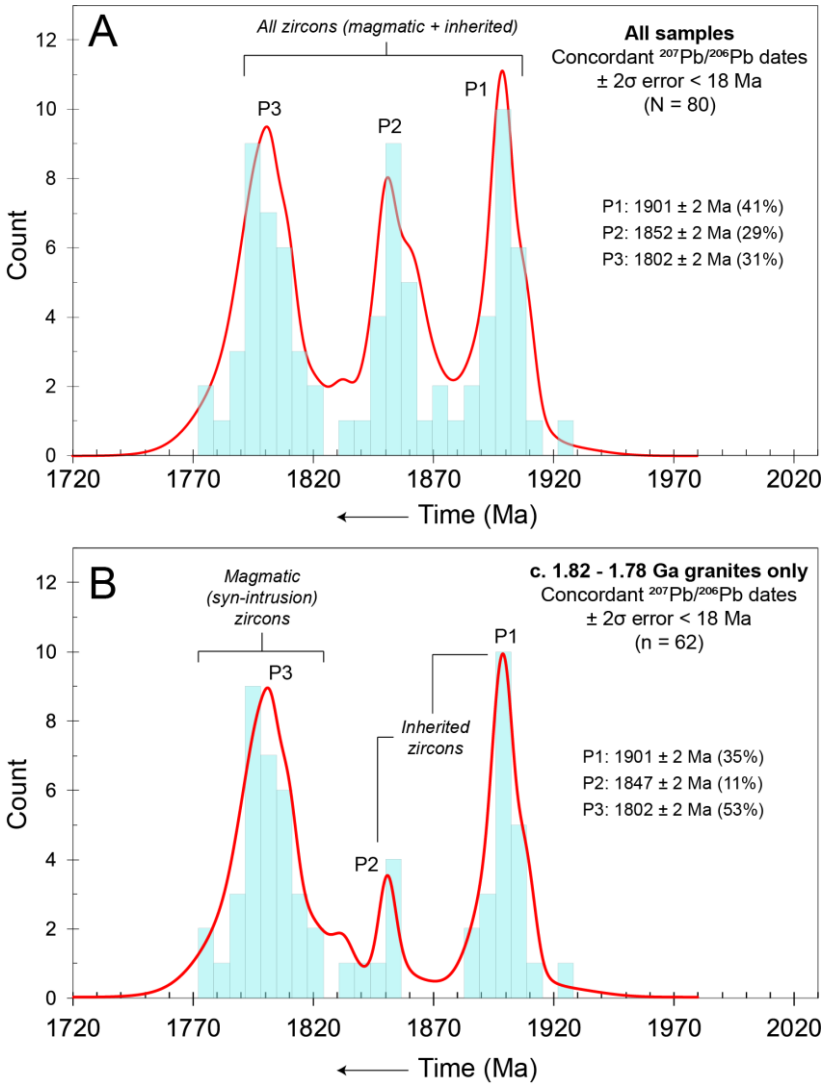

Figure 28. Combined probability density plots and binned frequency histograms for concordant single zircon $^{207}Pb/^{206}Pb$ dates with 2σ errors ≤ 18 Ma (median error). The plots show the temporal distribution of igneous and inherited age signatures in **A.** all dated samples, and **B.** granites with c. 1.81–1.78 Ga crystallisation ages. P1–P3 peak values and relative fractions are based on a Gaussian deconvolution of the probability density curves (red lines) using the method of Sambridge & Compston (1994). Background histogram bin size = 7 Ma.

From a regional perspective, the new U-Pb dates are consistent with previously reported c. 1.82–1.77 Ga igneous ages for Late Svecofennian granitic rocks both in western Bergslagen and elsewhere across the district (e.g., Patchett et al. 1987, Romer & Smeds 1994, Öhlander & Romer 1996, Persson & Persson 1997, Romer & Smeds 1997, Andersen et al. 2009, Johansson 2019, Johansson 2020). The new ages are also coeval with continental arc-type magmatism associated with the adjacent Transscandinavian Igneous Belt (TIB); namely c. 1.81–1.79 Ga TIB-1a mafic-felsic plutonic rocks occurring in the Östergötland-North Öland areas to the south of Bergslagen (e.g., Kleinhanns et al. 2015, Salin et al. 2019) and c. 1.79–1.77 Ga TIB-1b mafic-felsic plutonic rocks occurring along the western and north-western margins of Bergslagen (e.g., Rutanen & Andersson 2009), and in the Småland-South Öland areas in southern Sweden (Johansson 2016, Salin et al. 2019). This temporal overlap at c. 1.81–1.77 Ga suggests the prevailing subduction regime produced different petrogenetic outcomes depending on relative position within the arc system, with the dated GP-suite granites marking infracrustal felsic magmatism within an upper plate retro-arc setting. Alternatively, spatially decoupled tectonic processes could have been active at the same time producing compositionally distinct magmatism in separate lithotectonic terranes (see below).

Although the geochronology samples in this study are from a limited geographical area and the U-Pb results partly reflect the analysis of metamict zircons, the c. 30-to-40-million-year age range for the dated granitic rocks is shorter than previous estimates for the duration of GP-related magmatism in Bergslagen based on regional geochronology assessments. For example, in the compilation of Stephens et al. (2009), zircon and monazite U-Pb ages indicate GP suite granitic rocks formed during a protracted (c. 110 million year) episode from c. 1.86–1.75 Ga, with two successive events occurring from c. 1.86–1.83 Ga and c. 1.83–1.75 Ga. In the review of Stephens & Jansson (2020), igneous ages of GP suite granitic rocks mark two temporally discrete magmatic events. The first is an older c. 1.86–1.83 Ga event forming volumetrically minor leucogranite in eastern Bergslagen that post-dates regional high-strain deformation and migmatization (i.e., syn- to late-'Tectonic cycle 2' event described in Stephens & Jansson 2020). The second is a younger c. 1.82–1.75 Ga event representing a major granite-forming episode that may have overlapped with or directly followed late-orogenic (M_3/D_3?) metamorphism and crustal shortening (cf. Stephens & Andersson 2015). In contrast to the above assessments, Åhäll & Larsson (2000) identified a shorter c. 1.82–1.77 Ga emplacement episode for 'post-kinematic' granitic rocks within the Swedish Svecofennian domain and noted their contemporaneity with TIB-1 arc magmatism occurring to the west at that time.

Given the U-Pb dating results obtained from this study (Fig. 27, Table 4) and the large number of similar c. 1.82–1.78 Ga igneous ages for GP-type granites elsewhere in Bergslagen (cf. Åhäll & Larsson 2000), the emplacement of most GP-suite intrusions was likely confined to a relatively short tectonothermal epoch at c. 1.82–1.78 Ga. Recent redating of GP suite granites with previously determined younger (c. 1.75 Ga) and/or imprecise (> ± 20 Ma) U-Pb dates has yielded more robust c. 1.80–1.79 Ga crystallisation ages (e.g., Johansson 2019, Lynch et al. 2019) thus reenforcing the idea of a more temporally focused emplacement event for GP-suite granites.

In contrast to the above, the general paucity of 'GP-like' leucogranites with c. 1.85–1.84 Ga igneous ages (cf. Stephens & Jansson 2020) and the confinement of known examples to eastern Bergslagen (e.g., Forsmark area) suggests older GP-suite granites, although texturally and compositionally similar, lack consanguinity with the younger c. 1.82–1.78 Ga granites and probably mark an earlier phase of crustal anatexis in response to regional M_2/D_2 tectonothermal events at c. 1.85–1.83 Ga. Moreover, the absence of a clear spatial or genetic association between older c. 1.85 Ga granitic rocks assigned to the GP suite (e.g., Stephens et al. 2009) and known skarn- or pegmatite-hosted lithophile element mineralisation supports the idea that younger c. 1.82–1.78 Ga granites represent a temporally, compositionally, and genetically distinct plutonic

suite. Reassignment of older c. 1.85–1.83 Ga 'GP-type' leucogranites in Bergslagen to an alternative or new igneous suite is warranted to minimise the conflation of separate granite-forming episodes that developed in response to regional tectonothermal events occurring at different times.

Granite petrogenesis

The petrological and geochemical character of the investigated c. 1.8 Ga granitic rocks affirms the compositionally evolved and restricted nature of Late Svecofennian (GP-type) granites in western Bergslagen (cf. Sundblad et al. 1993, Bergman et al. 1995, Ahl et al. 2001, Stephens et al. 2009). The predominance of syenogranite to alkali feldspar granite types, their common association with late-stage aplite-pegmatite bodies, the relatively low abundance of mafic minerals (mainly biotite), and their high-silica and lithophile element contents (particularly for the skarn-proximal intrusions) attests to their highly differentiated nature. Moreover, the occurrence of intragranitic Mo ± F mineralisation within some intrusions (e.g., Pingstaberg, Bispbergs klack) and the spatiotemporal association between others and skarn W ± Mo ± F ± Cu mineralisation (e.g., Wigström-Högberget) further supports the idea that c. 1.8 Ga granitic rocks derived from 'specialised' felsic magmas with the potential to produce magmatic-hydrothermal Mo-W-Cu-F ± Sn mineralisation.

The comparable petrological, petrophysical and geochemical features of the investigated granitic rocks and their overlapping c. 1.82–1.78 Ga emplacement ages justifies their assessment as a grouped, cogenetic igneous suite. Overall, the main geochemical trends indicate variable degrees of fractionation for the GP-suite samples, with skarn-proximal intrusions in the NW having compositions that indicate the highest degree of differentiation (e.g., Figs. 19–22). Decreasing FeOt and MgO values relative to TiO_2, and covariation trends evident for certain high field strength elements (e.g., Ta, Zr, V, Sc) are consistent with plagioclase, biotite, magnetite, and zircon fractionation (Fig. 19). Relative to an average upper continental crust composition (Taylor & McLennan 1981), the c. 1.8 Ga granitic rocks have elevated Rb, Th, U, K, and heavy (H)REE contents, and show depletions in Ba, Sr, P, Ti and light (L)REE values which further emphasises compositional traits mainly controlled by variable K-feldspar, plagioclase, and mafic mineral abundances (cf. Fig. 20B–C).

Chondrite-normalized REE signatures corroborate a regional 'fractionation trend' for the c. 1.8 Ga granitic rocks and show a systematic flattening of REE patterns when comparing the SE intrusions to those in the NW (Fig. 21B–C). In particular, the REE patterns for skarn-proximal barren and mineralised granites reflect lower La_N/Yb_N values, have more pronounced negative Eu anomalies, show progressive HREE enrichments, and have lower total REE abundances compared to the skarn-distal intrusions that straddle the WBBZ (e.g., Fig. 21 & 22A–B). Although the REE patterns for skarn-proximal and mineralised samples may partly reflect fluid-rock interactions that cause the preferential leaching of LREEs (cf. Samson & Wood 2005), collinearity trends for total REE and La_N/Yb_N versus FeO, Zr/Hf and Gd_N/Yb_N values (Fig. 22A–C) suggests fractionation of plagioclase and REE-bearing accessory minerals (e.g., apatite, monazite, and fluorite) likely influenced the observed REE patterns.

Overall, the trace element data indicate parental magmas associated with the skarn-proximal granites in the NW underwent more pronounced degrees of differentiation during ascent and/or emplacement compared to granites in the SE and other comparable GP-suite intrusions in western Bergslagen. Additionally, local variability in the composition and relative oxidation state of melt source rocks and/or the degree of pre-melting element enrichment (via earlier weathering, metasomatism or anatexis) may have influenced granite compositional variations and mineralisation potential either side of the WBBZ (cf. Sato 2012, Romer & Kroner 2016).

Alternatively, local variations in the exposed erosion level may have resulted in the selective preservation of high crustal level, late-stage differentiated granites in the NW compared to marginally more deeper-seated bodies preserved SE of the WBBZ.

Tectonic discrimination diagrams provide additional insights into the petrogenesis of the c. 1.8 Ga granitic rocks (Fig. 29). On the classification plot of Sylvester (1989) for post-collisional granites (Fig. 29A), the analysed samples cluster mainly within the overlapping 'calc-alkaline-highly-fractionated' and 'alkaline' granitoid field reflecting their elevated silica and total alkali contents (cf. Ahl et al. 2001). On the discrimination plots for alkaline/anorogenic (A-type) granites of Whalen et al. (1987), the samples show a weak linear spread between the 'A-type' and 'highly fractionated felsic granite' fields (Fig. 29B–C) reflecting major and trace element compositional variations with increasing degree of fractionation (cf. Fig. 20C). These plots also highlight compositional overlaps for highly evolved I-, S- and A-type granites which tend to converge toward the 'highly fractionated felsic granite' field with increasing magmatic differentiation (cf. Whalen et al. 1987). On a Ce versus Ga/Al plot (Fig. 29D), the granitic rocks fall within the A-type granite field with a trend toward lower Ce values for the skarn-proximal mineralised granitic rocks reflecting LREE depletion that may be partly controlled by subsolidus alkali metasomatism (cf. Fig. 21C). On the ternary plots for A-type granites from Eby (1992), the samples mainly fall within the A2 field for A-type granites formed by the remelting of continental crust that previously underwent an earlier tectonic/weathering cycle (Fig. 29E). This classification is consistent with the setting and emplacement ages of the granites which mark the waning stages of regional c. 1.9–1.8 Ga orogenesis in Bergslagen.

On trace element diagrams that discriminate between continental arc, slab failure and A-type granitoids (Fig. 30), a subset of 27 samples filtered for ASI values < 1.1 were plotted to further assess the origins of the granitic rocks. Although these diagrams are not recommended for granitoid samples with SiO_2 contents > 70 wt. % (and ASI values > 1.1 also), high-silica samples with Nb + Y > 60 ppm and Ta + Yb > 6 ppm may be used to assess A-type granite affinities (cf. Whalen & Hildebrand 2019). For the plots that utilise REE ratios (Fig. 30A–B; Hildebrand & Whalen 2017; Hildebrand et al. 2018), the samples form a negative linear array from the slab failure to arc fields, with skarn-distal barren granites in the SE and NW mainly plotting within the former field. Given their low Sr/Y contents (< 10), moderately sloping to flat normalized REE signatures (e.g., Fig. 21), and their restricted unimodal (granitic) character, these data trends likely reflect granite parental magma fractionation rather than petrogenetic setting. This interpretation, particularly for the skarn-distal barren granites, is supported by compositional dissimilarities between GP-suite granitic rocks and 'adakite-like' slab failure magmas which typically show high Sr/Y (> 20) and La/Yb (> 10) ratios, and lack pronounced negative Eu anomalies (i.e., Eu/Eu* > 0.9).

On plots that incorporate immobile high field strength elements (e.g., Ta, Nb, Y; cf. Whalen and Hildebrand 2019), the samples straddle the slab failure and A-type boundary, with most falling within the A-type granite field (Fig. 30C–F). On the Nb/Y vs Nb + Y and Nb vs Y plots (Fig. 30D & F, respectively), the samples fall within the A2 field for A-type granites suggesting anatexis of pre-existing (c. 1.85–1.90 Ga) continental source rocks, likely geochemically modified by earlier subduction-related processes, was a major control on granite melt formation (cf. Fig. 29E). Overall, these signatures indicate parental magmas formed via anatexis of a feldspar-rich, mafic to intermediate granulitic source at lower to mid crustal levels. The melts underwent a degree of compositional modification during ascent and emplacement in a late-orogenic setting, producing a suite of A-type granites with a meta-igneous source heritage.

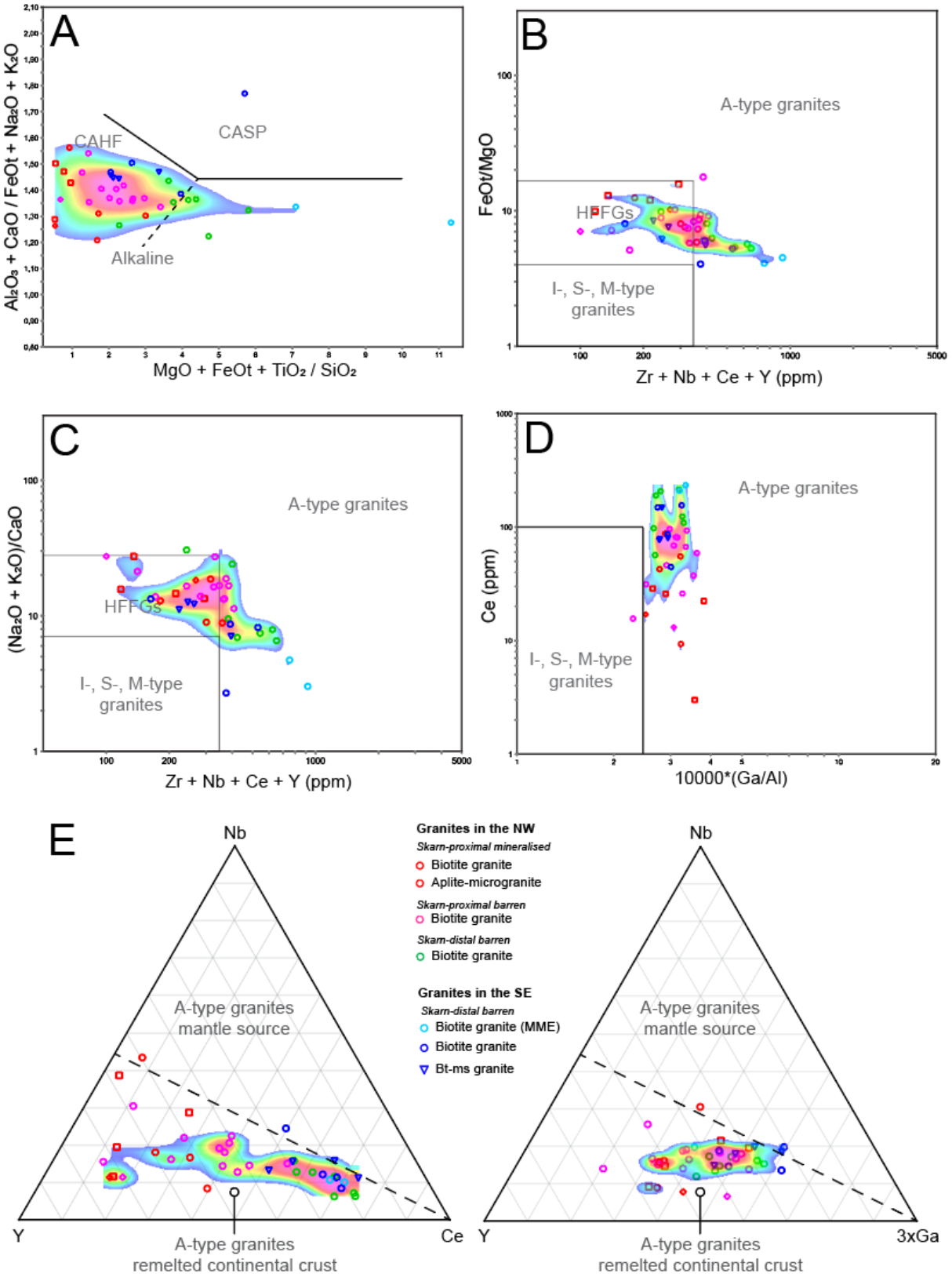

Figure 29. Granitoid discrimination plots for the c. 1.8 Ga granitic rocks. Background point density clouds are based on the number of sample points within a 30 × 30 unitless grid cell and visualise sample distribution maxima (red-pink shades) and geochemical data trends. Legend in E apllies to all plots. **A.** Collisional granites plot from Sylvester (1989). **B.** Ce vs 10000*Ga/Al (Whalen et al. 1987). **C.** FeOt/MgO vs Zr+Nb+Ce+Y (Whalen et al. 1987). **D.** (Na_2O+K_2O)/CaO vs Zr+Nb+Ce+Y (Whalen et al. 1987). **E.** Nb-Y-Ce and Nb-Y-3xGa ternary plots for A-type granites (Eby 1992). Abbreviations; A = anorogenic, I = igneous, S = sedimentary, M = mantle, CASP = Calc-alkaline and strongly peraluminous, CAHF = calc-alkaline and highly fractionated. HFFGs = highly fractionated felsic granites (both I- and S-types).

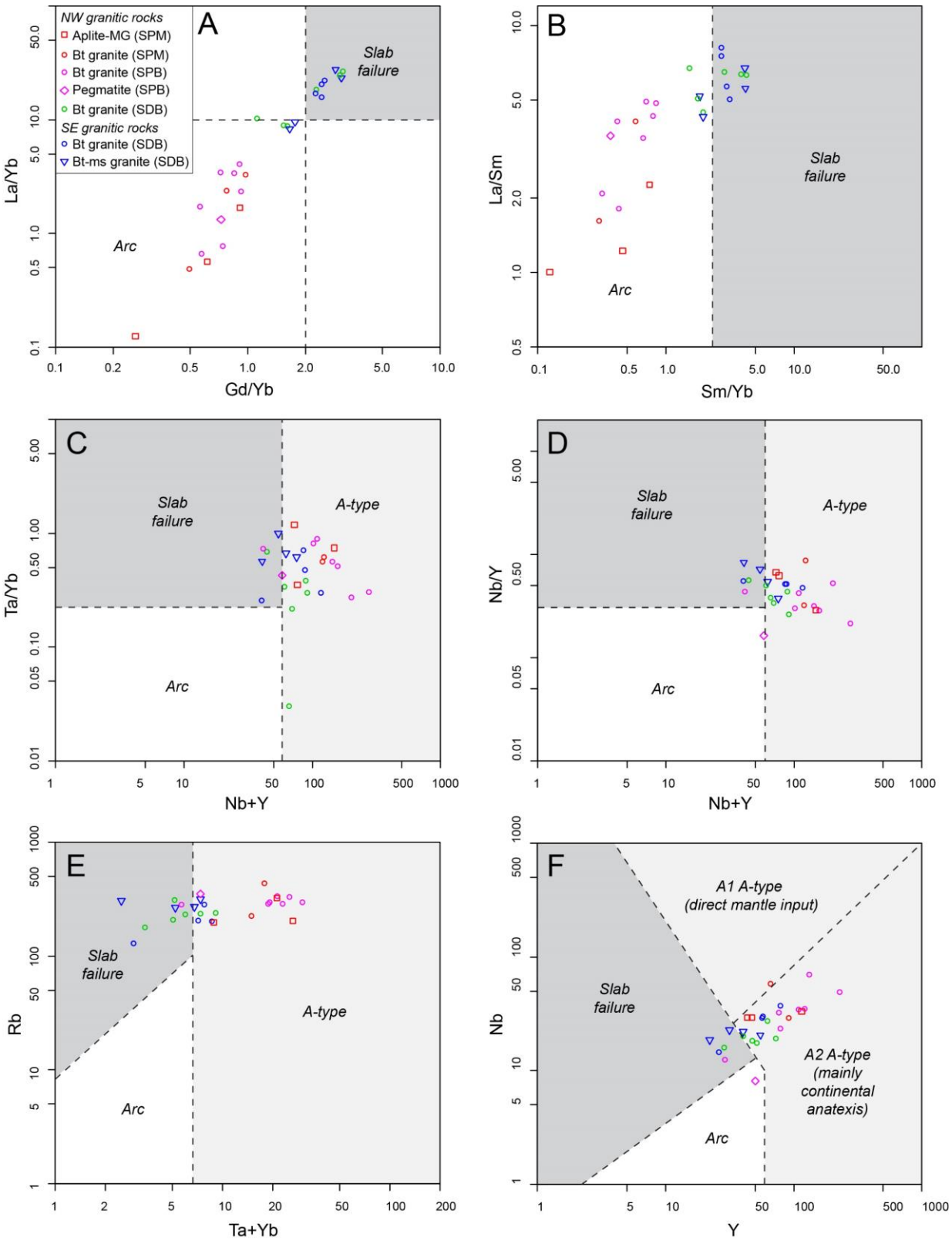

Figure 30. Selected tectonic discrimination diagrams (Hildebrand & Whalen 2017; Hildebrand et al. 2018; Whalen & Hildebrand 2019) showing GP-suite granitic samples with ASI values < 1.1 from western Bergslagen. Legend and SiO_2, Sr/Y ranges in plot (A) apply to other plots also. **A.** La/Yb v. Gd/Yb. **B.** La/Sm v. Sm/Yb. **C.** Ta/Yb v. Nb + Y. **D.** Nb/Y v. Nb + Y. **E.** Rb v. Ta + Yb. **F.** Nb v. Y. The A1 and A2 fields in plots D and F are for within-plate mantle-related and recycled continental crust A-type granites, respectively, and are from Eby (1992). Abbreviations: MG = microgranite; ORG = oceanic ridge granite, SPM = skarn-proximal mineralised, SPB = skarn-proximal barren, SDB = skarn-distal barren.

Based on the Sm-Nd isotopic results from this work (Table 6) and published data, potential source components for GP granite parental magmas are c. 1.90 - 1.89 Ga meta-igneous and/or metasedimentary rocks, with a possible subordinate input of reworked c. 1.86–1.84 Ga meta-igneous rocks (Fig. 31). The mainly positive initial εNd values suggest a juvenile crustal source without input of older, more isotopically mature (i.e., negative) crustal material, as envisaged by the Nd isotopic evolution of the Archean Norrbotten craton. The remelting of pre-existing Bergslagen continental crust likely resulted in felsic magma production and granite formation at c. 1.80 Ga. Possible tectonic mechanisms that drove anatexis are the upwelling of lithospheric mantle melts into the base of the crust and/or decompression melting associated with a phase of tectonic relaxation and extension during regional transpressive deformation. Coeval TIB-1 magmatism at c. 1.8 Ga also suggests that ongoing subduction processes could have contributed to the generation of granite parental melts in the overriding plate through the input of mafic melts or advective heat supply to lower to middle crustal levels.

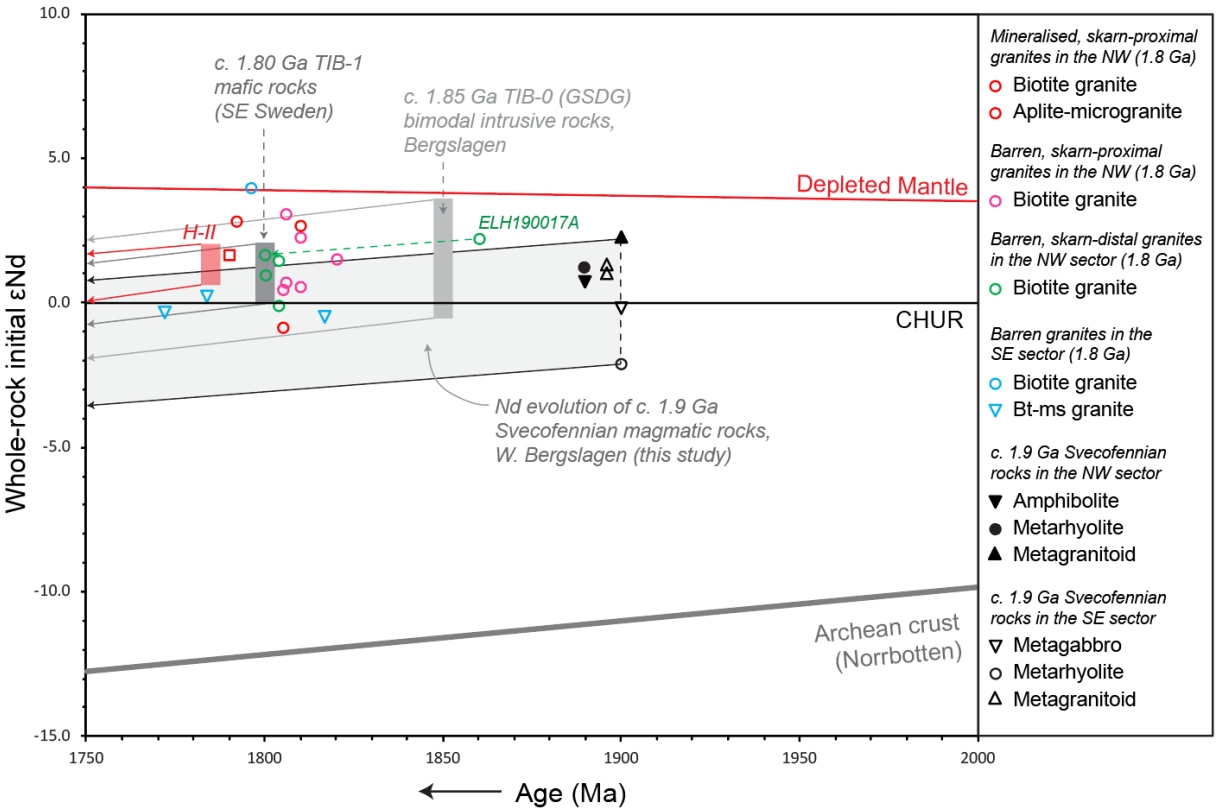

Figure 31. Initial εNd versus time plot for Svecofennian c. 1.8 Ga granite and c. 1.9 Ga intrusive and metasupracrustal rocks in western Bergslagen. Age distributions based on U-Pb dating results listed in Table 4, without errors depicted. Data points for sample ELH190017A (Malingsbo granite) connected by dashed green line represent initial εNd values calculated at 1.86 Ga and 1.80 Ga (see main text for discussion). Depleted mantle evolution line from DePaolo (1981). Norrbotten Archean crust evolution line based on Öhlander et al. (1987). Data range for c. 1.85 Ga TIB-0 bimodal intrusive rocks taken from Patchett et al. (1987), Valbracht et al. (1994), and Andersson (1997) — as listed in Stephens et al. (2009) as 'GSDG suite' rocks. Data range for c. 1.80 Ga TIB-1 mafic rocks from Andersson et al. (2007). Data range for the Hedesunda granite (H-II), northern Bergslagen, from Johansson (2020).

A petrogenetic association between the GP suite granites and a regional metamorphic event is presently unclear. Since localised migmatization and deformation is envisaged at c. 1.84–1.81 Ga in Bergslagen (Stephens & Andersson 2015, Stephens & Jansson 2020), GP suite granites may represent a delayed, indirect anatectic response to focused episodes of deformation and tectonic activity at c. 1.8 Ga, although the present data suggests deformation mainly predates GP granite emplacement. Overall, the spatial distribution of GP suite granites suggests these rocks predominantly record a magmatic 'flare-up' at c. 1.82–1.78 Ga in Bergslagen. Such focused felsic, and alkaline magmatic episodes typically mark a waning orogenic stage during a switch from net compressive to extensional tectonics. A younger example is the emplacement of Late Devonian granites associated with Mo ± W ± F ± Sn mineralisation in the Appalachian orogen of eastern Canada (e.g., Van Staal 2007).

Metallogenic implications

In general, GP suite granitic rocks in western Bergslagen have compositional features consistent with evolved granites associated with lithophile and/or critical element mineralisation typically found in late-orogenic, post-subduction settings (cf. Černý et al. 2005, Pirajno 2009, Ludington & Plumlee 2009, Richards 2011, Lehmann 2021). Specifically, their high-silica, total alkali and lithophile element contents (e.g., Th, U, Rb), and the association of some intrusions with intragranitic or skarn Mo ± W ± F ± Cu mineralisation (e.g., Pingstaberg and Wigström-Högberget, respectively) attests to the evolved or 'specialised' nature of the intrusions. The occurrence of rare metal-bearing pegmatites (Li, Ta, Nb, Yb) within or adjacent to c. 1.8 Ga granitic rocks elsewhere in Bergslagen (e.g., Smeds 1994, Romer & Smeds 1997) further highlights the proclivity of GP suite parental magmas to develop highly fractionated, incompatible element-enriched granitic intrusions with mineralisation potential.

Both a temporal and genetic link between c. 1.8 Ga granitic rocks in the NW sector and known skarn W ± F ± Cu ± Mo deposits and prospects is supported by the molybdenite Re-Os dating results (Table 5). In summary, granite- and skarn-hosted molybdenite samples gave Re-Os ages between 1802 and 1770 Ma (n = 5) and thus identify a mineralisation epoch that overlaps with the zircon U-Pb ages obtained for the dated granitic intrusions (cf. Fig. 27). At the Wigström deposit, skarn-hosted molybdenite dated to c. 1800 Ma overlaps with an imprecise zircon U-Pb date of c. 1.79 Ga for a microgranite dyke in the deposit hanging wall (Fig. 26D, Table 4) and an imprecise igneous age of c. 1.79 Ga for the adjacent Högberget granite as reported by Plan (2020). Likewise, disseminated molybdenite from the Bispbergs klack granite yielded a Re-Os age of 1792 ± 10 Ma which overlaps with the zircon U-Pb age of 1787 ± 24 Ma acquired for the same intrusion (cf. Fig. 26F & Table 4). Overall, these correlations highlight contemporaneity between leucogranite emplacement at c. 1.8 Ga and regional W ± Mo ± F mineralisation, while the elemental and mineralogical tenor of the proximal skarn systems and the generally evolved character of the leucogranites indirectly affirms a genetic relationship.

A trend toward more evolved, metalliferous granites in NW Bergslagen is shown by granite redox signatures (e.g., Fe_2O_3/FeO ratios, Fig. 23A) and covariation trends between F and other mineralisation-related elements such as S, Mo, Cu, K_2O (Fig. 23C–F). For the skarn-proximal granites, Fe_2O_3/FeO ratios suggest an intermediate (mildly oxidized) redox state which could have supressed early sulfide precipitation in the melt, leading to the retention of Mo, Cu and U in parental magmas (e.g., Blevin 2004, Richards 2015). Elevated F contents for the skarn-proximal granites, although partly reflecting subsolidus metasomatic effects, also suggests volatile elements (e.g., F, Cl, B, S) could have helped lower the melt solidus thus prolonging magma fractionation and increasing the potential for parental magmas to evolve and develop late-stage, fluid- and lithophile element-enriched residual melts (e.g., Pirajno 2009, Bartels et al. 2011).

Although granite parental magma composition likely represents a key controlling factor for the development of 1.8 Ga skarn and intragranitic mineralisation in Bergslagen, other local factors at the site of deposition may also have been important. For example, bulk fluid composition, syn-emplacement brittle deformation (e.g., hydrofracturing and faulting), and the availability of lithological trap rocks (e.g., marble horizons) are other key factors that likely contributed to the development of the skarn W deposits in the study area.

From an exploration perspective, the assessment or 'screening' of leucogranites favourable for lithophile and/or critical element (W-F ± Mo ± Cu) mineralisation in Bergslagen or other parts of the Paleoproterozoic bedrock in Sweden should focus on identifying evolved intrusions with 'Late Svecofennian' ages (i.e., c. 1.81–1.78 Ga). Such granites should exhibit petrological and/or geochemical evidence of high degrees of magma fractionation and lithophile element enrichment including internal aplite-pegmatite variants, potassic ± greisen alteration, and elevated SiO_2, total alkali, Rb, Ta, Th, U, and Y contents (cf. Candela 1993, Černý et al. 2005). Lithogeochemical analysis of FeO, B and F contents should also be undertaken to aid the identification of potentially metalliferous intrusions and assess favourable geochemical trends. A close spatial proximity (< 1 km) between potentially productive granites and supracrustal marble horizons is considered a favourable condition for exocontact skarn W-F ± Mo ± Cu mineralisation (cf. Pirajno 2009). Additionally, since elevated volatile element contents (e.g., Li, F, Be, H_2O) in late-stage magmas can aid residual melt migration and pegmatite zonation (e.g., Černý 1992), more distal environs (> 1–8 km) adjacent to suitable granites may be prospective for rare metal-bearing pegmatite discovery.

CONCLUSIONS

The following main conclusions can be taken from this study:

1. Late Orosirian (c. 1.8 Ga) granitic rocks in western Bergslagen assigned to the Granite-Pegmatite (GP) intrusive rock suite (e.g., Stephens et al. 2009) predominantly comprise locally deformed to more commonly massive syenogranite to alkali feldspar granite (*sensu stricto*).

2. The granites are medium- to coarse-grained, equigranular to K-feldspar megacrystic intrusions containing biotite as the main mafic mineral. Country rock xenoliths and larger inlier blocks are relatively common (e.g., Malingsbo batholith), while mafic microgranular enclaves also occur in some granites (e.g., Enkullen granite). Late-stage pegmatite-aplite segregations, dykes and vein dykes are relatively common feature also and are typically unzoned.

3. Geochemically, the granites are high-silica, peraluminous, ferroan intrusions with elevated total alkali, Th, U, and Rb contents, and depleted CaO, MgO, TiO_2, P_2O_5, Ba, Sr, Zr and total REE concentrations. Based on major and trace element contents, they exhibit fractionated I-type to A2-type signatures reflecting a late-orogenic, within plate tectonic setting. Major and trace element geochemical trends indicate an increasing degree of differentiation from SE to NW across the Western Bergslagen boundary zone (WBBZ), with intrusions proximal to skarn tungsten mineralisation or containing disseminated Mo ± F mineralisation in the NW representing the most compositionally evolved bodies.

4. Granite samples from Hörken, Pingstaberg, and Wigström have similar density, magnetic susceptibility, and magnetic remanence properties. The granite at the Wigström deposit has a lower density and a higher magnetic remanence than the Malingsbo granite, but the two granites cannot be separated based on magnetic susceptibility. On a regional scale, a trend toward lower magnetic susceptibility and density values is evident for barren to mineralisation-proximal granites.

5. Zircon U-Pb SIMS dating constrains the timing of granite emplacement to c. 1.82–1.78 Ga, with older tectonothermal events also identified at c. 1.85 G and 1.89 Ga. Inherited zircons in the c. 1.8 Ga granitic rocks mark two source component events at c. 1.90 and 1.85 Ga which overlap with major periods of Orosirian continental growth in the Swedish Svecofennian domain. The inherited age peaks and the occurrence of xenoliths in GP suite granitic rocks support the idea of parental magmas mainly derived from reworked Svecofennian continental crust.

6. The combined geochemical and Sm-Nd isotopic data suggest granite parental magmas formed by anatexis of existing Svecofennian juvenile continental crust. Input of sub-continental lithospheric material as a potential heat source that drove crustal melting events may also have occurred.

7. Re-Os ages for intragranitic and skarn-hosted molybdenite overlap with the zircon U-Pb dating results and identify a relatively short, c. 1.80–1.77 Ga granite-related metallogenic epoch in western Bergslagen.

8. Multiple factors operating at different scales likely contributed to granite- and skarn-related W ± F ± Mo ± Cu mineralisation in western Bergslagen. These include the overall 'late-orogenic' tectonic setting, parental magma composition and degree of fractionation, and local deposit-scale controls such as the availability of wall rock carbonate horizons susceptible to skarn metasomatism by magmatic fluids, and syn-emplacement brittle deformation that would have promoted focused fluid exsolution.

9. From an exploration perspective, the identification or 'screening' of granitic rocks with potential for critical element (W ± Mo ± F) mineralisation either in Bergslagen or other parts of the Paleoproterozoic bedrock of Sweden should focus on leucogranites with 'Late Svecofennian' ages (c. 1.81–1.78 Ga) and comparable petrological, geochemical and petrophysical properties to those outlined in points 2, 3 and 4 above.

ACKNOWLEDGMENTS

We thank George Morris, Jenny Andersson, and Alexander Lewerentz (SGU) for assistance with zircon sample preparation and imaging. Anders Plan (Lund University) is thanked for additional zircon preparation work and interesting discussions on Bergslagen granite-skarn systems. Heejin Joen, Martin Whitehouse and Kerstin Lindén are thanked for assistance with zircon U-Pb SIMS analysis at the Nordsim Lab, Stockholm. Karin Högdahl (Uppsala University) and David Selby (Durham University, UK) are thanked for assistance with molybdenite sample preparation and the Re-Os geochronology work. Reviews by Magnus Ripa, Lena Persson and Ildikó Antal Lundin (SGU) improved this report.

REFERENCES

Abdel-Rahman, A.-F.M., 2001: Peraluminous plutonism: Nature and origin of the Moly Max leucogranite and its coast plutonic complex granitic host-rocks, northwestern British Columbia. *The Canadian Mineralogist* 39, 1181–1196.

Åberg, G. & Bjurstedt, S., 1988: Radiometric dating of the serorogenic Svecokarelian Enkullen and Fjällberg granites, south central Sweden. *Geologiska Föreningens i Stockholm Förhandlingar 108,* 73–77.

Åhäll, K.-I. & Larson, S. Å. 2000: Growth-related 1.85–1.55 Ga magmatism in the Baltic shield; a review addressing the tectonic characteristics of Svecofennian, TIB 1-related, and Gothian events. *GFF 122,* 193–206.

Ahl, M., Bergman, S., Bergström, U., Eliasson, T., Ripa, M. & Weihed, P., 2001: Geochemical classification of plutonic rocks in central and northern Sweden. *Sveriges geologiska undersökning Rapporter och Meddelanden 106,* 82 pp.

Andersen, T., Andersson, U.B., Graham, S., Åberg, G. & Simonsen, S.I., 2009: Granitic magmatism by melting of juvenile continental crust: new constraints on the source of Palaeoproterozoic granitoids in Fennoscandia from Hf isotopes in zircon. *Journal of the Geological Society, London 166*, 233–247

Andersson, U.B., 1997: Petrogenesis of some Proterozoic granitoid suites and associated basic rocks in Sweden (geochemistry and isotope geology). *Sveriges geologiska undersökning Rapporter och meddelanden 91,* 216 pp.

Andersson, U. B., Rutanen, H., Johansson, Å., Mansfeld, J. & Rimša, A., 2007: Characterization of the Paleoproterozoic mantle beneath the Fennoscandian Shield: Geochemistry and isotope geology (Nd, Sr) of~ 1.8 Ga mafic plutonic rocks from the Transscandinavian Igneous Belt in southeast Sweden. *International Geology Review 49,* 587–625.

Arndt, N.N. & Goldstein, S.L., 1987: Use and abuse of crust-formation ages. *Geology 15,* 893–895.

Artemieva, I. M., Thybo, H., Jakobsen, K., Sørensen, N. K. & Nielsen, L. S., 2017: Heat production in granitic rocks: Global analysis based on a new data compilation GRANITE2017. *Earth-Science Reviews 172*, 1–26.

Baker, T., Pollard, P.J., Mustard, R., Mark, G. & Graham, J.L., 2005: A comparison of granite-related tin, tungsten, and gold-bismuth deposits: Implications for exploration. *Society of Economic Geologists Newsletter 61,* 5–17.

Ballouard, C., Poujol, M., Boulvais, P., Barnquest, Y., Tartese, R. & Vigneresse, J.-L., 2016: Nb-Ta fractionation in peraluminous granites: A marker of the magmatic-hydrothermal transition. *Geology* 44, 231–234.

Bartels, A., Vetere, F., Holtz, F., Behrens, H. & Linnen, R.L., 2011: Viscosity of flux-rich pegmatitic melts. *Contributions to Mineralogy and Petrology 162*, 51–60.

Bergman, S., Lynch, E. & Berggren, R., 2020: Styrning av W-Mo-mineralisering i granit-pegmatitsvitens intrusioner i Bergslagen. *SGU-rapport 2020:07*. Sveriges geologiska undersökning, 19 pp.

Bergman, S., Stephens, M.B., Andersson, J., Kathol, B. & Bergman, T., 2012: Sveriges berggrund, skala 1:1 miljon. *Sveriges geologiska undersökning K 423*.

Bergman, T., 2012: Western Bergslagen W-Mo. *In* P. Eilu (Ed.): Mineral deposits and metallogeny of Fennoscandia. *Geological Survey of Finland Special Paper 53*, 162.

Bergman, T., Schöberg, H. & Sundblad, K., 1995: Geochemistry, age, and origin of the Högberget granite, western Bergslagen, Sweden. *GFF 117*, 87–95.

Beunk, F.F. & Kuipers, G., 2012: The Bergslagen ore province, Sweden: Review and update of an accreted orocline, 1.9–1.8 Ga BP. *Precambrian Research 216–219*, 95–119.

Billström, K., Åberg, G. & Öhlander, B., 1988: Isotopic and geochemical data of the Pingstaberg Mo-bearing granite in Bergslagen, south central Sweden. *Geologie en Mijnbouw 67*, 255–263.

Blengini, G.A., Latunussa, C.E.L., Eynard, U., Torres de Matos, C., Wittmer, D., Georgitzikis, K., Pavel, C., Carrara, S., Mancini, L., Unguru, M., Blagoeva, D., Mathieux, F. & Pennington, D., 2020: *European Commission, Study on the EU's list of Critical Raw Materials – Final Report (2020).* Publications Office of the European Union, Luxembourg, 153 pp.

Blevin, P.L., 2004: Redox and compositional parameters for interpreting the granitoid metallogeny of eastern Australia: Implications for gold-rich ore systems. *Resource Geology 54*, 241–252.

Blevin, P.L. & Chappell, B.W., 1995: Chemistry, origin and evolution of mineralized granites in the Lachlan Fold Belt, Australia: The metallogeny of I- and S-type granites. *Economic Geology 83,* 305–316.

Boynton, W.V., 1984: Geochemistry of the rare earth elements: meteorite studies. *In P.* Henderson (ed.): *Rare Earth Element Geochemistry*. Elsevier, 63–114.

Candela, P.A., 1997: A review of shallow, ore-related granites: Textures, volatiles and ore metals. *Journal of Petrology 38*, 1619–1633.

Černý, P., 1991: Rare-element granitic pegmatites. Part II: Regional to global environments and petrogenesis. *Geoscience Canada 18*, 2, 68–81.

Černý, P., 1992: Regional zoning of pegmatite populations and its interpretation. *Mitteilungen der Österreichischen Mineralogischen Gesellschaft 137*, 99–107.

Černý, P., Blevin, P.L., Cuney, M. & London, D., 2005: Granite-related ore deposits. *Economic Geology 100th Anniversary Volume*, 337–370.

Chappell, B.W. & White, A.J.R., 2001: Two contrasting granite types: 25 years later. *Australian Journal of Earth Sciences 48,* 489–499.

Chappell, B. W., Bryant, C. J. & Wyborn, D., 2012: Peraluminous I-type granites. *Lithos 153*, 142–153.

Condie, K.C., Belousova, E., Griffin W.L., Sircombe S.R., 2009: Granitoid events in space and time: Constraints from igneous and detrital age spectra. *Gondwana Research 15,* 228–242.

DePaolo, D.J., 1981: Neodymium isotopes in the Colorado Front Range and crust-mantle evolution in the Proterozoic. *Nature 291,* 193–196.

Eby, G. N., 1992: Chemical subdivision of the A-type granitoids: petrogenetic and tectonic implications. *Geology 20,* 641–644.

Faure, G. & Mensing, T.M., 2005 Isotopes. *Principles and Applications*. 3rd Ed., John Wiley & Sons, Inc., Hoboken, New Jersey. 897 pp.

Frost, B. R., Barnes, C. G., Collins, W. J., Arculus, R. J., Ellis, D. J. & Frost, C. D., 2001: A geochemical classification for granitic rocks. *Journal of petrology 42*, 2033–2048.

Halley, S., 2020: Mapping magmatic and hydrothermal processes from routine exploration geochemical analysis. *Economic Geology* 115, 489–503.

Hayes, T.S., Miller, M.M., Orris, G.J. & Piatak, N.M., 2017: Fluorine. *In* K.J. Schulz, J.H. DeYoung Jr, R.R. Seal II & D.C. Bradley (eds.): Critical mineral resources of the United States—Economic and environmental geology and prospects for future supply: *U.S. Geological Survey, Professional Paper 1802,* Chapter G, G1–G80.

Hellingwerf, R.H. & Baker, J.H., 1985: Wall-rock alteration and tungsten and molybdenum mineralizations associated with older granites in western Bergslagen, Sweden. *Economic geology 80*, 479–487.

Hellingwerf, R.H., Baker, J.H. & Van Raaphorst, J.G., 1987: Sulphur isotope data of Proterozoic molybdenites from western Bergslagen, Sweden. *Geologiska Föreningens i Stockholm Förhandlingar 109*, 33–38.

Herrmann, M., Söderlund, U, Scherstén, A., Næraa, T., Holm-Alwmark, S. & Alwmark, C., 2021: The effect of low-temperature annealing on discordance of U–Pb zircon ages. *Scientific Reports 11*:7079.

Hildebrand, R.S. & Whalen, J.B., 2017: The tectonic setting and origin of Cretaceous batholiths within the North American Cordillera: the case for slab failure magmatism and its significance for crustal growth. Geological Society of America, Special Paper 532, 1–113.

Hildebrand, R.S., Whalen, J.B. & Bowring, S.A., 2018: Resolving the crustal composition paradox by 3.8 billion years of slab failure magmatism and collisional recycling of continental crust. *Tectonophysics 734–735*, 69–88.

Högdahl, K., Gromet, L.P. & Broman, C., 2001: Low P - T Caledonian resetting of U-rich Paleoproterozoic zircons, central Sweden. *American Mineralogist 86*, 534–546.

Holmquist, P. J., 1906: Studien über die Granite von Schweden. *Bulletin of the Geological Institution of Uppsala VII*, 77–269.

Hübner, H., 1971: Molybdenum and tungsten occurrences in Sweden. *Sveriges geologiska undersökning Ca 46*, 29 pp.

Irber, W., 1999: The lanthanide tetrad effect and its correlation with K/Rb, Eu/Eu*, Sr/Eu, Y/Ho, and Zr/Hf of evolving peraluminous granitic suites. *Geochimica et Cosmochimica Acta 63*, 489–508.

Johansson, Å., 2016: U–Pb SIMS dating of some granitoids from eastern Blekinge, southern Sweden. *GFF 138,* 430–444.

Johansson, Å., 2019: A refined U–Pb age for the Stockholm granite at Frescati, east-central Sweden. *GFF 141*, 40–47.

Johansson, Å., 2020: The Paleoproterozoic Hedesunda granite complex, east-central Sweden, a composite intrusion. *International Journal of Earth Sciences 109,* 1991–2022.

Kesler, S.E., 2005: Ore-forming fluids. *Elements 1,* 13–18.

Kleinhanns, I.C., Whitehouse, M.J., Nolte, N., Baero, W., Wilsky, F., Hansen, B.T. & Schoenberg, R., 2015: Mode and timing of granitoid magmatism in the Västervik area (SE Sweden, Baltic Shield): Sr–Nd isotope and SIMS U-Pb age constraints. *Lithos 212–215,* 321–337.

Kurhila, M., Mänttäri, I, Vaasjoki, M., Rämö, O.T. & Nironen, M., 2011: U–Pb geochronological constraints of the late Svecofennian leucogranites of southern Finland. *Precambrian Research 190*, 1–24.

Lassner, E. & Schubert, W.-D., 2005: The history of tungsten (wolfram). International Tungsten Industry Association, Newsletter, June 2005, 6–11.

Lehmann, B., 2021: Formation of tin ore deposits: A reassessment. *Lithos 402–403,* 105756.

Le Bas, M.J. & Streckeisen, A.L., 1991: The IUGS systematics of igneous rocks. *Journal of the Geological Society*, *London 148,* 825–833.

Liew, T.C. & Hofmann, A.W., 1988: Precambrian crustal components, plutonic associations, plate environment of the Hercynian fold belt of central Europe: Indications from a Nd and Sr isotopic study. *Contributions to Mineralogy and Petrology 98*, 129–138.

Ludington, S. & Plumlee, G. S., 2009: Climax-type porphyry molybdenum deposits. *US Geological Survey Open-file Report 1215*.

Ludwig, K.R., 2012: User's manual for Isoplot 3.75. A geochronological toolkit for Microsoft Excel. *Berkeley Geochronology Center Special Publication No. 5,* 75 pp.

Lugmair, G.W. & Marti, K., 1978: Lunar initial $^{143}Nd/^{144}Nd$: differential evolution line of the lunar crust and mantle. *Earth and Planetary Science Letters 39,* 349–357.

Lundström, I., 1983: Beskrivning till berggrundskartan Lindesberg SV. *Sveriges geologiska undersökning Af 126*, 140 pp.

Lynch, E., Ripa, M., Selby, D. & Antal Lundin, I., 2019: Mo mineralization in western Bergslagen, Sweden, marks pre- and late-collisional tectonothermal events during Svecokarelian orogenesis. 15th Biennial Meeting of the Society for Geology Applied to Mineral Deposits. Glasgow, England.

Magnusson, N. H., 1940: Ljusnarsbergs malmtrakt. Berggrund och malmfyndigheter. *Sveriges geologiska undersökning Ca 30*, 1–188.

Magnusson, N.H. & Lundqvist, G., 1932: Beskrivning till kartbladet Nya Kopparberget. *Sveriges geologiska undersökning Aa175,* 1–91.

Meinert, L. D., 1995: Compositional variation of igneous rocks associated with skarn deposits – chemical evidence for a genetic connection between petrogenesis and mineralization. *Mineralogical Association of Canada Short Course Series 23*, 401–418.

Middlemost, E.A.K., 1994: Naming materials in the magma/igneous rock system. *Earth Science Reviews 37,* 215–224.

Mielke, P. & Winkler, H.G.F., 1979: Eine bessere Berechnung der Mesonorm für granitische Gesteine. *Neues Jahrbuch für Mineralogie-Abhandlungen 10,* 471–480.

Öhlander, B. & Romer, R.L. 1996. Zircon ages of granites occurring along the central Swedish gravity low, *GFF 118,* 217–225.

Öhlander, B., Skiöld, T., Hamilton, P. J. & Claesson, L. Å., 1987: The western border of the Archaean province of the Baltic Shield: evidence from northern Sweden. *Contributions to Mineralogy and Petrology 95*, 437–450.

Ohlsson, L.-G., 1979: Tungsten occurrences in central Sweden. *Economic Geology 74*, 1012–1034.

Pavel, C.C., Tzimas, E., Alves Dias, P. & Blagoeva, D.T., 2020: Raw and processed materials used in the European defense industry. *In* R. Fangueiro & S. Rana (eds.): *Advanced Materials for Defense 4,* Proceedings in Materials, Springer, pp. 1–16.

Partzsch, L., 2018: The new EU Conflict Minerals Regulation: Normative power in international relations? *Global Policy 9*, 479–488.

Patchett, P. J., Todt, W. & Gorbatschev, R., 1987: Origin of continental crust of 1.9–1.7 Ga age: Nd isotopes in the Svecofennian orogenic terrains of Sweden. *Precambrian Research 35,* 145–60.

Persson, L. & Persson, P.-O., 1997: U-Pb datings of the Hedesunda and Åkersberga granites of south-central Sweden. *GFF 119,* 91–95.

Pirajno, F., 2009: *Hydrothermal Processes and Mineral Systems*. Springer, Dordrecht, 1250 pp.

Pirajno, F., 2013: Effects of Metasomatism on Mineral Systems and Their Host Rocks: Alkali Metasomatism, Skarns, Greisens, Tourmalinites, Rodingites, Black-Wall Alteration and Listvenites. In: Metasomatism and the Chemical Transformation of Rock. Lecture Notes in Earth System Sciences. Springer, Berlin, Heidelberg, 203–251.

Plan, A., 2020: *Resolving temporal links between the Högberget granite and the Wigström tungsten skarn deposit in Bergslagen (Sweden) using trace elements and U-Pb LA-ICPMS on complex zircons*. Master´s thesis, no 580. Department of Geology, Lund University, 58 pp.

Richards, J.P., 2011: Magmatic to hydrothermal metal fluxes in convergent and collided margins. *Ore Geology Reviews 40,* 1–26.

Richards, J.P., 2015: The oxidation state, and sulfur and Cu contents of arc magmas: implications for metallogeny. *Lithos 233*, 27–45.

Ripa, M. & Antal Lundin, I., 2020: Relationen mellan Mo-mineraliserad GP-granit och scheelitförande exoskarn i Pingstaberg. *SGU-rapport 2020:10*. Sveriges geologiska undersökning, 17 pp.

Romer, R.L. & Öhlander, B., 1994: U-Pb age of the Yxsjöberg tungsten-skarn deposit, Sweden. *GFF 116,* 161–166.

Romer, R.L. & Smeds, S.-A., 1994: Implications of U-Pb ages of columbite-tantalites from granitic pegmatites for the Palaeoproterozoic accretion of 1.90–1.85 Ga magmatic arcs to the Baltic Shield. *Precambrian Research 67,* 141–158.

Romer, R.L. & Smeds, S.-A., 1997: U–Pb columbite chronology of post-kinematic Palaeoproterozoic pegmatites in Sweden. *Precambrian Research 82,* 85–99.

Romer, R.L. & Kroner, U., 2016: Phanerozoic tin and tungsten mineralization—Tectonic controls on the distribution of enriched protoliths and heat sources for crustal melting. *Gondwanan Research 31,* 60–95.

Rudnick, R.L. & Gao, S., 2014: Composition of the Continental Crust. *In* H.D. Holland & K.K. Turekian (eds.): Treatise on Geochemistry, (Second Edition), Volume 4, Elsevier, Oxford, 1–51.

Rutanen, H. & Andersson, U.B., 2009: Mafic plutonic rocks in a continental-arc setting: geochemistry of 1.87-1.78 Ga rocks from south-central Sweden and models of their palaeotectonic setting. *Geological Journal 44,* 241–279.

Salin, E., Sundblad, K., Woodard, J. & O'Brien, H., 2019: The extension of the Transscandinavian Igneous Belt into the Baltic Sea region. *Precambrian Research 328*, 287–308.

Sambridge, M.S., & Compston, W., 1994: Mixture modeling of multi-component data sets with application to ion-probe zircon ages. *Earth and Planetary Science Letters 128,* 373–390.

Samson, I.M. & Wood, S.A., 2005: The rare earth elements: behaviour in hydrothermal fluids and concentration in hydrothermal mineral deposits, exclusive of alkaline settings. *In* R.L. Linnen & I.M. Samson (eds): *Rare-element Geochemistry and Mineral Deposits*. Geological Association of Canada, Short Course Notes 17, 269–298.

Sato, K., 2012: Sedimentary crust and metallogeny of granitoid affinity: Implications from the geotectonic histories of the circum-Japan Sea region, central Andes and southeastern Australia. *Resource Geology 62,* 329–351.

Schoene, B., 2014: U–Th–Pb geochronology. *In* H.D. Holland & K.K. Turekian (eds.): Treatise on Geochemistry (Second Edition), Elsevier, Oxford, 341–378.

Selby, D. & Creaser, R.A., 2001: Re-Os geochronology and systematic in molybdenite from the Endako porphyry molybdenum deposit, British Columbia, Canada. *Economic Geology 96,* 1461–1467.

Smeds, S.-A., 1994: Zoning and fractionation trends of a peraluminous NYF granitic pegmatite field at Falun, south-central Sweden. *GFF 116,* 175–184.

Smoliar, M.I., Walker, R.J. & Morgan, J.W., 1996: Re–Os isotope constraints on the age of Group IIA, IIIA, IVA, and IVB iron meteorites. *Science 271,* 1099–1102.

Stacey, J.S. & Kramers, J.D., 1975: Approximation of terrestrial lead isotope evolution by a two-stage model. *Earth and Planetary Science Letters 26*, 207–221.

Steiger, R.H. & Jäger, E., 1977: Convention on the use of decay constants in geo- and cosmo-chronology. *Earth and Planetary Science Letters 36*, 359–362.

Stein, H.J., 2006: Low-rhenium molybdenite by metamorphism in northern Sweden: recognition, genesis, and global implications. *Lithos 87,* 300–327.

Stein, H.J., Sundblad, K., Markey, R.J. & Morgan, J.W., 1996: New Tools, New Interpretations: A Re-Os Revelation at the Skarn Deposits of Pitkäranta, Russia. Abstract, Goldschmidt Conference, Heidelberg, 594.

Stephens, M.B. & Andersson, J., 2015: Migmatization related to mafic underplating and intra- or back-arc spreading above a subduction boundary in a 2.0–1.8Ga accretionary orogen, Sweden. *Precambrian Research 264,* 235–257.

Stephens, M.B. & Jansson, N.F., 2020: Paleoproterozoic (1.9–1.8 Ga) syn-orogenic magmatism, sedimentation and mineralization in the Bergslagen lithotectonic unit, Svecokarelian orogen. *In* M. B. Stephens & J. Bergman Weihed (eds): *Sweden: Lithotectonic Framework, Tectonic Evolution and Mineral Resources.* Geological Society, London, Memoirs, 50, 155–206.

Stephens, M.B., Ripa, M., Lundström, I., Persson, L., Bergman, T., Ahl, M., Wahlgren, C.-H., Persson, P.-O. & Wickström, L., 2009: Synthesis of the bedrock geology in the Bergslagen region, Fennoscandian Shield, south-central Sweden. *Sveriges geologiska undersökning Ba 58*, 259 s.

Strömberg, A.G.B., 1983: Berggrundskartan Ludvika SV. *Sveriges geologiska undersökning Af 158*.

Suikkanen, E. & Rämö O.T., 2019: Episyenites – Characteristic, genetic constraints, and mineral potentil. *Mining, Mineralogy and Exploration 36,* 861–878.

Sundblad, K. & Bergman, T., 1997: "Late Svecofennian" granitoids. *In* M. Ahl, U.B. Andersson, T. Lundqvist & K. Sundblad (eds.): Rapakivi granites and related rocks in central Sweden. *Sveriges geologiska undersökning Ca 87*, 7–15.

Sundblad, K., Ahl, M. & Schöberg, H., 1993: Age and geochemistry of granites associated with Mo-mineralizations in western Bergslagen, Sweden. *Precambrian Research 64,* 319–335.

Sylvester, P.J., 1989: Post-collisional alkaline granites. *Journal of Geology 97,* 261–280.

Taylor, S.R. & McLennan, S.M., 1981: The composition and evolution of the continental crust: Rare earth element evidence from sedimentary rocks. *Philosophical Transactions of the Royal Society of London, Series A 301,* 381–399.

Valbracht, P.J., Oen, I.S. & Beunk, F.F., 1994: Sm-Nd isotope systematics of 1.9-1.8-Ga granites from western Bergslagen, Sweden: inferences on a 2.1-2.0-Ga crustal precursor. *Chemical Geology 112,* 21–37.

Van Staal, C.R., 2007: Pre-Carboniferous tectonic evolution and metallogeny of the Canadian Appalachians. *In* W.D. Goodfellow (ed.): *Mineral Deposits of Canada: A Synthesis of Major Deposit-Types, District Metallogeny, the Evolution of Geological Provinces, and Exploration Methods.* Geological Association of Canada, Mineral Deposits Division, Special Publication 5, 793–818.

Wahlgren, C.-H. & Stephens, M.B., 2020: Småland lithotectonic unit dominated by Paleoproterozoic (1.8 Ga) syn-orogenic magmatism, Svecokarelian orogen. *In* M. B. Stephens & J. Bergman Weihed (eds): *Sweden: Lithotectonic Framework, Tectonic Evolution and Mineral Resources.* Geological Society, London, Memoirs, 50, 207–235.

Wang, X.-S., Williams-Jones, A.E., Hu, R.-Z., Shang, L.-B. & Bi, X.-W., 2021: The role of fluorine in granite-related tungsten ore genesis: Results of experiments and modeling. *Geochimica et Cosmochimica Acta 292,* 170–187.

Webster, J.D., Thomas, R., Rhede, D., Forster, H.J. & Seltmann, R., 1997: Melt inclusions in quartz from an evolved peraluminous pegmatite: Geochemical evidence for strong tin enrichment in fluorine-rich and phosphorus-rich residual liquids. *Geochimica et Cosmochimica Acta 61,* 2589–2604.

Whalen, J.B. & Hildebrand, R.S., 2019: Trace element discrimination of arc, slab failure, and A-type granitic rocks. *Lithos 348–349*, 105179.

Whalen, J.B., Currie, K.L. & Chappell, B.W., 1987: A-type granites: geochemical characteristics, discrimination and petrogenesis. *Contributions to Mineralogy and Petrology 95,* 407–419.

Whitehouse, M.J. & Kamber, B.S., 2005: Assigning dates to thin gneissic veins in high-grade metamorphic terranes: a cautionary tale from Akilia, southwest Greenland. *Journal of Petrology 46*, 291–318.

Whitehouse, M.J., Kamber, B.S. & Moorbath, S., 1999: Age significance of U–Th–Pb zircon data from Early Archaean rocks of west Greenland: a reassessment based on combined ion-microprobe and imaging studies. *Chemical Geology 160*, 201–224.

Wiedenbeck, M., Hanchar, J.M., Peck, W.H., Sylvester, P., Valley, J., Whitehouse, M., Kronz, A., Morishita, Y., Nasdala, L., Fiebig, J., Franchi, I., Girard, J.P., Greenwood, R.C., Hinton, R., Kita, N., Mason, P.R.D., Norman, M., Ogasawara, M., Piccoli, P.M., Rhede, D., Satoh, H., Schulz-Dobrick, B., Skår, O., Spicuzza, M.J., Terada, K., Tindle, A., Togashi, S., Vennemann, T., Xie, Q. & Zheng, Y.F., 2004: Further characterisation of the 91500 zircon crystal. *Geostandards and Geoanalytical Research 28,* 9–39.

Wilson, M., 1989: *Igneous petrogenesis—a global tectonic approach.* Unwin and Hyman, London, 466 pp.

Woodward, J., Sundblad, K. & Schöberg, H., 2009: Disturbance of U-Pb in zircons by Mo-W-mineralising magmatic fluids in the late Svecofennian Bipsbergs klack granite, Sweden. Geological Society of America, Annual Meeting, Portland, 158-9. Abstract.

Zuber, J.A., 1985: Geological interpretation of gravity and aeromagnetic surveys over the Fellingsbro-Blixterboda granite. *Geologiska Föreningens i Stockholm Förhandlingar 107,* 203–213.

APPENDIX 1: DESCRIPTIONS OF GEOCHEMISTRY SAMPLES

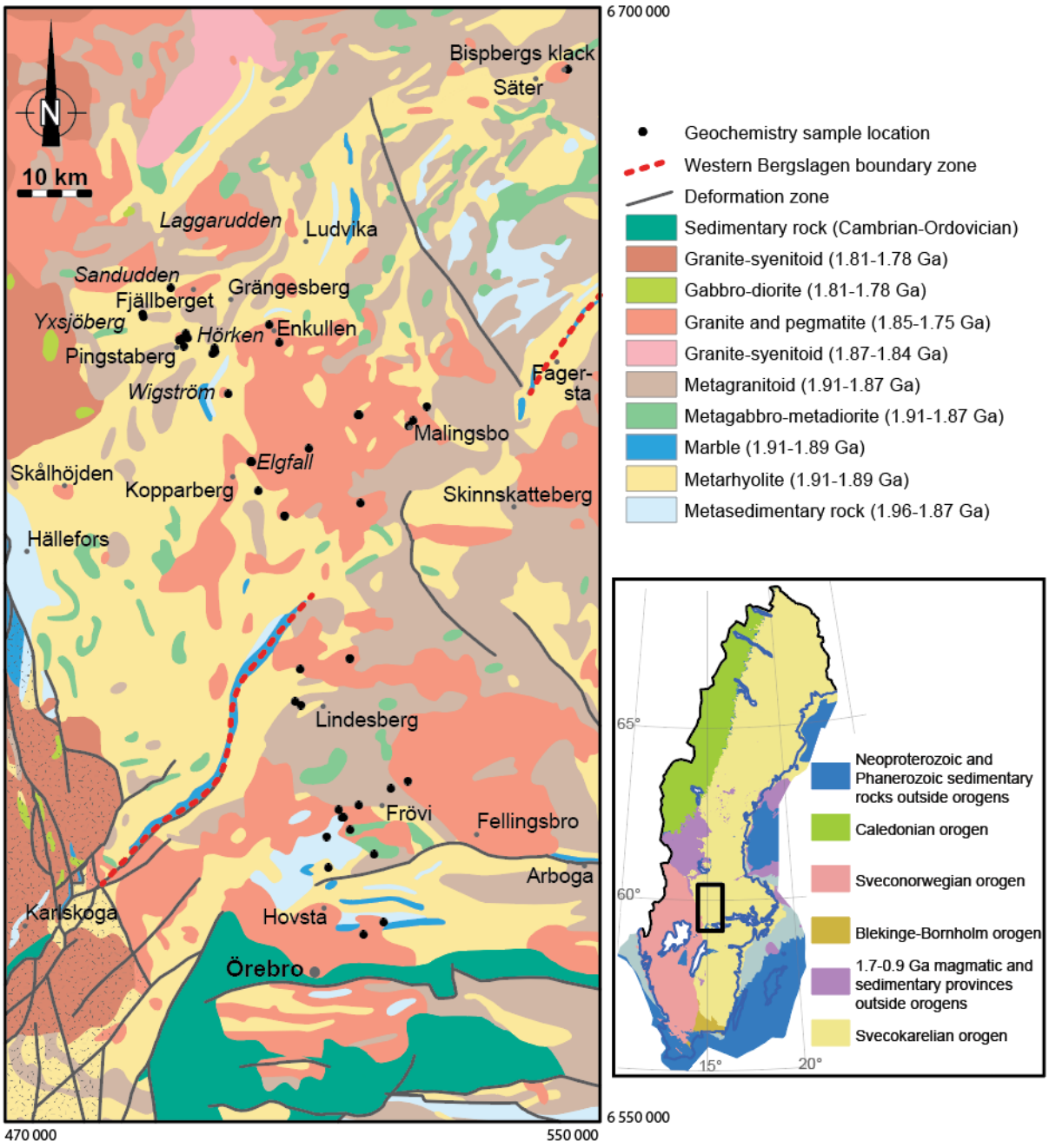

Figure A1. Geological map of the study area, western Bergslagen, showing the locations of geochemistry samples corresponding to those listed in Table A1 below.

Table A1. List of samples used in this study (n = 48).

Sample ID	Easting[1]	Northing[1]	Location or name	Sample Type	Brief description
Granitic rocks in the SE sector					
STB181047A	517613	6575164	Örebro (Kränglan)	Outcrop	Biotite granite
STB191008A	509211	6606027	Andsjöbäcken	Outcrop	Metagranitoid, foliated
STB191022A	516954	6592605	NÖ Ersboda	Outcrop	Metagranitoid, foliated
STB191023A	514977	6590932	NÖ Ersboda	Outcrop	Metagranitoid, foliated, cut by leucogranite
STB181051A	514750	6590987	Frövi (Ervalla)	Outcrop	Biotite-muscovite granite, equigranular, massive
STB191003A	509125	6610879	Fornaboda	Outcrop	Biotite-muscovite granite, equigranular, massive; amphibolite xenolith/contact
STB191044A	523570	6595826	NÖ Hagaberg	Outcrop	Biotite granite, megacrystic, massive, mafic enclaves
STB191052A	515838	6589292	Frövi (Ervalla)	Outcrop	Biotite granite, megacrystic, massive
STB191045A	520332	6576815	Ängsberget	Outcrop	Biotite-muscovite granite, equigranular to megacrystic, massive
STB191020A	514297	6592006	N Sundby	Outcrop	Biotite-muscovite granite, equigranular, massive
STB191027A	519016	6586052	Väringberget	Outcrop	Biotite granite, equigranular, massive, xenolith
STB191031A	512884	6584206	Väringberget	Outcrop	Biotite granite, equigranular, massive, xenolith
STB191036A	515806	6612348	S Stora Aspasjön	Outcrop	Biotite granite, equigranular, massive, partly weathered
Other rock samples in the SE sector					
STB181050A	512680	6588338	Frövi (Ervalla)	Outcrop	Metatexite: quartzofeldspathic gneiss with pink granitic veins and segregations.
STB191005A	508418	6606561	Lindesberg (Hidingen)	Outcrop	Meta-rhyolite to -dacite, foliated
STB191043A	521293	6594922	Frövi (Pikaboda)	Outcrop	Metagabbro
Barren, skarn-distal granitic rocks in the NW sector					
ELH190002A	524300	6644418	Malingsbo east	Outcrop	Biotite granite, equigranular, weakly foliated to massive
ELH190016A	516876	6645179	Malingsbo central	Outcrop	Biotite granite, equigranular, weakly foliation to massive
ELH190017A	517062	6645214	Malingsbo central	Outcrop	Biotite granite, seriate to megacrystic, weak foliation to massive
ELH190029A	517204	6633271	Malingsbo south	Outcrop	Biotite granite, megacrystic, weak foliation with augen texture
ELH190049A	506285	6654963	Enkullen	Outcrop	Biotite granite, equigranular, massive, mafic enclaves and rare xenoliths
ELH190051A	504934	6657263	Enkullen	Outcrop	Biotite granite, equigranular, massive, mafic enclaves
ELH200018A	510247	6640657	Malingsbo west	Outcrop	Biotite granite, megacrystic, weak foliation to massive
Barren, skarn-proximal granites in the NW sector					
ELH190039A	506988	6631558	Malingsbo SW	Outcrop	Biotite granite, equigranular, weakly foliated to massive, local pegmatite
ELH190039B	506988	6631558	Malingsbo SW	Outcrop	Granitic pegmatite, massive
ELH190042B	503493	6634931	Malingsbo SW (Gruvberget)	Outcrop	Biotite granite, equigranular, massive

Sample ID	Easting[1]	Northing[1]	Location or name	Sample Type	Brief description
ELH190063A	493978	6655535	Pingstaberg	Outcrop	Biotite granite, equigranular, massive
ELH190067A	499437	6648018	Wigström	Outcrop	Biotite granite, equigranular, massive
ELH190072A	493454	6654385	Pingstaberg	Outcrop	Metagranitoid, foliated
ELH190077A	493149	6655373	Pingstaberg	Outcrop	Biotite granite, equigranular, massive
ELH190078A	493138	6655310	Pingstaberg	Outcrop	Biotite granite, equigranular, massive
ELH200019A	497306	6653364	Hörken	Outcrop	Biotite granite, equigranular, massive
ELH200020A	497676	6653649	Hörken	Outcrop	Biotite granite, equigranular, massive
ELH200081A	491664	6662316	Sandudden	Outcrop	Biotite granite, equigranular, massive
ELH200105A	497607	6654102	Hörken	Drill core	Biotite granite, equigranular, massive
ELH200109A	502488	6638889	Elgfall	Drill core	Biotite granite, equigranular, massive
ELH200109B	502488	6638889	Elgfall	Drill core	Biotite microgranite, equigranular, massive
Mineralised ± altered skarn-proximal granitic rocks in the NW sector					
ELH170002A	492894	6655258	Pingstaberg	Outcrop	Biotite granite, equigranular, massive, disseminated sulfides and fluorite, sericite-altered
ELH190054A	545140	6691617	Bispbergs klack	Outcrop	Biotite granite, equigranular, massive, disseminated sulfides, sericite-altered
ELH190060A	493696	6656073	Pingstaberg	Outcrop	Aplite-microgranite, equigranular, massive, sericite-altered
ELH190073A	492888	6655252	Pingstaberg	Outcrop	Biotite granite, equigranular, massive, disseminated sulfides, sericite-altered
ELH190073B	492888	6655252	Pingstaberg	Outcrop	Biotite granite, equigranular, massive, disseminated sulfides, sericite-altered
ELH190073C	492888	6655252	Pingstaberg	Outcrop	Granitic pegmatite, equigranular, massive, disseminated sulfides, altered
ELH200096A	502591	6638897	Elgfall	Outcrop	Biotite granite, pegmatitic, massive, sericite-altered
ELH200106A	487901	6658733	Yxsjöbyn	Drill core	Aplite-microgranite, sericite-altered, massive, disseminated sulfides
ELH200107A	488006	6658328	Yxsjöbyn	Drill core	Aplite-microgranite, sericite-altered, massive, disseminated sulfides
Other rock samples in the NW sector					
ELH190003A	523697	6643640	Malingsbo east	Outcrop	Amphibolite, foliated
ELH190026A	526116	6646272	Malingsbo east	Outcrop	Meta-rhyolite, foliated, banded

Notes: 1 = Sweref99 TM coordinates; drill core samples show drill hole collar coordinates at surface.